Constraints on the spin-parity and anomalous HVV couplings of the Higgs boson in proton collisions at 7 and 8 TeV

V. Khachatryan *et al.*[*]
(CMS Collaboration)
(Received 12 November 2014; published 13 July 2015)

The study of the spin-parity and tensor structure of the interactions of the recently discovered Higgs boson is performed using the $H \to ZZ, Z\gamma^*, \gamma^*\gamma^* \to 4\ell$, $H \to WW \to \ell\nu\ell\nu$, and $H \to \gamma\gamma$ decay modes. The full data set recorded by the CMS experiment during the LHC run 1 is used, corresponding to an integrated luminosity of up to 5.1 fb^{-1} at a center-of-mass energy of 7 TeV and up to 19.7 fb^{-1} at 8 TeV. A wide range of spin-two models is excluded at a 99% confidence level or higher, or at a 99.87% confidence level for the minimal gravitylike couplings, regardless of whether assumptions are made on the production mechanism. Any mixed-parity spin-one state is excluded in the ZZ and WW modes at a greater than 99.999% confidence level. Under the hypothesis that the resonance is a spin-zero boson, the tensor structure of the interactions of the Higgs boson with two vector bosons ZZ, $Z\gamma$, $\gamma\gamma$, and WW is investigated and limits on eleven anomalous contributions are set. Tighter constraints on anomalous HVV interactions are obtained by combining the HZZ and HWW measurements. All observations are consistent with the expectations for the standard model Higgs boson with the quantum numbers $J^{PC} = 0^{++}$.

DOI: 10.1103/PhysRevD.92.012004 PACS numbers: 14.80.Bn, 12.60.-i, 13.88.+e

I. INTRODUCTION

The observation of a new boson [1–3] with a mass around 125 GeV and properties consistent with the standard model (SM) Higgs boson [4–10] was reported by the ATLAS and CMS Collaborations in 2012. The discovery was followed by a comprehensive set of measurements [11–27] of its properties to determine if the new boson follows the SM predictions or if there are indications for physics beyond the SM (BSM).

The CMS experiment analyzed the full data set collected during the CERN LHC run 1 and measured the properties of the Higgs-like boson H, using its decay modes to two electroweak gauge bosons $H \to ZZ \to 4\ell$ [11–13], $H \to WW \to \ell\nu\ell\nu$ [14], and $H \to \gamma\gamma$ [15], where ℓ denotes $e^\pm$ or $\mu^\pm$, and WW denotes W^+W^-. The results showed that the spin-parity properties of the new boson are consistent with the expectations for the scalar SM Higgs boson. In particular, the hypotheses of a pseudoscalar, vector, and pseudovector boson were excluded at a 99.95% confidence level (CL) or higher, and several spin-two boson hypotheses were excluded at a 98% C.L. or higher. The investigated spin-two models included two bosons with gravitonlike interactions and two bosons with higher-dimension operators and opposite parity. The spin-zero results included the first constraint of the f_{a3} parameter, which probes the tensor structure of the HZZ interactions and is defined as the fractional pseudoscalar cross section, with $f_{a3} = 1$ corresponding to the pure pseudoscalar hypothesis. The ATLAS experiment has also excluded at a 98% C.L. or higher the hypotheses of a pseudoscalar, vector, pseudovector, and graviton-inspired spin-two boson with minimal couplings and several assumptions on the boson production mechanisms [22].

In this paper, an extended study of the spin-parity properties of the Higgs boson and of the tensor structure of its interactions with electroweak gauge bosons is presented using the $H \to ZZ$, $Z\gamma^*$, $\gamma^*\gamma^* \to 4\ell$, where the interference between the three intermediate states is included, and $H \to WW \to \ell\nu\ell\nu$ decay modes at the CMS experiment. The study focuses on testing for the presence of anomalous effects in HZZ and HWW interactions under spin-zero, -one, and -two hypotheses. The $HZ\gamma$ and $H\gamma\gamma$ interactions are probed for the first time using the 4ℓ final state. Constraints are set on eleven anomalous coupling contributions to the HVV interactions, where V is a gauge vector boson, under the spin-zero assumption of the Higgs boson, extending the original measurement of the f_{a3} parameter [11,12]. The exotic-spin study is extended to the analysis of mixed spin-one states, beyond the pure parity states studied earlier [12,14], and ten spin-two hypotheses of the boson under the assumption of production either via gluon fusion or quark-antiquark annihilation, or without such an assumption. This corresponds to thirty spin-two models, beyond the six production and decay models studied earlier [11,12,14]. The $H \to \gamma\gamma$ decay channel is also studied in the context of exotic spin-two scenarios, and the

[*]Full author list given at the end of the article.

Published by the American Physical Society under the terms of the Creative Commons Attribution 3.0 License. Further distribution of this work must maintain attribution to the author(s) and the published article's title, journal citation, and DOI.

 © 2015 CERN, for the CMS Collaboration

results presented in Ref. [15] are combined with those obtained in the $H \to ZZ$ and $H \to WW$ channels [12,14].

The experimental approaches used here are similar to those used by CMS to study the spin-parity and other properties of the new resonance [11–15], and use the techniques developed for such measurements [28–33]. The analysis is based on theoretical and phenomenological studies that describe the couplings of a Higgs-like boson to two gauge bosons. They provide techniques and ideas for measuring the spin and CP properties of a particle interacting with vector bosons [28–57]. Historically, such techniques have been applied to the analysis of meson decays to four-body final states [58–62].

The paper is organized as follows. First, the phenomenology of spin-parity and anomalous HVV interactions is described in Sec. II. The experimental apparatus, simulation, and reconstruction techniques are discussed in Sec. III. The analysis techniques are introduced in Sec. IV. The exclusion of exotic spin-one and spin-two scenarios is shown in Sec. V. Finally, for the spin-zero scenario, comprehensive studies of the tensor structure of HVV interactions are presented in Sec. VI. The results are summarized in Sec. VII.

II. PHENOMENOLOGY OF SPIN-PARITY AND ANOMALOUS HVV INTERACTIONS

The production and decay of H are described by its interactions with a pair of vector bosons VV, such as $ZZ, Z\gamma, \gamma\gamma, WW$, and gg, or with a fermion-antifermion pair. The relevant phenomenology for the interactions of spin-zero, -one, and -two bosons, as motivated by earlier studies [28,29,31–33,53], is presented below. In the following, the spin-parity state is generically denoted as J^P, with $J = 0, 1$, or 2, while the quantum numbers of the SM Higgs boson are expected to be $J^{PC} = 0^{++}$. However, the interactions of the observed state do not necessarily conserve C-parity or CP-parity, and the general scattering amplitudes describe the spin-parity properties of the new boson and its anomalous couplings with a pair of vector bosons or fermions.

A. Decay of a spin-zero resonance

The scattering amplitude describing the interaction between a spin-zero H and two spin-one gauge bosons VV, such as $ZZ, Z\gamma, \gamma\gamma, WW$, or gg, includes only three independent invariant tensor structures with the coupling parameters a_i^{VV} that can have both real and imaginary parts and, in general, are form factors which can depend on the squared Lorentz-invariant four-momenta of V_1 and V_2, q_{V1}^2 and q_{V2}^2. In the following, the terms up to q_V^2 are kept in the expansion under the assumption of small contributions from anomalous couplings,

$$A(HVV) \sim \left[a_1^{VV} + \frac{\kappa_1^{VV} q_{V1}^2 + \kappa_2^{VV} q_{V2}^2}{(\Lambda_1^{VV})^2}\right] m_{V1}^2 \epsilon_{V1}^* \epsilon_{V2}^* + a_2^{VV} f_{\mu\nu}^{*(1)} f^{*(2),\mu\nu} + a_3^{VV} f_{\mu\nu}^{*(1)} \tilde{f}^{*(2),\mu\nu}, \tag{1}$$

where $f^{(i)\mu\nu} = \epsilon_{Vi}^{\mu} q_{Vi}^{\nu} - \epsilon_{Vi}^{\nu} q_{Vi}^{\mu}$ is the field strength tensor of a gauge boson with momentum q_{Vi} and polarization vector ϵ_{Vi}, $\tilde{f}_{\mu\nu}^{(i)} = \frac{1}{2}\epsilon_{\mu\nu\rho\sigma} f^{(i),\rho\sigma}$ is the dual field strength tensor, the superscript * designates a complex conjugate, m_{V1} is the pole mass of the Z or W vector boson (while the cases with the massless vector bosons are discussed below), and Λ_1 is the scale of BSM physics and is a free parameter of the model [31]. A different coupling in the scattering amplitude in Eq. (1) typically leads to changes of both the observed rate and the kinematic distributions of the process. However, the analysis presented in this paper does not rely on any prediction of the overall rate and studies only the relative contributions of different tensor structures.

In Eq. (1), VV stands for $ZZ, Z\gamma, \gamma\gamma, WW$, and gg. The tree-level SM-like contribution corresponds to $a_1^{ZZ} \neq 0$ and $a_1^{WW} \neq 0$, while there is no tree-level coupling to massless gauge bosons, that is, $a_1^{VV} = 0$ for $Z\gamma, \gamma\gamma$, and gg. Small values of the other couplings can be generated through loop effects in the SM, but their SM values are not accessible experimentally with the available data. Therefore, the other terms can be ascribed to anomalous couplings which are listed for HZZ, HWW, $HZ\gamma$, and $H\gamma\gamma$ in Table I. Among those, considerations of symmetry and gauge invariance require $\kappa_1^{ZZ} = \kappa_2^{ZZ} = -\exp(i\phi_{\Lambda1}^{ZZ})$, $\kappa_1^{\gamma\gamma} = \kappa_2^{\gamma\gamma} = 0$, $\kappa_1^{gg} = \kappa_2^{gg} = 0$, $\kappa_1^{Z\gamma} = 0$ and $\kappa_2^{Z\gamma} = -\exp(i\phi_{\Lambda1}^{Z\gamma})$. While not strictly required, the same symmetry is considered in the WW case $\kappa_1^{WW} = \kappa_2^{WW} = -\exp(i\phi_{\Lambda1}^{WW})$. In the above, $\phi_{\Lambda1}^{VV}$ is the phase of the anomalous coupling with Λ_1^{VV}, which is either 0 or π for real couplings. In the following, the ZZ labels for the ZZ interactions will be omitted, and therefore the couplings a_1, a_2, a_3, and Λ_1 are not labeled explicitly with a ZZ superscript, while the superscript is kept for the other VV states.

The parity-conserving interaction of a pseudoscalar (CP-odd state) corresponds to the a_3^{VV} terms, while the other terms describe the parity-conserving interaction of a scalar (CP-even state). The a_3^{VV} terms appear in the SM only at a three-loop level and receive a small contribution. The a_2^{VV} and Λ_1^{VV} terms appear in loop-induced processes and give small contributions $O(10^{-3}$–$10^{-2})$. The dominant contributions to the SM expectation of the $H \to Z\gamma$ and $\gamma\gamma$ decays are $a_2^{Z\gamma}$ and $a_2^{\gamma\gamma}$, which are predicted to be $a_2^{Z\gamma} \simeq -0.007$ and $a_2^{\gamma\gamma} \simeq 0.004$ [63]. The $a_i^{Z\gamma}$ and $a_i^{\gamma\gamma}$ coupling terms contribute to the $H \to 4\ell$ process through the $H \to Z\gamma^*$ and $\gamma^*\gamma^* \to 4\ell$ decays with off-shell intermediate photons. Anomalous couplings may be enhanced with BSM contributions and generally acquire a nontrivial dependence

TABLE I. List of anomalous HVV couplings considered in the measurements assuming a spin-zero Higgs boson. The definition of the effective fractions is discussed in the text and the translation constant is given in each case. The effective cross sections correspond to the processes $H \to VV \to 2e2\mu$ and $H \to WW \to \ell\nu\ell\nu$ and the Higgs boson mass $m_H = 125.6$ GeV using the JHUGEN [28,29,31] calculation. The cross-section ratios for the $HZ\gamma$ and $H\gamma\gamma$ couplings include the requirement $\sqrt{q_V^2} \geq 4$ GeV.

Interaction	Anomalous Coupling	Coupling Phase	Effective Fraction	Translation Constant
HZZ	Λ_1	$\phi_{\Lambda 1}$	$f_{\Lambda 1}$	$\sigma_1/\tilde{\sigma}_{\Lambda 1} = 1.45 \times 10^4$ TeV^{-4}
	a_2	ϕ_{a2}	f_{a2}	$\sigma_1/\sigma_2 = 2.68$
	a_3	ϕ_{a3}	f_{a3}	$\sigma_1/\sigma_3 = 6.36$
HWW	Λ_1^{WW}	$\phi_{\Lambda 1}^{WW}$	$f_{\Lambda 1}^{WW}$	$\sigma_1^{WW}/\tilde{\sigma}_{\Lambda 1}^{WW} = 1.87 \times 10^4$ TeV^{-4}
	a_2^{WW}	ϕ_{a2}^{WW}	f_{a2}^{WW}	$\sigma_1^{WW}/\sigma_2^{WW} = 1.25$
	a_3^{WW}	ϕ_{a3}^{WW}	f_{a3}^{WW}	$\sigma_1^{WW}/\sigma_3^{WW} = 3.01$
$HZ\gamma$	$\Lambda_1^{Z\gamma}$	$\phi_{\Lambda 1}^{Z\gamma}$	$f_{\Lambda 1}^{Z\gamma}$	$\sigma_1'/\tilde{\sigma}_{\Lambda 1}^{Z\gamma} = 5.76 \times 10^3$ TeV^{-4}
	$a_2^{Z\gamma}$	$\phi_{a2}^{Z\gamma}$	$f_{a2}^{Z\gamma}$	$\sigma_1'/\sigma_2^{Z\gamma} = 2.24 \times 10^{-3}$
	$a_3^{Z\gamma}$	$\phi_{a3}^{Z\gamma}$	$f_{a3}^{Z\gamma}$	$\sigma_1'/\sigma_3^{Z\gamma} = 2.72 \times 10^{-3}$
$H\gamma\gamma$	$a_2^{\gamma\gamma}$	$\phi_{a2}^{\gamma\gamma}$	$f_{a2}^{\gamma\gamma}$	$\sigma_1'/\sigma_2^{\gamma\gamma} = 2.82 \times 10^{-3}$
	$a_3^{\gamma\gamma}$	$\phi_{a3}^{\gamma\gamma}$	$f_{a3}^{\gamma\gamma}$	$\sigma_1'/\sigma_3^{\gamma\gamma} = 2.88 \times 10^{-3}$

on Lorentz-invariant quantities and become complex. The different contributions to the amplitude can therefore be tested without making assumptions about the complex phase between different contributions. When the particles in the loops responsible for these couplings are heavy in comparison to the Higgs boson mass parameters, the couplings are real.

Under the assumption that the couplings are constant and real, the above formulation is equivalent to an effective Lagrangian notation for the HZZ, HWW, $HZ\gamma$, and $H\gamma\gamma$ interactions

$$\begin{aligned} L(HVV) \sim\; & a_1 \frac{m_Z^2}{2} H Z^\mu Z_\mu - \frac{\kappa_1}{(\Lambda_1)^2} m_Z^2 H Z_\mu \Box Z^\mu \\ & - \frac{1}{2} a_2 H Z^{\mu\nu} Z_{\mu\nu} - \frac{1}{2} a_3 H Z^{\mu\nu} \tilde{Z}_{\mu\nu} \\ & + a_1^{WW} m_W^2 H W^{+\mu} W_\mu^- - \frac{1}{(\Lambda_1^{WW})^2} m_W^2 \\ & \times H(\kappa_1^{WW} W_\mu^- \Box W^{+\mu} + \kappa_2^{WW} W_\mu^+ \Box W^{-\mu}) \\ & - a_2^{WW} H W^{+\mu\nu} W_{\mu\nu}^- - a_3^{WW} H W^{+\mu\nu} \tilde{W}_{\mu\nu}^- \\ & + \frac{\kappa_2^{Z\gamma}}{(\Lambda_1^{Z\gamma})^2} m_Z^2 H Z_\mu \partial_\nu F^{\mu\nu} - a_2^{Z\gamma} H F^{\mu\nu} Z_{\mu\nu} \\ & - a_3^{Z\gamma} H F^{\mu\nu} \tilde{Z}_{\mu\nu} - \frac{1}{2} a_2^{\gamma\gamma} H F^{\mu\nu} F_{\mu\nu} - \frac{1}{2} a_3^{\gamma\gamma} H F^{\mu\nu} \tilde{F}_{\mu\nu}, \end{aligned} \tag{2}$$

where the notations are the same as in Eq. (1) and H is the real Higgs field, Z_μ is the Z field, W_μ is the W field, F_μ is the γ^* field, $V_{\mu\nu} = \partial_\mu V_\nu - \partial_\nu V_\mu$ is the bosonic field strength, the dual field strengths are defined as $\tilde{V}_{\mu\nu} = \frac{1}{2}\epsilon_{\mu\nu\rho\sigma} V^{\rho\sigma}$, and $\Box$ is the d'Alembert operator. The SM-like terms with tree-level couplings a_1 and a_1^{WW} are associated with dimension-three operators, and the rest of the terms tested correspond to operators of dimension five. Operators of higher dimension are neglected in this study.

In the analysis, the physics effects of the eleven anomalous couplings listed in Table I are described, where the hypothesis of the Higgs boson mass $m_H = 125.6$ GeV is used, which is the best-fit value in the study of the $H \to VV \to 4\ell$ and $H \to WW \to \ell\nu\ell\nu$ channels [12,14]. The scenarios are parametrized in terms of the effective fractional cross sections f_{ai} and their phases ϕ_{ai} with respect to the two dominant tree-level couplings a_1 and a_1^{WW} in the $H \to VV \to 4\ell$ and $H \to WW \to \ell\nu\ell\nu$ processes, respectively. In the $H \to VV$ decay the q_V^2 range does not exceed approximately 100 GeV due to the kinematic bound, supporting the expansion up to q_V^2 in Eq. (1). Even though the expansion with only three anomalous contributions in Eq. (1) may become formally incomplete when large values of $f_{ai} \sim 1$ are considered, this remains a valuable test of the consistency of the data with the SM. Moreover, certain models, such as models with a pseudoscalar Higgs boson state, do not require a sizable contribution of higher terms in the q_V^2 expansion even for $f_{ai} \sim 1$. Therefore, the full range $0 \leq f_{ai} \leq 1$ is considered in this study.

The effective fractional ZZ cross sections f_{ai} and phases ϕ_{ai} are defined as follows:

$$f_{\Lambda 1} = \frac{\tilde{\sigma}_{\Lambda 1}/(\Lambda_1)^4}{|a_1|^2\sigma_1 + |a_2|^2\sigma_2 + |a_3|^2\sigma_3 + \tilde{\sigma}_{\Lambda 1}/(\Lambda_1)^4 + \cdots},$$
$$\phi_{\Lambda 1},$$
$$f_{a2} = \frac{|a_2|^2\sigma_2}{|a_1|^2\sigma_1 + |a_2|^2\sigma_2 + |a_3|^2\sigma_3 + \tilde{\sigma}_{\Lambda 1}/(\Lambda_1)^4 + \cdots},$$
$$\phi_{a2} = \arg\left(\frac{a_2}{a_1}\right),$$
$$f_{a3} = \frac{|a_3|^2\sigma_3}{|a_1|^2\sigma_1 + |a_2|^2\sigma_2 + |a_3|^2\sigma_3 + \tilde{\sigma}_{\Lambda 1}/(\Lambda_1)^4 + \cdots},$$
$$\phi_{a3} = \arg\left(\frac{a_3}{a_1}\right), \tag{3}$$

where σ_i is the cross section of the process corresponding to $a_i = 1$, $a_{j\neq i} = 0$, while $\tilde{\sigma}_{\Lambda 1}$ is the effective cross section of the process corresponding to $\Lambda_1 = 1$ TeV, given in units of fb $\times$ TeV^4. The effective fractional WW cross sections are defined in complete analogy with the definitions for ZZ as shown in Eq. (3). The definition in Eq. (3) is independent of the collider energy because only the decay rates of the processes $H \to VV \to 4\ell$ and $H \to WW \to \ell\nu\ell\nu$ affect the ratio. It also has the advantage of the f_{ai} parameters being bounded between 0 and 1, and being uniquely defined, regardless of the convention used for the coupling constants. In the four-lepton final state, the cross section of the $H \to VV \to 2e2\mu$ final state is used, as this final state is not affected by the interference between same-flavor leptons in the final state.

In an analogous way, the effective fractional cross sections and phases of $Z\gamma$ and $\gamma\gamma$, generically denoted as $V\gamma$ below, in the $H \to VV \to 2e2\mu$ process are defined as

$$f_{ai}^{V\gamma} = \frac{|a_i^{V\gamma}|^2\sigma_i^{V\gamma}}{|a_1|^2\sigma_1' + |a_i^{V\gamma}|^2\sigma_i^{V\gamma} + \cdots},$$
$$\phi_{ai}^{V\gamma} = \arg\left(\frac{a_{ai}^{V\gamma}}{a_1}\right), \tag{4}$$

where the requirement $\sqrt{q_{Vi}^2} \geq 4$ GeV is used in the cross-section calculations for all processes, including the ZZ tree-level process with a_1 as indicated with σ_1'. This requirement on q_{Vi}^2 is introduced to restrict the definition to a region without infrared divergence and to define the fractions within the empirically relevant range. The ellipsis ($\ldots$) in Eqs. (3) and (4) indicates any other contribution not listed explicitly.

Given the measured values of the effective fractions, it is possible to extract the ratios of the coupling constants a_i/a_1, the scale of BSM physics Λ_1, or the ratios of the $Z\gamma^*$ ($\gamma^*\gamma^*$) cross sections with respect to the SM predictions in any parametrization. Following Eq. (1) the translation of the f_{ai} measurements can be performed as

$$\frac{|a_i|}{|a_1|} = \sqrt{f_{ai}/f_{a1}} \times \sqrt{\sigma_1/\sigma_i},$$
$$\Lambda_1\sqrt{|a_1|} = \sqrt[4]{f_{a1}/f_{\Lambda 1}} \times \sqrt[4]{\tilde{\sigma}_{\Lambda 1}/\sigma_1}, \tag{5}$$

where the cross-section ratios for a 125.6 GeV Higgs boson are given in Table I, and the fraction $f_{a1} = (1 - f_{\Lambda 1} - f_{a2} - f_{a3} - \ldots)$ corresponds to the effective SM tree-level contribution, which is expected to dominate. The ellipsis in the f_{a1} definition indicates any other contribution, such as $Z\gamma^*$ and $\gamma^*\gamma^*$, where relevant.

The couplings of the Higgs boson to $Z\gamma$ and $\gamma\gamma$ are generally much better measured in the decays with the on-shell gauge bosons $H \to Z\gamma$ and $\gamma\gamma$ [15,19,23,25]. Therefore, the measurements of the $HZ\gamma$ and $H\gamma\gamma$ anomalous couplings are provided mostly as a feasibility study without going into detailed measurements of correlations of parameters. Once a sufficient number of events is accumulated for the discovery of these modes in the $H \to VV \to 4\ell$ channel with a high-luminosity LHC, the study of CP properties can be performed with the $HZ\gamma$ and $H\gamma\gamma$ couplings [56,64].

The couplings of a spin-zero particle to W and Z bosons can be related given the assumption of certain symmetries. For example, in the case of the custodial singlet Higgs boson, the relation is $a_1^{WW} = a_1$ [65,66]. Generally, these couplings could have a different relationship and the HVV couplings are controlled by two free parameters. When one parameter is expressed as the f_{ai} fraction in the HZZ coupling, the other parameter can be chosen as a ratio of anomalous couplings in the $H \to ZZ$ and $H \to WW$ channels

$$r_{ai} = \frac{a_i^{WW}/a_1^{WW}}{a_i/a_1} \quad \text{or} \quad R_{ai} = \frac{r_{ai}|r_{ai}|}{1 + r_{ai}^2}. \tag{6}$$

Using Eq. (5) the effective fractions f_{ai}^{WW} and f_{ai} can be related as

$$f_{ai} = [1 + r_{ai}^2(1/f_{ai}^{WW} - 1)\sigma_i^{WW}\sigma_1/(\sigma_1^{WW}\sigma_i)]^{-1}. \tag{7}$$

In this way, the measurement of f_{ai}^{WW} can be converted to f_{ai} and vice versa, and the combination of the results in the ZZ and WW channels can be achieved.

B. Decay of a spin-one resonance

In the case of a spin-one resonance, the amplitude of its interaction with a pair of massive gauge bosons, ZZ or WW, consists of two independent terms, which can be written as

$$A(X_{J=1}VV) \sim b_1^{VV}[(\epsilon_{V1}^* q)(\epsilon_{V2}^*\epsilon_X) + (\epsilon_{V2}^* q)(\epsilon_{V1}^*\epsilon_X)] + b_2^{VV}\epsilon_{\alpha\mu\nu\beta}\epsilon_X^\alpha\epsilon_{V1}^{*\mu}\epsilon_{V2}^{*\nu}\tilde{q}^\beta, \tag{8}$$

where ϵ_X is the polarization vector of the boson X with spin one, $q = q_{V1} + q_{V2}$ and $\tilde{q} = q_{V1} - q_{V2}$ [28,29]. Here the $b_1^{VV} \neq 0$ coupling corresponds to a vector particle, while the

$b_2^{VV} \neq 0$ coupling corresponds to a pseudovector. The $Z\gamma$ interactions of the spin-one particle are not considered, while the $\gamma\gamma$ and gg interactions are forbidden by the Landau-Yang theorem [67,68], where the gg case is justified by the assumption that the state X is color-neutral. Here, and throughout this paper, a boson with an exotic spin is denoted as X to distinguish it from a spin-zero Higgs boson H.

Similarly, the lowest order terms in the scattering amplitudes can be mapped to the corresponding terms in the effective Lagrangian

$$\begin{aligned} L(X_{J=1}VV) \sim & \, b_1 \partial_\mu X_\nu Z^\mu Z^\nu + b_2 \epsilon_{\alpha\mu\nu\beta} X^\alpha Z^\mu \partial^\beta Z^\nu \\ & + b_1^{WW} \partial_\mu X_\nu (W^{+\mu} W^{-\nu} + W^{-\mu} W^{+\nu}) \\ & + b_2^{WW} \epsilon_{\alpha\mu\nu\beta} X^\alpha (W^{-\mu} \partial^\beta W^{+\nu} + W^{+\mu} \partial^\beta W^{-\nu}). \end{aligned} \quad (9)$$

Despite the fact that the experimental observation [1–3] of the $H \to \gamma\gamma$ decay channel prevents the observed boson from being a spin-one particle, it is still important to experimentally study the spin-one models in the decay to massive vector bosons in the case that the observed state is a different one. The CMS and ATLAS experiments have already tested the compatibility of the observed boson with the $J^P = 1^+$ and 1^- hypotheses [12,22], where CMS has tested this using both production-independent and production-dependent methods. The compatibility of the data with the hypothesis of the boson being a mixture of the 1^+ and 1^- states is now tested, allowing for the presence of each of the terms in the scattering amplitude in Eq. (8). A continuous parameter that uniquely describes the presence of the corresponding terms b_1^{VV} and b_2^{VV} is defined as an effective fractional cross section

$$f_{b2}^{VV} = \frac{|b_2^{VV}|^2 \sigma_{b2}}{|b_1^{VV}|^2 \sigma_{b1} + |b_2^{VV}|^2 \sigma_{b2}}, \quad (10)$$

where σ_{bi} is the cross section of the process corresponding to $b_i^{VV} = 1, b_{j\neq i}^{VV} = 0$ in the $X \to ZZ \to 2e2\mu$ or $WW \to \ell\nu\ell\nu$ final state and $\sigma_{b1} = \sigma_{b2}$. This effective fraction is used in the analysis to test if the data favor the SM Higgs boson scalar hypothesis or some particular mixture of the vector and pseudovector states.

C. Decay of a spin-two resonance

In the case of a general spin-two resonance, its decay to a pair of massive vector bosons, ZZ or WW, is considered in their sequential decay to four leptons, but not with $Z\gamma^*$ and $\gamma^*\gamma^*$, as those are generally suppressed by the $\gamma^* \to \ell^+\ell^-$ selection. The decay to two on-shell photons $X \to \gamma\gamma$ is also considered. The corresponding XVV amplitude is used to describe the $X \to ZZ$ and WW, as well as $gg \to X$, processes

$$\begin{aligned} A(X_{J=2}VV) \sim \Lambda^{-1} \Bigg[& 2c_1^{VV} t_{\mu\nu} f^{*1,\mu\alpha} f^{*2,\nu}{}_{\alpha} + 2c_2^{VV} t_{\mu\nu} \frac{q_\alpha q_\beta}{\Lambda^2} f^{*1,\mu\alpha} f^{*2,\nu\beta} \\ & + c_3^{VV} t_{\beta\nu} \frac{\tilde{q}^\beta \tilde{q}^\alpha}{\Lambda^2} (f^{*1,\mu\nu} f^{*2}_{\mu\alpha} + f^{*2,\mu\nu} f^{*1}_{\mu\alpha}) + c_4^{VV} t_{\mu\nu} \frac{\tilde{q}^\nu \tilde{q}^\mu}{\Lambda^2} f^{*1,\alpha\beta} f^{*2}_{\alpha\beta} \\ & + m_V^2 \left(2c_5^{VV} t_{\mu\nu} \epsilon_{V1}^{*\mu} \epsilon_{V2}^{*\nu} + 2c_6^{VV} t_{\mu\nu} \frac{\tilde{q}^\mu q_\alpha}{\Lambda^2} (\epsilon_{V1}^{*\nu} \epsilon_{V2}^{*\alpha} - \epsilon_{V1}^{*\alpha} \epsilon_{V2}^{*\nu}) + c_7^{VV} t_{\mu\nu} \frac{\tilde{q}^\mu \tilde{q}^\nu}{\Lambda^2} \epsilon_{V1}^* \epsilon_{V2}^* \right) + c_8^{VV} t_{\mu\nu} \frac{\tilde{q}^\mu \tilde{q}^\nu}{\Lambda^2} f^{*1,\alpha\beta} \tilde{f}^{*2}_{\alpha\beta} \\ & + m_V^2 \left(c_9^{VV} t^{\mu\alpha} \frac{\tilde{q}_\alpha \epsilon_{\mu\nu\rho\sigma} \epsilon_{V1}^{*\nu} \epsilon_{V2}^{*\rho} q^\sigma}{\Lambda^2} + c_{10}^{VV} t^{\mu\alpha} \frac{\tilde{q}_\alpha \epsilon_{\mu\nu\rho\sigma} q^\rho \tilde{q}^\sigma (\epsilon_{V1}^{*\nu} (q\epsilon_{V2}^*) + \epsilon_{V2}^{*\nu} (q\epsilon_{V1}^*))}{\Lambda^4} \right) \Bigg], \end{aligned} \quad (11)$$

where $t^{\mu\nu}$ is the wave function of a spin-two particle X given by a symmetric traceless tensor, m_V is the mass of the considered gauge boson, and Λ is the scale of BSM physics [28,29]. The couplings c_1^{VV} and c_5^{VV} correspond to the parity-conserving interaction of a spin-two tensor with minimal gravitylike couplings. As in the spin-zero case, the couplings c_i^{VV} are, in general, momentum-dependent form factors. In this analysis it is assumed that the form factors are momentum-independent constants and, thus, only the lowest q_i^2 order terms in the scattering amplitude are considered.

The terms in Eq. (11) can be mapped to the corresponding terms (operators up to dimension seven) in the effective Lagrangian

$$\begin{aligned} L(X_{J=2}ZZ) \sim \Lambda^{-1} \Bigg(& -c_1 X_{\mu\nu} Z^{\mu\alpha} Z^\nu{}_\alpha + \frac{c_2}{\Lambda^2} (\partial_\alpha \partial_\beta X_{\mu\nu}) Z^{\mu\alpha} Z^{\nu\beta} + \frac{c_3}{\Lambda^2} X_{\beta\nu} [\partial^\alpha, [\partial^\beta, Z^{\mu\nu}]] Z_{\mu\alpha} + \frac{c_4}{2\Lambda^2} X_{\mu\nu} [\partial^\mu, [\partial^\nu, Z^{\alpha\beta}]] Z_{\alpha\beta} \\ & + c_5 m_Z^2 X_{\mu\nu} Z^\mu Z^\nu + \frac{2c_6 m_Z^2}{\Lambda^2} \partial_\alpha X_{\mu\nu} [\partial^\mu, Z^\nu] Z^\alpha - \frac{c_7 m_Z^2}{2\Lambda^2} X_{\mu\nu} [\partial^\mu, [\partial^\nu, Z_\alpha]] Z^\alpha + \frac{c_8}{2\Lambda^2} X_{\mu\nu} [\partial^\mu, [\partial^\nu, Z^{\alpha\beta}]] \tilde{Z}_{\alpha\beta} \\ & - \frac{c_9 m_Z^2}{\Lambda^2} \epsilon_{\mu\nu\rho\sigma} \partial^\sigma X^{\mu\alpha} Z_\nu \partial_\alpha Z^\rho + \frac{c_{10} m_Z^2}{\Lambda^4} \epsilon_{\mu\nu\rho\sigma} \partial^\rho \partial^\beta X^{\mu\alpha} [\partial^\sigma, [\partial_\alpha, Z^\nu]] Z_\beta \Bigg). \end{aligned} \quad (12)$$

TABLE II. List of spin-two models with the production and decay couplings of an exotic X particle. The subscripts m (minimal couplings), h (couplings with higher-dimension operators), and b (bulk) distinguish different scenarios.

J^P Model	$gg \to X$ Couplings	$q\bar{q} \to X$ Couplings	$X \to VV$ Couplings
2_m^+	$c_1^{gg} \neq 0$	$\rho_1 \neq 0$	$c_1^{VV} = c_5^{VV} \neq 0$
2_{h2}^+	$c_2^{gg} \neq 0$	$\rho_1 \neq 0$	$c_2^{VV} \neq 0$
2_{h3}^+	$c_3^{gg} \neq 0$	$\rho_1 \neq 0$	$c_3^{VV} \neq 0$
2_h^+	$c_4^{gg} \neq 0$	$\rho_1 \neq 0$	$c_4^{VV} \neq 0$
2_b^+	$c_1^{gg} \neq 0$	$\rho_1 \neq 0$	$c_1^{VV} \ll c_5^{VV} \neq 0$
2_{h6}^+	$c_1^{gg} \neq 0$	$\rho_1 \neq 0$	$c_6^{VV} \neq 0$
2_{h7}^+	$c_1^{gg} \neq 0$	$\rho_1 \neq 0$	$c_7^{VV} \neq 0$
2_h^-	$c_8^{gg} \neq 0$	$\rho_2 \neq 0$	$c_8^{VV} \neq 0$
2_{h9}^-	$c_8^{gg} \neq 0$	$\rho_2 \neq 0$	$c_9^{VV} \neq 0$
2_{h10}^-	$c_8^{gg} \neq 0$	$\rho_2 \neq 0$	$c_{10}^{VV} \neq 0$

The study of a subset of these ten terms in $X \to ZZ$, WW, and $\gamma\gamma$ decays and $gg \to X$ production has already been performed by the CMS and ATLAS experiments [11,12,14,15,22]. In this analysis the study of spin-two hypotheses is completed by considering the remaining terms in the spin-two VV scattering amplitude in Eq. (11) and different production scenarios. Ten spin-two scenarios are listed in Table II. Both $q\bar{q}$ production, discussed in Sec. II D, and gluon fusion, described by Eq. (11), of a spin-two state are considered. In the $X \to \gamma\gamma$ decay channel, the full list of models is not analyzed.

The spin-two model with minimal couplings, which is common to $X \to ZZ$, WW, and $\gamma\gamma$, represents a massive gravitonlike boson as suggested in models with warped extra dimensions (ED) [69,70]. The individual results for the 2_m^+ model were presented for the $X \to ZZ$, WW, and $\gamma\gamma$ decays earlier [12,14,15]. A combination is reported here.

A modified minimal coupling model 2_b^+ is also considered, where the SM fields are allowed to propagate in the bulk of the ED [71], corresponding to $c_1^{VV} \ll c_5^{VV}$ in the XZZ or XWW couplings only. Moreover, eight spin-two models with higher-dimension operators are considered for the XZZ and XWW couplings. The above list of ten spin-two decay models and several production mechanisms does not exhaust all the possible scenarios with mixed amplitudes, but it does provide a comprehensive sample of spin-two alternatives to test the validity of the SM-like $J^P = 0^+$ hypothesis.

D. Production of a resonance

While the above discussion of Eqs. (1), (8), and (11) is focused on the decay $H \to VV$, these amplitudes also describe production of a resonance via gluon fusion, weak vector boson fusion (VBF) with associated jets, or associated production with a weak vector boson VH. All these mechanisms, along with the $t\bar{t}H$ production, are considered in the analysis of the spin-zero hypothesis of the H boson, where the gluon fusion production dominates. It is possible to study HVV interactions using the kinematics of particles produced in association with the Higgs boson, such as VBF jets or vector boson daughters in VH production. While the q_V^2 range in the $H \to VV$ process does not exceed approximately 100 GeV due to the kinematic bound, in the associated production no such bound exists, and therefore consideration of more restricted ranges of q_V^2 might be required [31], bringing an additional uncertainty to such a study. Instead, the analysis presented here is designed to minimize the dependence on the production mechanism focusing on the study of the $H \to VV$ decay kinematics. In the case of a spin-zero particle, there is no spin correlation between the production process and decay, which allows for production-independent studies. In the case of a nonzero spin particle, it is possible to study decay information only without dependence on the polarization of the resonance, and therefore without dependence on the production mechanism.

The production of a on-shell Higgs boson is considered in this analysis. In gluon fusion, about 10% of $H \to ZZ$ and $H \to WW$ events are produced off-shell, with a Higgs boson invariant mass above 150 GeV [72]. A similar effect appears in VBF production [13], while it is further suppressed for other production mechanisms. However, this off-shell contribution depends on the width of the Higgs boson [73]. A relative enhancement of the off-shell with respect to the on-shell production is expected in models with anomalous HVV couplings [13,57]. Therefore, it is possible to study anomalous HVV interactions using the kinematics of the Higgs boson produced off-shell, including relative off-shell enhancement. However, such a study requires additional assumptions about the width of the Higgs boson, its production mechanisms, and the extrapolation of the coupling constants in Eqs. (1), (8), and (11) to q_H^2 values significantly larger than 100 GeV. Therefore, the study of anomalous HVV couplings with the off-shell Higgs boson is left for a future work. Instead, the $H \to ZZ$ events with an invariant ZZ mass above 140 GeV are not considered, effectively removing off-shell effects and associated model dependence. In the $H \to WW$ analysis, the event selection discussed below reduces the off-shell contribution to less than 2%. Even though this contribution may increase with anomalous HVV couplings, no such enhancement has been observed in the $H \to ZZ$ study [13], which limits it to be less than 5 times the SM expectation at a 95% C.L. This constraint is expected to be further improved with more data and additional final states studied. In the present analysis, any off-shell contribution in the study of the on-shell production and $H \to WW$ decay is neglected.

Since the production of a color-neutral spin-one resonance is forbidden in gluon fusion, its dominant production mechanism is expected to be quark-antiquark annihilation.

The production mechanisms of a spin-two boson are expected to be gluon fusion and quark-antiquark annihilation, as, for example, in the ED models in Refs. [69–71]. While gluon fusion is expected to dominate over the $q\bar{q}$ production of a spin-two state, the latter is a possibility in the effective scattering amplitude with form factors. Therefore, the $q\bar{q} \to X$ production of both spin-one and spin-two resonances and the $gg \to X$ production of a spin-two resonance are considered. The fractional contribution of the $q\bar{q}$ process to the production of a spin-two resonance is denoted as $f(q\bar{q})$ and can be interpreted as the fraction of events produced with $J_z = \pm 1$. For both spin-one and spin-two states, the analysis of the $X \to ZZ \to 4\ell$ decay mode is also performed without dependence on the production mechanism, allowing coverage of other mechanisms including associated production.

For the analysis of the $q\bar{q} \to X$ production, the general scattering amplitudes are considered for the interaction of the spin-one and spin-two bosons with fermions,

$$‘A(X_{J=1}f\bar{f}) = \epsilon_X^{\mu}\bar{u}_2(\gamma_\mu(\rho_1 + \rho_2\gamma_5) + \frac{m_f\tilde{q}_\mu}{\Lambda^2}(\rho_3 + \rho_4\gamma_5))u_1, \quad (13)$$

$$A(X_{J=2}f\bar{f}) = \frac{1}{\Lambda}t^{\mu\nu}\bar{u}_2(\gamma_\mu\tilde{q}_\nu(\rho_1 + \rho_2\gamma_5) + \frac{m_f\tilde{q}_\mu\tilde{q}_\nu}{\Lambda^2}(\rho_3 + \rho_4\gamma_5))u_1, \quad (14)$$

where m_f is the fermion mass, u_i is the Dirac spinor, and Λ is the scale of BSM physics [28,29]. The couplings ρ_i are assumed to be the same for all quark flavors. This assumption, along with the choice of ρ_i couplings in general, has little effect on the analysis since this affects only the expected longitudinal boost of the resonance from different mixtures of parton production processes without affecting its polarization, whose projection on the parton collision axis is always $J_z = \pm 1$, since the ρ_3 and ρ_4 terms are suppressed in the annihilation of light quarks. Therefore, $q\bar{q}$ production leads to a resonance with polarization $J_z = \pm 1$ along the parton collision axis, while gluon fusion leads to $J_z = 0$ or ± 2. In the case of minimal c_1^{gg} coupling, only $J_z = \pm 2$ is possible. The terms proportional to m_V^2 in Eq. (11) are absent for couplings to massless vector bosons, either $gg \to X$ in production or $X \to \gamma\gamma$ in decay. Therefore, the list of models in Table II covers ten decay couplings to massive vector bosons but only five couplings for the massless gluons.

The presence of an additional resonance can be inferred from the kinematics of the decay products when separation in invariant mass alone is not sufficient. For example, composite particles can have multiple narrow states with different spin-parity quantum numbers and nearly degenerate masses. Some examples of this phenomenon include ortho/para-positronia, χ_b and χ_c particles where the mass splitting between the different J^P states is orders of magnitude smaller than their mass [74–76].

In an approach common to both the spin-one and spin-two scenarios, the production of a second resonance with different J^P quantum numbers but close in mass to the SM Higgs-like state can be probed. The two states are assumed to be sufficiently separated in mass or produced by different mechanisms, so that they do not interfere, but still closer than the experimental mass resolution

$$\Gamma_{J^P} \quad \text{and} \quad \Gamma_{0^+} \ll |m_{J^P} - m_{0^+}| \ll \delta_m \sim 1\ \text{GeV}. \quad (15)$$

The fractional cross section $f(J^P)$ is defined as follows:

$$f(J^P) = \frac{\sigma_{J^P}}{\sigma_{0^+} + \sigma_{J^P}}, \quad (16)$$

where σ_{J^P} (σ_{0^+}) is the cross section of the process corresponding to the J^P (0^+) model defined at the LHC energy of 8 TeV and, in the case of the ZZ channel, for the $X \to ZZ \to 2e2\mu$ decay mode. In this case the notation J^P refers to a model name and, in practice, should reflect all relevant model properties, including spin, parity, production, and decay modes. It should be noted that the effective fractions f_{ai} and $f(J^P)$ have a distinct nature. The fractions f_{ai} denote the effective fractions related to the corresponding a_i terms within the scattering amplitude of a given state, and are used in measurements that consider interference effects between different parts of the amplitude.

III. THE CMS DETECTOR, SIMULATION, AND RECONSTRUCTION

The central feature of the CMS apparatus is a superconducting solenoid of 6 m internal diameter, providing a magnetic field of 3.8 T. Within the superconducting solenoid volume are a silicon pixel and strip tracker, a lead tungstate crystal electromagnetic calorimeter (ECAL), and a brass/scintillator hadron calorimeter, each composed of a barrel and two endcap sections. Muons are measured in gas-ionization detectors embedded in the steel flux-return yoke outside the solenoid. Extensive forward calorimetry complements the coverage provided by the barrel and endcap detectors. A more detailed description of the CMS detector, together with a definition of the coordinate system used and the relevant kinematic variables, can be found in Ref. [77].

The data samples used in this analysis are the same as those described in Refs. [12–15], corresponding to an integrated luminosity of 5.1, (4.9) fb^{-1} collected in 2011 at a center-of-mass energy of 7 TeV and 19.7 (19.4) fb^{-1} in 2012 at 8 TeV in the case of the $H \to VV \to 4\ell$ and $H \to \gamma\gamma$ ($H \to WW \to \ell\nu\ell\nu$) channels. The integrated luminosity is measured using data from the CMS hadron forward calorimeter system and the pixel detector [78,79]. The uncertainties in the integrated luminosity measurement are 2.2% and 2.6% in the 2011 and 2012 data sets, respectively.

A. Monte Carlo simulation

The simulation of the signal process is essential for the study of anomalous couplings in HVV interactions, and all the relevant Monte Carlo (MC) samples are generated following the description in Sec. II. A dedicated simulation program, JHUGen 4.8.1 [28,29,31], is used to describe anomalous couplings in the production and decay to two vector bosons of spin-zero, spin-one, and spin-two resonances in hadron-hadron collisions, including all the models listed in Tables I and II. For the spin-zero and spin-one studies, interference effects are included by generating mixed samples produced with either of the different tensor structures shown in Eqs. (1) and (8).

For gluon fusion production of a spin-zero state, the kinematics of the Higgs boson decay products and of an associated jet are not affected by the anomalous Hgg interactions, and therefore the next-to-leading-order (NLO) QCD effects are introduced in production with the SM couplings through the POWHEG [80–82] event generator. It is also found that the NLO QCD effects that are relevant for the analysis of a spin-zero state are well approximated with the combination of leading-order (LO) QCD matrix elements and parton showering [31]. Therefore, JHUGen at LO QCD is adopted for the simulation of anomalous interactions in all the other production processes where it is important to model the correlations between production and the kinematics of the final-state particles, such as in VBF and VH production of a spin-zero state, $q\bar{q} \to X$ production of a spin-one state, and $q\bar{q}$ and $gg \to X$ production of a spin-two state. In the case of a spin-two X boson, the LO QCD modeling of production avoids a potentially problematic p_{T} spectrum of the X boson appearing at NLO with nonuniversal $Xq\bar{q}$ and Xgg couplings [54] allowed in this study. In all cases, the decays $H/X \to ZZ/Z\gamma^*/\gamma^*\gamma^* \to 4\ell$, $H/X \to WW \to \ell\nu\ell\nu$, and $H/X \to \gamma\gamma$ are simulated with JHUGen, including all spin correlations in the production and decay processes and interference effects between all contributing amplitudes.

To increase the number of events in the simulated samples for each hypothesis studied, the MELA package [2,28,29,31] is adopted to apply weights to events in any $H \to VV \to 4\ell$ or $H \to WW \to \ell\nu\ell\nu$ spin-zero sample to model any other spin-zero sample. The same reweighting technique has also been used in the study of the $q\bar{q}$ and $gg \to ZZ/Z\gamma^*$ backgrounds.

All MC samples are interfaced with PYTHIA 6.4.24 [83] for parton showering and further processing through a dedicated simulation of the CMS detector based on Geant4 [84]. The simulation includes overlapping pp interactions (pileup) matching the distribution of the number of interactions per LHC beam crossing observed in data.

Most of the background event simulation is unchanged since Refs. [12–15]. In the $H \to VV \to 4\ell$ analysis, the $q\bar{q} \to ZZ/Z\gamma^*$ process is simulated with POWHEG. The $gg \to ZZ/Z\gamma^*$ process is simulated with both GG2ZZ 3.1.5 [85] and MCFM 6.7 [86–88], where the Higgs boson production K-factor is applied to the LO cross section [13]. In the $H \to WW \to \ell\nu\ell\nu$ analysis, the WZ, ZZ, VVV, Drell-Yan (DY) production of Z/γ^*, $W+$jets, $W\gamma^*$, and $q\bar{q} \to WW$ processes are generated using the MadGraph 5.1 event generator [89], the $gg \to WW$ process using the GG2WW 3.1 generator [90], and the $t\bar{t}$ and tW processes are generated with POWHEG. The electroweak production of the nonresonant $WW+2$jets process, which is not part of the inclusive $WW+$jets sample, has been generated using the PHANTOM 1.1 event generator [91] including terms of order (α_{EM}^6). The TAUOLA package [92] is used in the simulation of τ-lepton decays to account for τ-polarization effects.

B. Event reconstruction

The analysis uses the same event reconstruction and selection as in the previous measurements of the properties of the Higgs boson in the $H \to VV \to 4\ell$ [12,13], $H \to WW \to \ell\nu\ell\nu$ [14], and $H \to \gamma\gamma$ [15] channels. The data from the CMS detector and the simulated samples are reconstructed using the same algorithms.

For the $H \to VV \to 4\ell$ and $H \to WW \to \ell\nu\ell\nu$ analyses described in this paper, events are triggered by requiring the presence of two leptons, electrons or muons, with asymmetric requirements on their transverse momenta, p_{T}. Several single-lepton triggers with relatively tight lepton identification are used for the $H \to WW$ analysis. A triple-electron trigger is also used for the $H \to VV \to 4\ell$ analysis. For the $H \to \gamma\gamma$ analysis, the events are selected by diphoton triggers with asymmetric transverse energy thresholds and complementary photon selections. The particle-flow (PF) algorithm [93,94] is used to reconstruct the observable particles in the event. The PF event reconstruction consists of reconstructing and identifying each single particle with an optimized combination of all subdetector information.

The $H \to VV \to 4\ell$ and $H \to WW \to \ell\nu\ell\nu$ analyses require four and two lepton candidates (electrons or muons), respectively, originating from a vertex with the largest $\sum p_T^2$ of all tracks associated with it. Electron candidates are defined by a reconstructed charged-particle track in the tracking detector pointing to an energy deposition in the ECAL. The electron energy is measured primarily from the ECAL cluster energy. Muon candidates are identified by signals of charged-particle tracks in the muon system that are compatible with a track reconstructed in the central tracking system. Electrons and muons are required to be isolated. Electrons are reconstructed within the geometrical acceptance, $|\eta| < 2.5$, and for $p_{\mathrm{T}} > 7$ GeV.

TABLE III. Number of background and signal events expected in the SM, and number of observed candidates, for the $H \to VV \to 4\ell$ analysis after the final selection in the mass region $105.6 < m_{4\ell} < 140.6$ GeV. The signal and ZZ background are estimated from MC simulation, while the $Z + X$ background is estimated from data. Only systematic uncertainties are quoted.

	$4e$		4μ		$2e2\mu$	
Channel Energy	7 TeV	8 TeV	7 TeV	8 TeV	7 TeV	8 TeV
$q\bar{q} \to ZZ$	0.84 ± 0.10	2.94 ± 0.33	1.80 ± 0.11	7.65 ± 0.49	2.24 ± 0.28	8.86 ± 0.68
$gg \to ZZ$	0.03 ± 0.01	0.20 ± 0.05	0.06 ± 0.02	0.41 ± 0.10	0.07 ± 0.02	0.50 ± 0.13
$Z + X$	0.62 ± 0.14	2.77 ± 0.62	0.22 ± 0.09	1.19 ± 0.48	1.06 ± 0.29	4.29 ± 1.10
Background	1.49 ± 0.17	5.91 ± 0.71	2.08 ± 0.14	9.25 ± 0.69	3.37 ± 0.40	13.65 ± 1.30
Signal	0.70 ± 0.11	3.09 ± 0.47	1.24 ± 0.14	5.95 ± 0.71	1.67 ± 0.26	7.68 ± 0.98
Observed	1	9	3	15	6	16

Muons are reconstructed within $|\eta| < 2.4$ and $p_T > 5$ GeV [95].

Photons, used in the $H \to \gamma\gamma$ analysis, are identified as ECAL energy clusters not linked to the extrapolation of any charged-particle trajectory to the ECAL. Jets, used in the $H \to WW$ analysis, are reconstructed from the PF candidates, clustered with the anti-k_t algorithm [96,97] with a size parameter of 0.5. The jet momentum is determined as the vector sum of all particle momenta in the jet. Identification of b-quark decays is used to reject backgrounds containing top quarks that subsequently decay to a b quark and a W boson in the $H \to WW$ analysis. The missing transverse energy vector $\vec{E}_T^{\text{miss}}$ is defined as the negative vector sum of the transverse momenta of all reconstructed particles (charged or neutral) in the event, with $E_T^{\text{miss}} = |\vec{E}_T^{\text{miss}}|$.

C. Four-lepton event selection

To study the $H \to VV \to 4\ell$ decay, events are selected with at least four identified and isolated electrons or muons. A $V \to \ell^+\ell^-$ candidate originating from a pair of leptons of the same flavor and opposite charge is required. The $\ell^+\ell^-$ pair with an invariant mass m_1 nearest to the nominal Z boson mass is retained and is denoted Z_1 if it is in the range $40 \leq m_1 \leq 120$ GeV. A second $\ell^+\ell^-$ pair, denoted Z_2, is required to have $12 \leq m_2 \leq 120$ GeV. If more than one Z_2 candidate satisfies all criteria, the pair of leptons with the highest scalar p_T sum is chosen. At least one lepton should have $p_T \geq 20$ GeV, another one $p_T \geq 10$ GeV, and any oppositely charged pair of leptons among the four selected must satisfy $m_{\ell\ell} \geq 4$ GeV. Events are restricted to a window around the observed 125.6 GeV resonance, $105.6 \leq m_{4\ell} \leq 140.6$ GeV.

After the selection, the dominant background for $H \to VV \to 4\ell$ originates from the $q\bar{q} \to ZZ/Z\gamma^*$ and $gg \to ZZ/Z\gamma^*$ processes and is evaluated from simulation, following Refs. [12,13]. The other backgrounds come from the production of Z and WZ bosons in association with jets, as well as $t\bar{t}$, with one or two jets misidentified as an electron or a muon. The $Z + X$ background is evaluated using a tight-to-loose misidentification rate method [12]. The number of estimated background and signal events, and the number of observed candidates after the final selection in data in the narrow mass region around 125.6 GeV, is given in Table III.

D. Two-lepton event selection

In the case of the $H \to WW \to \ell\nu\ell\nu$ analysis, events with exactly one electron and one muon are selected. The leptons must have opposite charge and pass the full identification and isolation criteria presented in detail in Ref. [14]. The highest-p_T (leading) lepton should have $p_T > 20$ GeV, and the second one $p_T > 10$ GeV. Events are classified according to the number of selected jets that satisfy $E_T > 30$ GeV and $|\eta| < 4.7$. Two categories of events with exactly zero and exactly one jet are selected, in which the signal is produced mostly by the gluon fusion process. The $e\mu$ pair is required to have an invariant mass above 12 GeV, and a p_T above 30 GeV. Events are also required to have *projected* E_T^{miss} above 20 GeV, as defined in Ref. [14].

The main background processes from nonresonant WW production and from top-quark production, including top-quark pair ($t\bar{t}$) and single-top-quark (mainly tW) processes, are estimated using data. Instrumental backgrounds arising from misidentified ("nonprompt") leptons in $W +$ jets production and mismeasurement of $\vec{E}_T^{\text{miss}}$ in $Z/\gamma^* +$ jets events are also estimated from data. The contributions from other subdominant diboson (WZ and ZZ) and triboson (VVV) production processes are estimated from simulation. The $W\gamma^*$ cross section is measured from data. The shapes of the discriminant variables used in the signal extraction for the $W\gamma$ process are also obtained from data. The $Z/\gamma^* \to \tau^+\tau^-$ background process is estimated using $Z/\gamma^* \to \mu^+\mu^-$ events selected in data where the muons are replaced with simulated τ-lepton decays. To suppress the background from top-quark production, events that are identified as coming from top decays are rejected based on soft-muon and b-jet identification. The number of estimated background and signal events and the number of observed candidates after the final selection are given in Table IV. After all selection criteria are applied, the

TABLE IV. Number of background and signal events expected in the SM, and number of observed candidates, for the $H \to WW$ analysis after final selection. The signal and background are estimated from MC simulation and from data control regions, as discussed in the text. Only systematic uncertainties are quoted.

	0-jet		1-jet	
Channel Energy	7 TeV	8 TeV	7 TeV	8 TeV
WW	861 ± 12	4185 ± 63	249.9 ± 4.0	1268 ± 21
$WZ + ZZ + Z/\gamma^*$	22.7 ± 1.2	178.3 ± 9.5	26.4 ± 1.4	193 ± 11
$t\bar{t} + tW$	91 ± 20	500 ± 96	226 ± 14	1443 ± 46
$W +$ jets	150 ± 39	620 ± 160	60 ± 16	283 ± 72
$W\gamma^{(*)}$	68 ± 20	282 ± 76	10.1 ± 2.8	55 ± 14
Background	1193 ± 50	5760 ± 210	573 ± 22	3242 ± 90
Signal $gg \to H$	50 ± 10	227 ± 46	17.1 ± 5.5	88 ± 28
Signal VBF $+ VH$	0.44 ± 0.03	10.27 ± 0.41	2.09 ± 0.12	19.83 ± 0.81
Observed	1207	5747	589	3281

contribution from other Higgs boson decay channels is negligible.

E. Two-photon event selection

In the $H \to \gamma\gamma$ analysis, the energy of photons used in the global event reconstruction is directly obtained from the ECAL measurement. The selection requires a loose calorimetric identification based on the shape of the electromagnetic shower and loose isolation requirements on the photon candidates. For the spin-parity studies, the "cut-based" analysis described in Ref. [15] is used. This analysis does not use multivariate techniques for selection or classification of events, which allows for a categorization better suited for the study of the Higgs boson decay kinematics. The cosine of the scattering angle in the Collins-Soper frame, $\cos\theta^*$, is used to discriminate between the spin hypotheses. The angle is defined in the diphoton rest frame as that between the collinear photons and the line that bisects the acute angle between the colliding protons. To increase the sensitivity, the events are categorized using the same four diphoton event classes used in the cut-based analysis but without the additional classification based on p_T used there. Within each diphoton class, the events are binned in $|\cos\theta^*|$ to discriminate between the different spin hypotheses. The events are thus split into 20 event classes, four (η, R_9) [15] diphoton classes with five $|\cos\theta^*|$ bins each, for both the 7 and 8 TeV data sets, giving a total of 40 event classes. In Table V, the number of estimated background and signal events and the number of observed candidates are given after the final selection in an $m_{\gamma\gamma}$ range centered at $m_H = 125$ GeV and corresponding to the full width at half maximum for the signal distribution for each of the four (η, R_9) categories. The total expected number of selected signal events, summed over all categories and integrated over the full signal distribution, is 421 (94) at 8 TeV (7 TeV).

IV. ANALYSIS TECHNIQUES

The kinematics of the Higgs boson decay to four charged leptons, two charged leptons and two neutrinos, or two photons, and their application to the study of the properties of the Higgs boson have been extensively studied in the literature [28–31,36,38,42,42,43,45–49,51,53]. The schematic view of the production and decay information can be seen in Fig. 1 [28,59].

If the resonance has a nonzero spin, its polarization depends on the production mechanism. As a result, a

TABLE V. Number of background and signal events expected in the SM, and number of observed candidates, for the $H \to \gamma\gamma$ analysis after final selection. The four categories are defined as follows [15]: low $|\eta|$ indicates that both photons are in the barrel with $|\eta| < 1.5$ and high $|\eta|$ otherwise; high R_9 indicates that both photons have $R_9 > 0.94$ and low R_9 otherwise. The $m_{\gamma\gamma}$ range (GeV) centered at $m_H = 125$ GeV corresponds to the full width at half maximum for the signal distribution in each category. Only systematic uncertainties are quoted, which include uncertainty from the background $m_{\gamma\gamma}$ parametrization in the background estimates.

	(low $\lvert\eta\rvert$, high R_9)		(low $\lvert\eta\rvert$, low R_9)		(high $\lvert\eta\rvert$, high R_9)		(high $\lvert\eta\rvert$, low R_9)	
Channel Energy	7 TeV	8 TeV	7 TeV	8 TeV	7 TeV	8 TeV	7 TeV	8 TeV
Range $m_{\gamma\gamma}$	2.44	2.30	3.34	2.94	4.72	4.58	5.48	5.57
Background	230.1 ± 2.5	875 ± 5	604 ± 4	2210 ± 8	456 ± 8	1685 ± 9	911 ± 6	2045 ± 11
Signal	18.6 ± 2.3	74 ± 9	23.5 ± 3.0	103 ± 13	9.3 ± 1.3	38 ± 5	12.0 ± 1.6	57 ± 8
Observed	263	11047	647	1963	459	1638	913	1988

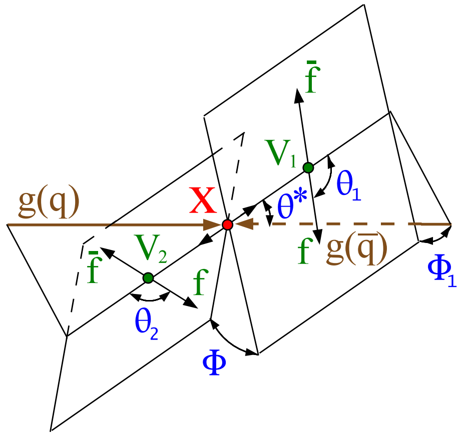

FIG. 1 (color online). Illustration of the production of a system X in a parton collision and its decay to two vector bosons gg or $q\bar{q} \to X \to ZZ, WW, Z\gamma$, and $\gamma\gamma$ either with or without sequential decay of each vector boson to a fermion-antifermion pair [28,59]. The two production angles θ^* and Φ_1 are shown in the X rest frame, and the three decay angles θ_1, θ_2, and Φ are shown in the V rest frames. Here X stands either for a Higgs boson, an exotic particle, or, in general, the genuine or misidentified VV system, including background.

nontrivial correlation of the kinematic distributions of production and sequential decay is observed for a resonance with nonzero spin, while there is no such direct correlation due to polarization for a spin-zero resonance. Furthermore, the kinematics and polarization of the vector bosons in the $H \to VV$ process depend on the initial polarization of the resonance and the tensor structure of the HVV interactions, and this affects the kinematics of the leptons in the $VV \to 4\ell$ or $\ell\nu\ell\nu$ decay.

The analysis of the HVV interactions requires the study of the kinematic distributions of the Higgs boson decay products compared to the prediction of the corresponding models. In the case of the $H \to VV \to 4\ell$ decay, the full kinematic information can be reconstructed with small experimental uncertainties. In the case of the $H \to WW \to \ell\nu\ell\nu$ decay, the two missing neutrinos lead to a loss of kinematic information, but in some cases the V-A nature of the $W \to \ell\nu$ coupling, compared to a different V-A coupling in the $Z \to \ell\ell$ decay, leads to more pronounced kinematic effects. In the following, the partial kinematic information used in the analysis of this decay mode is also introduced.

The spin-parity analysis of the $H \to \gamma\gamma$ decay is also possible, and this channel is studied in the context of the exotic spin-two hypothesis tested with respect to the SM hypothesis. However, only one angle θ^* out of the five identified in Fig. 1 is observable in this case. Its distribution is isotropic in the boson frame for any spin-zero model, and therefore such models cannot be distinguished in this way. Details of the reconstruction and analysis of the $\cos\theta^*$ distribution in the $H \to \gamma\gamma$ channel are discussed in Ref. [15].

The rest of this section is organized as follows. The kinematic observables reconstructed in the $H \to VV \to 4\ell$ and $H \to WW \to \ell\nu\ell\nu$ channels are discussed first. A matrix element likelihood approach is introduced next. Its goal is to reduce the number of observables to be manageable in the following analysis, while retaining full information for the measurements of interest. A maximum likelihood fit employs the template parametrization of the probability distribution of the kinematic observables using full simulation of the processes in the detector. This method is validated with the analytic parametrization of some of the multidimensional distributions using a simplified modeling of the detector response in the $H \to ZZ \to 4\ell$ channel. Systematic uncertainties and validation tests are also discussed.

A. Observables in the $H \to VV \to 4\ell$ analysis

The four-momenta of the $H \to 4\ell$ decay products carry eight independent degrees of freedom, which fully describe the kinematic configuration of a four-lepton system in its center-of-mass frame, except for an arbitrary rotation around the beam axis. These can be conveniently expressed in terms of the five angles $\vec{\Omega} \equiv (\theta^*, \Phi_1, \theta_1, \theta_2, \Phi)$ defined in Fig. 1, the invariant masses of the dilepton pairs, m_1 and m_2, and of the four-lepton system, $m_{4\ell}$. The boost of the H boson system in the laboratory frame, expressed as p_T and rapidity, depends on the production mechanism and generally carries some but limited discrimination power between either signal or background hypotheses originating from different production processes. These observables are not used in the analysis to remove the dependence of the results on the production model. For the same reason, information about particles produced in association with H bosons is not used either. This approach differs from the study reported in Ref. [12] where such observables were used to investigate the production mechanisms of the Higgs boson.

The distributions of the eight kinematic observables $(m_1, m_2, m_{4\ell}, \vec{\Omega})$ in data, as well as the expectations for the SM background, the Higgs boson signal, and some characteristic alternative spin-zero scenarios, are shown in Fig. 2. All distributions in Fig. 2, with the exception of the $m_{4\ell}$ distribution, are presented using events in the $m_{4\ell}$ range of 121.5–130.5 GeV to enhance the signal purity. The observables with their correlations are used in the analysis to establish the consistency of the spin and parity quantum numbers and tensor structure of interactions with respect to the SM predictions. These observables also permit a further discrimination of signal from background, increasing the signal sensitivity and reducing the statistical uncertainty in the measurements.

B. Observables in the $H \to WW \to \ell\nu\ell\nu$ analysis

Only partial reconstruction is possible in the $H \to WW \to \ell\nu\ell\nu$ decay. This channel features two isolated,

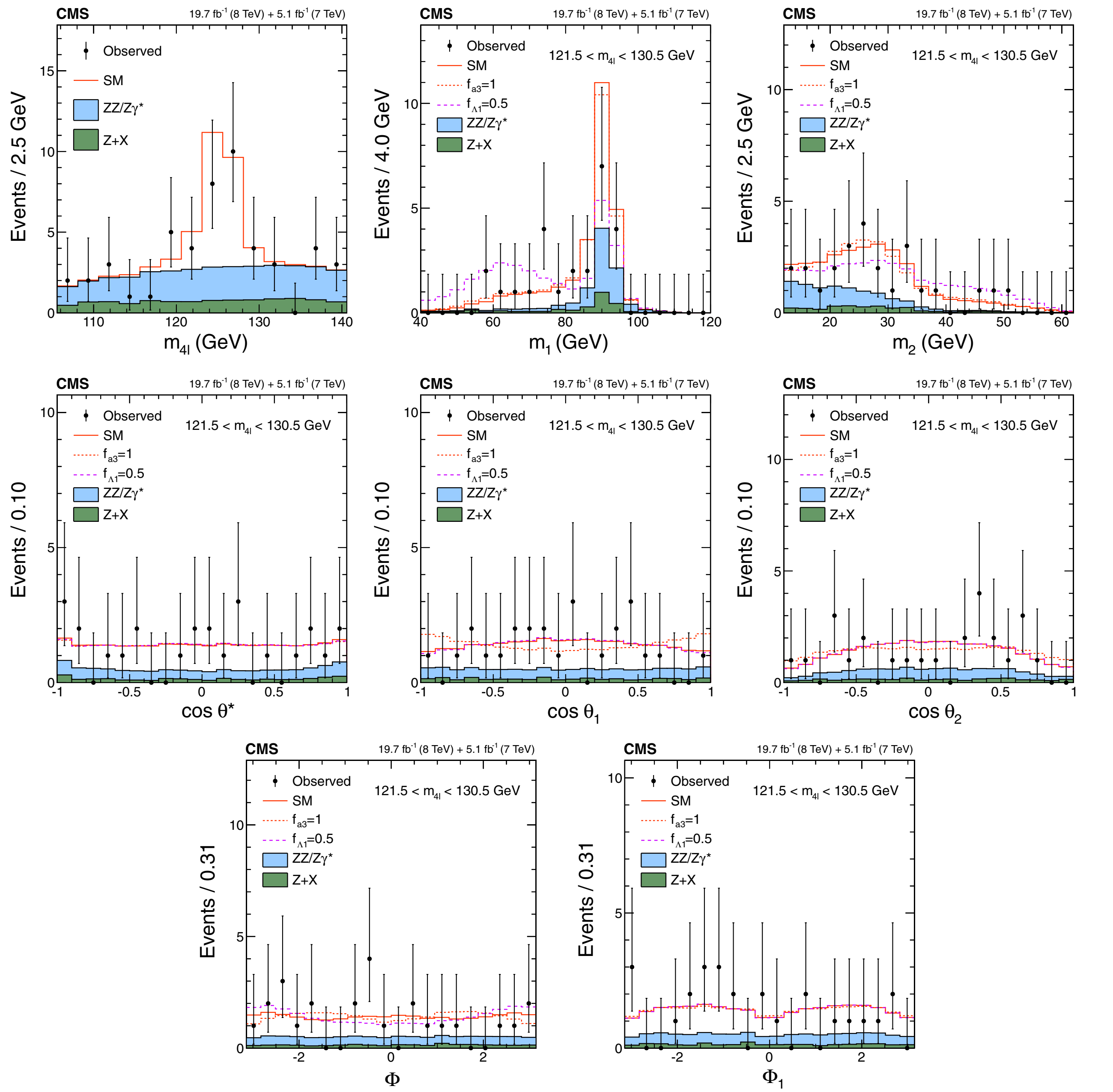

FIG. 2 (color online). Distributions of the eight kinematic observables used in the $H \to VV \to 4\ell$ analysis: $m_{4\ell}$, m_1, m_2, $\cos\theta^*$, $\cos\theta_1$, $\cos\theta_2$, Φ, and Φ_1. The observed data (points with error bars), the expectations for the SM background (shaded areas), the SM Higgs boson signal (open areas under the solid histogram), and the alternative spin-zero resonances (open areas under the dashed histograms) are shown, as indicated in the legend. The mass of the resonance is taken to be 125.6 GeV and the SM cross section is used. All distributions, with the exception of $m_{4\ell}$, are presented with the requirement $121.5 < m_{4\ell} < 130.5$ GeV.

high-p_T, charged leptons and E_T^{miss} due to the presence of neutrinos in the final state. The kinematic distributions of the decay products exhibit the characteristic properties of the parent boson. There are three main observables in this channel: the azimuthal opening angle between the two leptons ($\Delta\phi_{\ell\ell}$), which is correlated with the spin of the Higgs boson; the dilepton mass ($m_{\ell\ell}$), which is one of the most discriminating kinematic variables for a Higgs boson with low mass (it is also correlated to the spin and to $\Delta\phi_{\ell\ell}$); and the transverse mass (m_T) of the final state objects, which scales with the Higgs boson mass. The transverse mass is defined as $m_T^2 = 2p_T^{\ell\ell} E_T^{\text{miss}}(1 - \cos\Delta\phi(\ell\ell, \vec{E}_T^{\text{miss}}))$, where $p_T^{\ell\ell}$ is the dilepton transverse momentum and $\Delta\phi(\ell\ell, \vec{E}_T^{\text{miss}})$ is the azimuthal angle between the dilepton momentum and $\vec{E}_T^{\text{miss}}$.

Two observables are used in the final analysis, $m_{\ell\ell}$ and m_T. These two kinematic observables are independent quantities that effectively discriminate the signal against most of the backgrounds and between different signal models in the dilepton analysis in the 0-jet and 1-jet categories and have already been used in Ref. [14]. The signal region is defined by $m_{\ell\ell} < 200$ GeV and $60 \leq m_{\mathrm{T}} \leq 280$ GeV. The distributions of these observables for data, an expected SM Higgs signal, an alternative signal model with $f_{a3}^{WW} = -0.4$, and backgrounds are presented in Fig. 3.

C. Observables in the matrix element likelihood approach

A comprehensive analysis of the kinematics of the decay of a Higgs boson would include up to eight observables, as discussed above. In such an analysis, it is required to have a parametrization of the multidimensional distributions as a function of the parameters of interest. However, it becomes challenging to describe all the correlations of the observables and detector effects. It is possible to reduce the number of observables and keep the necessary information using the matrix element likelihood approach. In this approach, the kinematic information is stored in a discriminant designed for the separation of either background, the alternative signal components, or interference between those components. The parametrization of up to three observables can be performed with full simulation or data from the control regions. This approach is adopted in the $H \to VV \to 4\ell$ analysis. A similar approach is also possible in the $H \to WW \to \ell\nu\ell\nu$ channel, but the construction of the discriminants is more challenging because of the presence of unobserved neutrinos. Therefore, a simpler approach with the two observables defined above is used in this case.

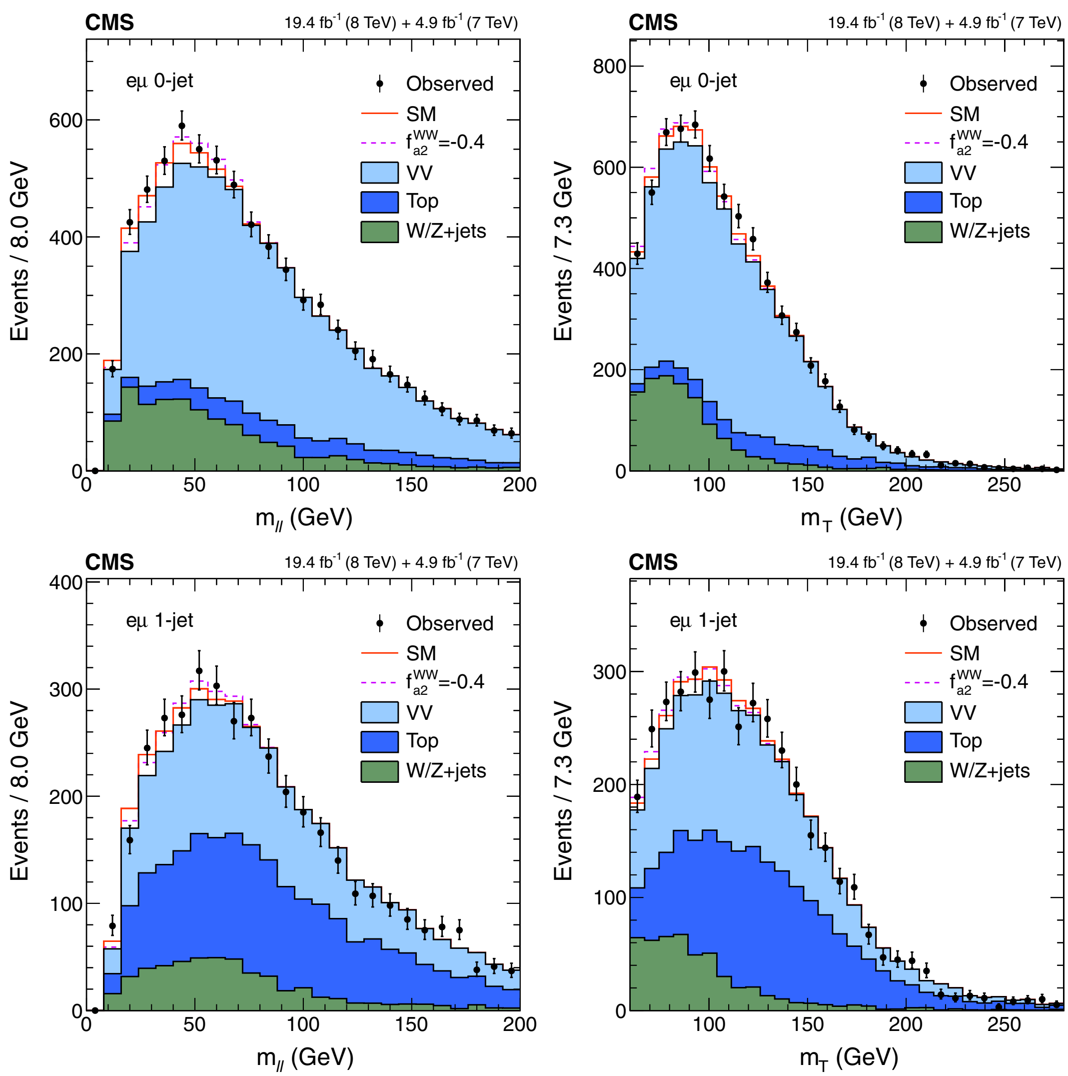

FIG. 3 (color online). Distributions of $m_{\ell\ell}$ (left) and m_{T} (right) for events with 0 jets (upper row) and 1 jet (lower row) in the $H \to WW \to \ell\nu\ell\nu$ analysis. The observed data (points with error bars), the expectations for the SM background (shaded areas), the SM Higgs boson signal (open areas under the solid histogram), and the alternative spin-zero resonance (open areas under the dashed histograms) are shown, as indicated in the legend. The mass of the resonance is taken to be 125.6 GeV and the SM cross section is used.

The use of kinematic discriminants in Higgs boson studies was introduced in previous CMS analyses [2,11–13] and feasibility studies [29,31], and here it is extended both to a number of new models and to new techniques. The construction of the kinematic discriminants follows the matrix element likelihood approach, where the probabilities for an event are calculated using the LO matrix elements as a function of angular and mass observables. In this way, the kinematic information, which fully characterizes the 4ℓ event topology of a certain process in its center-of-mass frame, is condensed to a reduced number of observables.

The kinematic discriminants used in this study are computed using the MELA package [2,28,29,31], which provides the full set of processes studied in this paper and uses JHUGEN matrix elements for the signal, gg or $q\bar{q} \to X \to ZZ/Z\gamma^*/\gamma^*\gamma^* \to 4\ell$, and MCFM matrix elements for the background, gg or $q\bar{q} \to ZZ/Z\gamma^*/\gamma^*\gamma^*/Z \to 4\ell$. This library of processes is also consistent with the MC simulation used, as discussed in Sec. III, and also includes other production and decay mechanisms. Within the MELA framework, an analytic parametrization of the matrix elements for signal [28,29] and background [30] was adopted in the previous CMS analyses, reported in Refs. [2,3,11]. The above matrix element calculations are validated against each other and tested with the MEKD package [98], which is based on MADGRAPH and FEYNRULES [99], for a subset of processes implemented in common. The analytic parametrizations of the spin-zero signal and $q\bar{q} \to ZZ/Z\gamma^* \to 4\ell$ background processes are available from an independent implementation [30,33,56] and are used in a multidimensional distribution parametrization without the calculation of discriminants.

Given several signal hypotheses defined for gg or $q\bar{q} \to X \to ZZ/Z\gamma^*/\gamma^*\gamma^* \to 4\ell$, and the main background hypotheses gg or $q\bar{q} \to ZZ/Z\gamma^*/\gamma^*\gamma^*/Z \to 4\ell$, the effective probabilities are defined for each event using a set of kinematic observables $(m_1, m_2, m_{4\ell}, \vec{\Omega})$

$$\begin{aligned}
\mathcal{P}_{\rm SM} &= \mathcal{P}^{\rm kin}_{\rm SM}(m_1, m_2, \vec{\Omega}|m_{4\ell}) \times \mathcal{P}^{\rm mass}_{\rm sig}(m_{4\ell}|m_H),\\
\mathcal{P}_{J^P} &= \mathcal{P}^{\rm kin}_{J^P}(m_1, m_2, \vec{\Omega}|m_{4\ell}) \times \mathcal{P}^{\rm mass}_{\rm sig}(m_{4\ell}|m_H),\\
\mathcal{P}^{\rm int}_{J^P} &= (\mathcal{P}^{\rm kin}_{\rm SM+J^P}(m_1, m_2, \vec{\Omega}|m_{4\ell}) - \mathcal{P}^{\rm kin}_{J^P}(m_1, m_2, \vec{\Omega}|m_{4\ell})\\
&\quad - \mathcal{P}^{\rm kin}_{\rm SM}(m_1, m_2, \vec{\Omega}|m_{4\ell})),\\
\mathcal{P}^{\rm int\perp}_{J^P} &= (\mathcal{P}^{\rm kin}_{\rm SM+J^P\perp}(m_1, m_2, \vec{\Omega}|m_{4\ell}) - \mathcal{P}^{\rm kin}_{J^P}(m_1, m_2, \vec{\Omega}|m_{4\ell})\\
&\quad - \mathcal{P}^{\rm kin}_{\rm SM}(m_1, m_2, \vec{\Omega}|m_{4\ell})),\\
\mathcal{P}_{q\bar{q}ZZ} &= \mathcal{P}^{\rm kin}_{q\bar{q}ZZ}(m_1, m_2, \vec{\Omega}|m_{4\ell}) \times \mathcal{P}^{\rm mass}_{q\bar{q}ZZ}(m_{4\ell}),\\
\mathcal{P}_{ggZZ} &= \mathcal{P}^{\rm kin}_{ggZZ}(m_1, m_2, \vec{\Omega}|m_{4\ell}) \times \mathcal{P}^{\rm mass}_{ggZZ}(m_{4\ell}),
\end{aligned} \tag{17}$$

where $\mathcal{P}^{\rm kin}(m_1, m_2, \vec{\Omega}|m_H) = |A(m_1, m_2, \vec{\Omega}|m_H)|^2$ are the probabilities computed from the LO matrix elements and are generally not normalized. The variable $\mathcal{P}^{\rm mass}(m_{4\ell}|m_H)$ is the probability as a function of the four-lepton reconstructed mass and is calculated using the $m_{4\ell}$ parametrization described in Refs. [11,12] including the $m_H = 125.6$ GeV hypothesis for signal. The probabilities $\mathcal{P}^{\rm int}_{J^P}$ parametrize interference between contributions from the SM and anomalous couplings, where J^P refers to a spin-zero tensor structure of interest, and they are allowed to have both positive and negative values. In the calculation of the mixed amplitude used for $\mathcal{P}^{\rm kin}_{\rm SM+J^P}$, the same coupling strengths are used as in the individual probabilities $\mathcal{P}^{\rm kin}_{\rm SM}$ and $\mathcal{P}^{\rm kin}_{J^P}$, and these couplings are required to provide equal cross sections for the two individual processes. The quantity $\mathcal{P}^{\rm int\perp}_{J^P}$ is constructed in the same way as $\mathcal{P}^{\rm int}_{J^P}$ except that the phase of the J^P amplitude is changed by $\pi/2$. The matrix element calculations in Eq. (17) are also used for the reweighting of simulated samples, as discussed in Sec. III.

Several kinematic discriminants are constructed for the main signal and background processes from the set of probabilities described above,

$$\begin{aligned}
\mathcal{D}_{\rm bkg} &= \frac{\mathcal{P}_{\rm SM}}{\mathcal{P}_{\rm SM} + c \times \mathcal{P}_{q\bar{q}ZZ}} = \Bigg[1 + c(m_{4\ell})\\
&\quad \times \frac{\mathcal{P}^{\rm kin}_{q\bar{q}ZZ}(m_1, m_2, \vec{\Omega}|m_{4\ell}) \times \mathcal{P}^{\rm mass}_{q\bar{q}ZZ}(m_{4\ell})}{\mathcal{P}^{\rm kin}_{\rm SM}(m_1, m_2, \vec{\Omega}|m_{4\ell}) \times \mathcal{P}^{\rm mass}_{\rm sig}(m_{4\ell}|m_H)}\Bigg]^{-1},\\
\mathcal{D}_{J^P} &= \frac{\mathcal{P}_{\rm SM}}{\mathcal{P}_{\rm SM} + \mathcal{P}_{J^P}} = \left[1 + \frac{\mathcal{P}^{\rm kin}_{J^P}(m_1, m_2, \vec{\Omega}|m_{4\ell})}{\mathcal{P}^{\rm kin}_{\rm SM}(m_1, m_2, \vec{\Omega}|m_{4\ell})}\right]^{-1},\\
\mathcal{D}_{\rm int} &= \frac{\mathcal{P}^{\rm int}_{J^P}(m_1, m_2, \vec{\Omega}|m_{4\ell})}{\mathcal{P}^{\rm kin}_{\rm SM} + \mathcal{P}^{\rm kin}_{J^P}}.
\end{aligned} \tag{18}$$

Here, the coefficient $c(m_{4\ell})$ is tuned to adjust the relative normalization of the signal and background probabilities for a given value of $m_{4\ell}$. The observable $\mathcal{D}_{\rm bkg}$ is used to separate signal from $q\bar{q} \to ZZ$, $gg \to ZZ$, and $Z + X$ backgrounds, using the $m_{4\ell}$ probability in addition to $\mathcal{P}^{\rm kin}$. The discriminant $\mathcal{D}_{J^P}$ is created to separate the SM signal from an alternative J^P state. The discriminant $\mathcal{D}_{\rm int}$ is created to isolate interference between the SM and anomalous coupling contributions. Since the analysis is designed to probe small anomalous couplings, interference between different anomalous contributions is a negligible effect and dedicated discriminants for those contributions are not considered. The variable $\mathcal{D}_{\rm int}$ is denoted as $\mathcal{D}_{CP}$ for interference between the a_1 and a_3 contributions because it is sensitive to CP violation [31].

To remove the dependence of the spin-one and spin-two discriminants on the production model, the probability $\mathcal{P}^{\rm kin}$ is averaged over the two production angles $\cos\theta^*$ and Φ_1, defined in Fig. 1, or equivalently the signal matrix element squared is averaged over the polarization of the resonance [31]. The production-independent discriminants are defined as

$$\mathcal{D}_{\rm bkg}^{\rm dec}=\left[1+\frac{c(m_{4\ell})}{4\pi}\frac{\mathcal{P}_{q\bar{q}ZZ}^{\rm mass}(m_{4\ell})}{\mathcal{P}_{\rm SM}^{\rm kin}(m_1,m_2,\vec{\Omega}|m_{4\ell})\times\mathcal{P}_{\rm sig}^{\rm mass}(m_{4\ell}|m_H)}\times\int d\Phi_1 d\cos\theta^*\mathcal{P}_{q\bar{q}ZZ}^{\rm kin}(m_1,m_2,\vec{\Omega}|m_{4\ell})\right]^{-1},$$

$$\mathcal{D}_{J^P}^{\rm dec}=\left[1+\frac{\frac{1}{4\pi}\int d\Phi_1 d\cos\theta^*\mathcal{P}_{J^P}^{\rm kin}(m_1,m_2,\vec{\Omega}|m_{4\ell})}{\mathcal{P}_{\rm SM}^{\rm kin}(m_1,m_2,\vec{\Omega}|m_{4\ell})}\right]^{-1}. \quad (19)$$

The decay kinematics of a spin-zero resonance are already independent of the production mechanism, due to the lack of spin correlations for any spin-zero particle. The small differences in the distributions of the production-independent discriminants with the different production mechanisms are due to detector acceptance effects and are treated as systematic uncertainties.

A complete list of all the discriminants used in the analysis is presented in Table VI. Some examples of the distributions as expected from simulation and as observed in data can be seen in Fig. 4 for all the discriminants used in the study of the spin-zero HZZ couplings. A complete list of the measurements performed and observables used is discussed in Secs. V and VI.

D. Maximum likelihood fit with the template method

The goal of the analysis is to determine if a set of anomalous coupling parameters $\vec{\zeta}$, defined both for the production and decay of a resonance with either spin zero, one, or two, is consistent, for a given set of observables $\vec{x}$, with the data. The coupling parameters $\vec{\zeta}$ are discussed in detail in Sec. II. They are summarized in Eqs. (1), (3), (4) and Table I for spin-zero, in Eqs. (8) and (10) for spin-one, and in Eqs. (11), (14) and Table II for spin-two. The observables $\vec{x}_i$ are defined for each event i, listed in Table VI, and discussed above. The extended likelihood function is defined for N candidate events as

$$\mathcal{L}=\exp\left(-n_{\rm sig}-\sum_k n_{\rm bkg}^k\right)\prod_i^N\left(n_{\rm sig}\times\mathcal{P}_{\rm sig}(\vec{x}_i;\vec{\zeta})+\sum_k n_{\rm bkg}^k\times\mathcal{P}_{\rm bkg}^k(\vec{x}_i)\right), \quad (20)$$

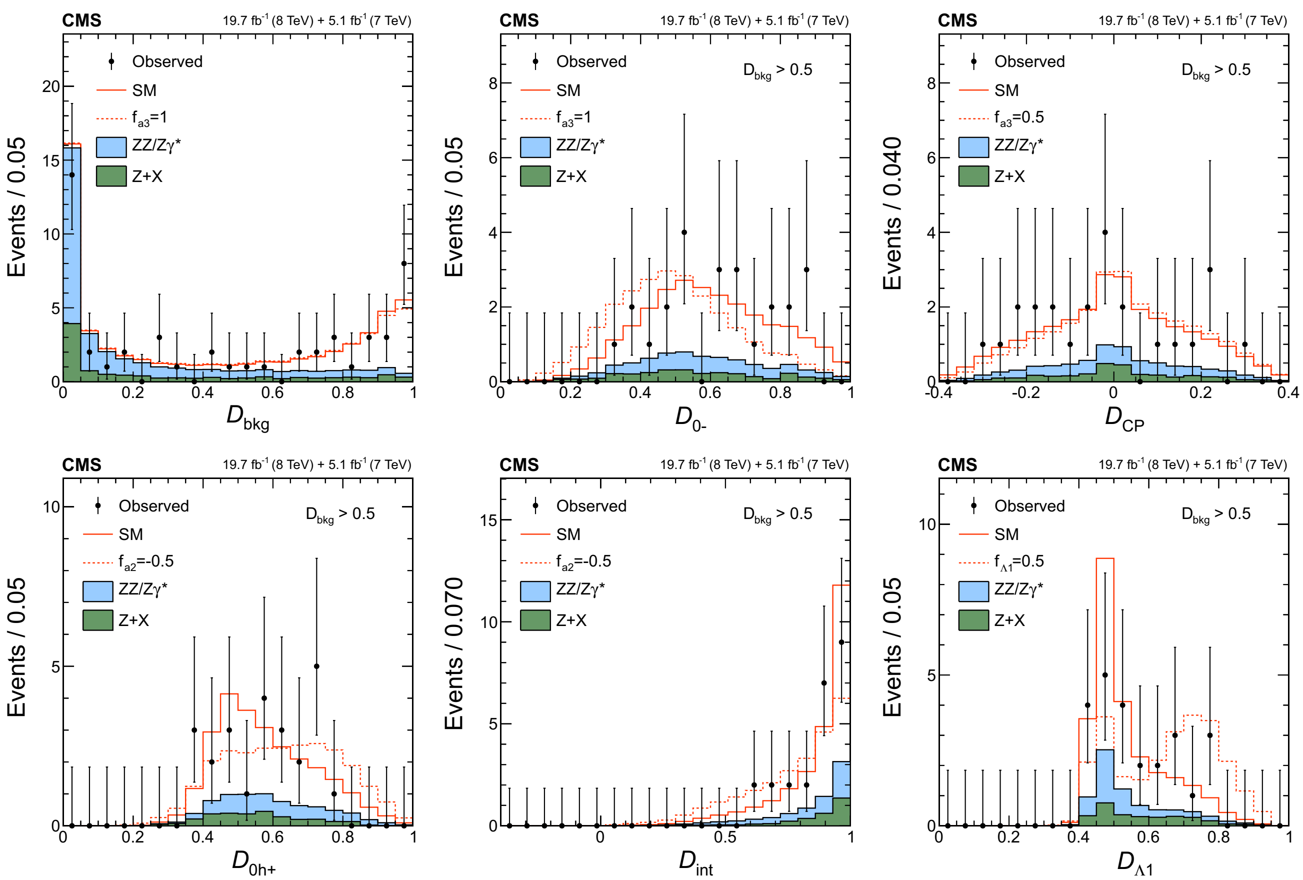

FIG. 4 (color online). Distributions of the kinematic discriminants for the observed data (points with error bars), the expectations for the SM background (shaded areas), the SM Higgs boson signal (open areas under the solid histogram), and the alternative spin-zero resonances (open areas under the dashed histograms) are shown, as indicated in the legend. The mass of the resonance is taken to be 125.6 GeV and the SM cross section is used. Top row from left to right: $\mathcal{D}_{\rm bkg}$, $\mathcal{D}_{0-}$, $\mathcal{D}_{CP}$; bottom row from left to right: $\mathcal{D}_{0h+}$, $\mathcal{D}_{\rm int}$, $\mathcal{D}_{\Lambda1}$. All distributions, with the exception of $\mathcal{D}_{\rm bkg}$, are shown with the requirement $\mathcal{D}_{\rm bkg}>0.5$ to enhance signal purity.

TABLE VI. List of observables $\vec{x}$ used in the analysis of the HVV couplings. The J^P notation for spin-two refers to the ten scenarios defined in Table II. The $H \to \gamma\gamma$ channel is illustrated with two main observables, where $\cos\theta^*$ represents categories constructed from the angular and other observables, and more details are given in Sec. III E and Ref. [15].

Measurement	Observables $\vec{x}$		
$f_{\Lambda 1}$	$\mathcal{D}_{\rm bkg}$	$\mathcal{D}_{\Lambda 1}$	
f_{a2}	$\mathcal{D}_{\rm bkg}$	$\mathcal{D}_{0h+}$	$\mathcal{D}_{\rm int}$
f_{a3}	$\mathcal{D}_{\rm bkg}$	$\mathcal{D}_{0-}$	$\mathcal{D}_{CP}$
$f_{\Lambda 1}^{WW}$	$m_{\rm T}$	$m_{\ell\ell}$	
f_{a2}^{WW}	$m_{\rm T}$	$m_{\ell\ell}$	
f_{a3}^{WW}	$m_{\rm T}$	$m_{\ell\ell}$	
$f_{\Lambda 1}^{Z\gamma}$	$\mathcal{D}_{\rm bkg}$	$\mathcal{D}_{\Lambda 1}^{Z\gamma}$	$\mathcal{D}_{\rm int}^{Z\gamma,\Lambda 1}$
$f_{a2}^{Z\gamma}$	$\mathcal{D}_{\rm bkg}$	$\mathcal{D}_{a2}^{Z\gamma}$	$\mathcal{D}_{\rm int}^{Z\gamma}$
$f_{a3}^{Z\gamma}$	$\mathcal{D}_{\rm bkg}$	$\mathcal{D}_{a3}^{Z\gamma}$	$\mathcal{D}_{CP}^{Z\gamma}$
$f_{a2}^{\gamma\gamma}$	$\mathcal{D}_{\rm bkg}$	$\mathcal{D}_{a2}^{\gamma\gamma}$	$\mathcal{D}_{\rm int}^{\gamma\gamma}$
$f_{a3}^{\gamma\gamma}$	$\mathcal{D}_{\rm bkg}$	$\mathcal{D}_{a3}^{\gamma\gamma}$	$\mathcal{D}_{CP}^{\gamma\gamma}$
spin-one $q\bar{q} \to X(f_{b2}) \to ZZ$	$\mathcal{D}_{\rm bkg}$	$\mathcal{D}_{1-}$	$\mathcal{D}_{1+}$
spin-one decay $X(f_{b2}) \to ZZ$	$\mathcal{D}_{\rm bkg}^{\rm dec}$	$\mathcal{D}_{1-}^{\rm dec}$	$\mathcal{D}_{1+}^{\rm dec}$
spin-two $q\bar{q} \to X(J^P) \to ZZ$	$\mathcal{D}_{\rm bkg}$	$\mathcal{D}_{J^P}^{q\bar{q}}$	
spin-two $gg \to X(J^P) \to ZZ$	$\mathcal{D}_{\rm bkg}$	$\mathcal{D}_{J^P}^{gg}$	
spin-two decay $X(J^P) \to ZZ$	$\mathcal{D}_{\rm bkg}^{\rm dec}$	$\mathcal{D}_{J^P}^{\rm dec}$	
spin-one $q\bar{q} \to X(f_{b2}^{WW}) \to WW$	$m_{\rm T}$	$m_{\ell\ell}$	
spin-two gg or $q\bar{q} \to X(J^P) \to WW$	$m_{\rm T}$	$m_{\ell\ell}$	
spin-two gg or $q\bar{q} \to X(2_m^+) \to \gamma\gamma$	$m_{\gamma\gamma}$	$\cos\theta^*$	

where $n_{\rm sig}$ is the number of signal events and $n_{\rm bkg}^k$ is the number of background events of type k. The probability density functions $\mathcal{P}_{\rm sig}(\vec{x}_i;\vec{\zeta})$ and $\mathcal{P}_{\rm bkg}^k(\vec{x}_i)$ are defined for the signal and background, respectively.

There are several event categories, such as $4e$, 4μ, and $2e2\mu$ in the $H \to VV \to 4\ell$ analysis, 0 and 1 jet in the $H \to WW \to \ell\nu\ell\nu$ analysis, or the 7 TeV and 8 TeV categories, and several types of background. The total signal yield $n_{\rm sig}$ is a free parameter to avoid using the overall signal event yield as a part of the discrimination between alternative hypotheses. However, when several channels are used in the same decay, such as $H \to VV \to 4e, 2e2\mu$, and 4μ, the relative yields between the channels depend on the terms considered in the tensor structure due to interference effects in the presence of identical leptons, and this information is exploited in the analysis.

The method adopted for all the measurements presented in this paper is a template method. The probability density functions $\mathcal{P}_{\rm sig}$ and $\mathcal{P}_{\rm bkg}^k$ are described as histograms (templates) with two or three dimensions (see observables in Table VI) and with up to 50 bins in each dimension. The number of dimensions used is limited by the number of simulated events that can be generated or the number of events in the control regions in data. However, an optimal construction of observables allows for the retention of all the necessary information for the measurement with up to three observables. The templates are built for signal and background from histograms of fully simulated events, or from control regions in data. In the $H \to VV \to 4\ell$ analyses, where the number of bins is larger than in the $H \to WW \to \ell\nu\ell\nu$ analysis, statistical fluctuations are removed using a smoothing algorithm [100,101].

The signal probability density functions $\mathcal{P}_{\rm sig}$ depend on the coupling parameters $\vec{\zeta}$. For spin-zero, these functions can be parametrized as a linear combination of the terms originating from the SM-like and anomalous amplitudes and their interference [31]

$$\begin{aligned}\mathcal{P}_{\rm sig}(\vec{x};\vec{\zeta} = \{f_{ai},\phi_{ai}\}) &= \left(1-\sum_{ai} f_{ai}\right)\mathcal{P}_{0^+}(\vec{x}) + \sum_{ai} f_{ai}\mathcal{P}_{ai}(\vec{x}) \\ &\quad + \sum_{ai}\sqrt{f_{ai}\left(1-\sum_{aj} f_{aj}\right)}\,\mathcal{P}_{ai,0^+}^{\rm int}(\vec{x};\phi_{ai}) \\ &\quad + \sum_{ai<aj}\sqrt{f_{ai}f_{aj}}\,\mathcal{P}_{ai,aj}^{\rm int}(\vec{x};\phi_{ai}-\phi_{aj}), \end{aligned} \tag{21}$$

where $\mathcal{P}_{ai}$ is the probability of a pure a_i term and $\mathcal{P}_{ai,aj}^{\rm int}$ describes the interference between the two terms, each parametrized as a template. Each term in Eq. (21) is extracted from the dedicated simulation and includes proper normalization. For spin-one or spin-two, in the case of a study of noninterfering states, there is only one fraction $f(J^P)$ and no interference contribution.

The likelihood in Eq. (20) can be used in two different ways. In both approaches, the likelihood is maximized with respect to the nuisance parameters which include the signal yield and constrained parameters describing the systematic uncertainties discussed in Sec. IV E. In one approach the likelihood is maximized to estimate the values of anomalous couplings, and the confidence intervals are determined from profile likelihood scans of the respective parameters. This is used for the measurement of anomalous couplings under the spin-zero hypothesis, as well as for the $f(J^P)$ measurements of the spin-one and spin-two hypotheses. The allowed 68% and 95% C.L. intervals are defined using the profile likelihood function, $-2\Delta\ln\mathcal{L} = 1.00$ and 3.84, for which exact coverage is expected in the asymptotic limit [102]. The approximate coverage has been tested with generated samples for several true parameter values, and the quoted results have been found to be conservative.

The other approach is used to distinguish an alternative spin-one or spin-two signal hypothesis from the SM Higgs boson. In this case, the test statistic $q = -2\ln(\mathcal{L}_{J^P}/\mathcal{L}_{0^+})$ is defined using the ratio of signal plus background likelihoods for two signal hypotheses. To quantify the consistency of the observed test statistic $q_{\rm obs}$ with respect to the SM Higgs boson hypothesis (0^+), the probability $p = P(q \leq q_{\rm obs}|0^+ + {\rm bkg})$ is assessed and converted into a number of standard deviations via the Gaussian one-sided tail integral. The consistency of the observed data with the alternative signal hypothesis (J^P) is assessed from $P(q \geq q_{\rm obs}|J^P + {\rm bkg})$. The $CL_{\rm s}$ criterion [103,104], defined as $CL_{\rm s} = P(q \geq q_{\rm obs}|J^P + {\rm bkg})/P(q \geq q_{\rm obs}|0^+ + {\rm bkg}) < \alpha$, is used for the final inference of whether a particular alternative signal hypothesis is excluded or not at a given confidence level $(1-\alpha)$. The following quantities are used to characterize the expected and observed results: (i) separation, defined as the tail area $A_{\rm tail}$ calculated at the value of q where the tails of the two distributions have identical area, (ii) the probability of each hypothesis to fluctuate beyond $q_{\rm obs}$, and (iii) the expected and observed $CL_{\rm s}$ value. Option (i) is used to characterize the expected results as this quantity is symmetric between the two hypotheses, and it is expressed as the number of standard deviations multiplied by two. Options (ii) and (iii) are used to characterize the observed results for exclusion of a particular hypothesis. The observed separation (ii) is also expressed as the number of standard deviations, and the sign is positive if the tail extends away or negative if it extends towards the median of the other hypothesis.

E. Analysis validation and systematic uncertainties

The validation of this analysis and the assignment of systematic uncertainties follows various aspects of the parametrization in Eq. (20). Estimates of the expected background yields and shapes of the probability distributions for signal and background are investigated. The performance of the fit has been tested using events from the full simulation discussed in Sec. III A and using events generated directly from probability distributions. Both approaches are found to give consistent expected results and unbiased parameter estimates in the fit for anomalous couplings for the full spectrum of measurements listed in Table VI. These tests rely on the proper simulation of the signal and background processes, and further studies propagate any systematic uncertainties in the simulation to the final results, which are specific to each final state. The overall signal yield is left unconstrained in the fit, and therefore the associated theoretical uncertainties do not affect the constraints on anomalous couplings.

The statistical uncertainties dominate over the systematic ones for all the results quoted in this paper. The systematic uncertainties in the $H \to VV \to 4\ell$ channel are generally the same as the ones investigated in Ref. [12]. Among the yield uncertainties, experimental systematic uncertainties are evaluated from data for the lepton trigger efficiency and combined object reconstruction, identification, and isolation efficiencies. The theoretical uncertainties on the ZZ background are described in Ref. [12], but the calculations have been updated using the recommendations in Ref. [105] and the treatment of the $gg \to ZZ/Z\gamma^*$ process follows Ref. [13]. The $Z+X$ uncertainties include the effects on both the expected yields and on the shape. The yield uncertainties are estimated to be 20%, 25%, and 40% for the $4e$, $2e2\mu$, and 4μ decay channels, respectively. The shape uncertainty is taken into account by considering the difference between the $Z+X$ and $q\bar{q} \to ZZ$ distributions for a particular final state, which was found to cover any potential biases in $Z+X$ parametrization. To account for the lepton momentum scale and resolution uncertainty in the $m_{4\ell}$ distribution, the alternative signal shapes are taken from the variations of both of these contributions, following Ref. [12].

In the $H \to WW \to \ell\nu\ell\nu$ analysis, the same treatment of the systematic uncertainties as in Ref. [14] has been performed. The uncertainty related to the size of the simulated samples is such that it is at least a factor of 2 smaller than the rest of the systematic uncertainties and varies from 1.0% for a Higgs boson signal to 20% for some of the backgrounds ($Z/\gamma^* \to \ell^+\ell^-$, $W+{\rm jets}$, and $V\gamma^{(*)}$). Systematic uncertainties are represented by individual nuisance parameters with log-normal distributions. An exception is applied to the $q\bar{q} \to WW$ normalization, which is an unconstrained parameter in the fit.

The analysis is optimized for the $gg \to H$ production mode, which has the largest cross section, as verified experimentally [12,14,15], and is characterized by low hadronic activity in the final state. Other production modes such as VBF, VH, and $t\bar{t}H$ are considered in the analysis, representing a small or negligible fraction of the signal. In the $H \to VV \to 4\ell$ analysis, only the exclusive four-lepton final state is reconstructed, and it has been verified that all observables are similar for all production mechanisms of a spin-zero particle. For the spin-one and spin-two models using decay-only observables, any residual dependence on the production mechanism is small and enters only through the difference in detector acceptance effects. Uncertainties in this approach are accounted for with alternative parametrization of the observable distributions, covering the difference between the gluon fusion and $q\bar{q}$ production mechanisms of a spin-two particle, or an equivalent variation for a spin-one particle production which reflects the difference in the boost of the resonance.

In the $H \to WW \to \ell\nu\ell\nu$ analysis, the VBF contribution, which has similar kinematics as $gg \to H$, represents 5% of the total Higgs boson signal in the 1-jet category, where it is the second-largest mode in terms of rate after $gg \to H$, and less than 0.5% in the 0-jet bin, where it is highly suppressed. The associated production VH, and in particular ZH, shows some differences in the observables compared to $gg \to H$ because of the additional vector bosons present in the final state, but it contributes less than 1% to the total signal yield in the 0- and 1-jet categories. There is no expected $t\bar{t}H$ contribution in the signal region after all selection requirements. For the measurements presented in Sec. V B, a full combination of all Higgs boson production mechanisms is considered in the parametrization, while the alternative exotic-spin hypotheses are produced via gg, $q\bar{q}$, or a combination of the two. For the measurements presented in Sec. VI D, the $gg \to H$ model is used to create the templates and the full variation of the distributions after the inclusion of all the production mechanisms according to the SM expectation is used for the evaluation of the systematic uncertainties. This approach is taken because *a priori* the fraction of various production mechanisms is not known for an arbitrary BSM model. However, those fractions have been experimentally constrained to be consistent with the SM expectations [12,14,15,21].

The correlations between the systematic uncertainties in the different categories and final states are taken into account. In particular, the main sources of correlated systematic uncertainties are those related to the experimental measurements such as the integrated luminosity, lepton and trigger selection efficiencies, lepton momentum scale, and the theoretical uncertainties affecting the background processes. Uncertainties in the background normalization or background model parameters from control regions and uncertainties of a statistical nature are uncorrelated.

It is instructive to validate the matrix element method with the study of spin-parity and anomalous interactions of the Z boson, which has already established SM properties [74]. An earlier CMS analysis tested the Z boson couplings to fermions in the two-body decay $q\bar{q} \to Z/\gamma^* \to \ell^+\ell^-$ [106], using a matrix element formalism similar to the one used in the Higgs boson studies [28] and established consistency with the SM. Here the study is extended to the four-lepton decay of the Z boson in the topology $q\bar{q} \to Z/\gamma^* \to \ell^+\ell^-\gamma^* \to 4\ell$ [107]. A hypothesis test is performed between the SM Z boson and an exotic Higgs-like resonance $gg \to H(91.2) \to ZZ \to 4\ell$ with the same mass and width as the Z boson. The mass window $80 < m_{4\ell} < 100$ GeV is used, just below the mass range used in the Higgs boson analysis. In addition, the nonresonant $q\bar{q} \to ZZ/Z\gamma^*/\gamma^*\gamma^* \to 4\ell$ contribution is parametrized, including interference with $q\bar{q} \to Z/\gamma^* \to \ell^+\ell^-\gamma^* \to 4\ell$ following the formalism of Eq. (21), and its effective fractional cross section is fitted in data in analogy to the f_{ai} parameters. The results show that the SM Z boson hypothesis is highly preferred in the data, and the small contribution of the production $q\bar{q} \to ZZ/Z\gamma^*/\gamma^*\gamma^* \to 4\ell$, including its phase, is consistent with the SM expectation. The alternative Higgs-like hypothesis $H(91.2)$ has been excluded with a C.L. > 99.99%.

F. Analysis validation with analytic parametrization of kinematic distributions

In the $H \to VV \to 4\ell$ channel, the template method discussed above can be extended to the complete set of eight kinematic observables $\vec{x} = (m_1, m_2, m_{4\ell}, \vec{\Omega})$ described in Sec. IV A and shown in Fig. 2. Such an approach would allow us to parametrize the data distributions directly without constructing the dedicated discriminants. However, the parametrization of templates in eight dimensions using full simulation is nearly impossible to perform because of the large number of events required. Therefore, a simplified approach is performed with parametrization of eight-dimensional distributions to cross-check a subset of results, specifically, measurements of the f_{a2} and f_{a3} parameters in the spin-zero studies (see Sec. VI). The signal and the dominant $q\bar{q} \to ZZ/Z\gamma^*$ background are parametrized analytically, and reconstruction effects are incorporated in the probability function numerically. About one-third of the background events coming from the $Z+X$ and $gg \to ZZ/Z\gamma^*$ processes are parametrized with the template approach in eight dimensions using generated events with detector effects incorporated using the same approximate numerical parametrization.

The likelihood construction follows Eq. (20), and the probability distribution is equivalent to Eq. (21). The normalization of the probability distributions in eight dimensions is one of the main computational challenges in this approach and is performed with MC integration. The final state with $2e$ and 2μ is split into $2e2\mu$ and $2\mu 2e$ subcategories where the distinction between them is determined by the flavor of the leptons from the Z_1 decay. Additionally, a narrower mass window (115–135 GeV) is used compared to the template method.

The analytic parametrization is the product of the differential decay cross section $d\sigma_{4\ell}$ and the production spectrum W_{prod}, written as

$$\mathcal{P}(\vec{p}_{\mathrm{T}}, Y, \Phi^*, \vec{x}|\vec{\zeta}) = W_{\mathrm{prod}}(\vec{p}_{\mathrm{T}}, Y, \Phi^*, \hat{s}) \times \frac{d\sigma_{4\ell}(m_{4\ell}, m_1, m_2, \vec{\Omega}|\vec{\zeta})}{dm_1^2 dm_2^2 d\vec{\Omega}}, \tag{22}$$

where $\vec{p}_{\mathrm{T}}$, Y, and Φ^* are the transverse momentum, rapidity, and azimuthal orientation of the four-lepton system illustrated in Fig. 1, and $\hat{s} = m_{4\ell}^2$ is the center-of-mass energy of the parton-parton system. In order to convert the above probability to an expression in terms of detector-level reconstructed observables, it is convoluted with a transfer function $T(\vec{x}'^{\mathrm{R}}|\vec{x}'^{\mathrm{G}})$ describing the detector response to produced leptons

$$\mathcal{P}(\vec{x}'^{\mathrm{R}}|\vec{\zeta}) = \int \mathcal{P}(\vec{x}'^{\mathrm{G}}|\vec{\zeta}) T(\vec{x}'^{\mathrm{R}}|\vec{x}'^{\mathrm{G}}) d\vec{x}'^{\mathrm{G}}, \tag{23}$$

where $\vec{x}' = (\vec{p}_{\mathrm{T}}, Y, \Phi^*, m_1, m_2, m_{4\ell}, \vec{\Omega})$ and the superscripts R and G denote reconstruction and generator level, respectively.

It is important to model accurately the lepton momentum response and the dependence of the efficiency on p_{T} and η, which can all significantly affect the shape of the distributions of the eight observables used in the likelihood function. The transfer functions are constructed from the fully simulated samples for both signal and background. Because of the excellent angular resolution of the CMS tracker, for the purpose of this measurement, the effect of the resolution on the direction of each lepton is negligible compared with the effect of the momentum resolution. As a result, the effect of the direction is neglected, and only the p_{T} response of the leptons is modeled. It is also assumed that the detector response for each lepton is independent of the other leptons so that the transfer function can be written as a product of the transfer functions for each individual lepton. Furthermore, an overall efficiency factor to account for inefficiencies in the lepton selection requirements is applied. The transfer functions are validated by comparing the full detector simulation with the generator-level samples, where track parameters are convolved with these functions.

The production spectrum W_{prod} in Eq. (22) is obtained empirically using simulation. The observables $(\vec{p}_{\mathrm{T}}, Y, \Phi^*)$ are found to be uncorrelated to a good approximation, and their distribution is modeled as a product of three one-dimensional distributions. Then these observables are integrated out to keep the parametrization with the eight main kinematic observables $\vec{x}^{\mathrm{R}}$. For the main background, $q\bar{q} \to ZZ/Z\gamma^*$, the four-lepton mass spectrum $m_{4\ell}$ is also modeled empirically. To construct the $m_{4\ell}$ model, the mass spectrum is parametrized with an empirical exponential function in several bins of rapidity using MC simulation. These distributions are interpolated between different bins in rapidity. The reconstructed $m_{4\ell}$ spectrum is parametrized between 115 and 135 GeV, while the generator-level spectrum is wider to model smearing into and out of this region.

There is no explicit analytic form for the differential cross section for the $Z+X$ and $gg \to ZZ/Z\gamma^*$ backgrounds. Instead, the likelihood is calculated by filling a multidimensional template histogram using very large samples of generator-level PYTHIA and MCFM events, respectively, with parton showering modeled by PYTHIA. These samples are smeared with transfer functions to account for detector effects. This approach is validated using the $q\bar{q} \to ZZ/Z\gamma^*$ analytic description and the corresponding templates, which have been confirmed to have a sufficient accuracy for the description of these backgrounds. The remaining discrepancies observed between the $Z+X$ background templates and the control regions used in the template analysis [12] are covered by assigning a corresponding systematic uncertainty. The systematic uncertainties in the lepton momentum scale and resolution are propagated using alternative parametrizations generated through variations of the transfer function for both signal and background. The sizes of these variations were determined to be consistent with the size of the lepton momentum and resolution systematic uncertainty in Ref. [12]. A systematic uncertainty in the production spectrum of the signal is included using variation of the p_{T} spectrum of the four-lepton system when averaging over the production spectrum. The parametrization of the $gg \to ZZ/Z\gamma^*$ and $Z+X$ background shape is varied using the alternative parametrization from the $q\bar{q} \to ZZ/Z\gamma^*$ background process.

V. STUDY OF EXOTIC SPIN-ONE AND SPIN-TWO SCENARIOS

The study of the exotic-spin J^P hypotheses of the observed boson with mass around 125 GeV using the $X \to ZZ$ and WW channels that have not been presented in previous publications [12,14] is summarized in this section. Mixed spin-one state hypotheses, as well as the spin-two models listed in Table VI, are examined. In addition, the fractional presence of J^P models of a state nearly degenerate in mass with the SM state are tested. In all cases, the template method is employed as discussed in Sec. IV D. The $X \to \gamma\gamma$ decay channel is also studied in the context of the exotic spin-two scenarios, and the results presented in Ref. [15] are combined with those obtained in the $X \to ZZ$ and WW channels [12,14]. All spin-one and spin-two scenarios studied are excluded, which motivates the detailed study of the spin-zero scenario in Sec. VI. All studies in this paper are presented under the hypothesis of a boson mass of $m_H = 125.6$ GeV, which is the combined value in the $H \to ZZ$ and WW channels [12,14]. The only exception is the analysis of the $X \to ZZ$, WW, and $\gamma\gamma$ channels combined that is performed with the $m_H = 125.0$ GeV hypothesis, which is the combined value for the three channels [12,14,15]. This mass difference has little effect on the results and it is in the same range as the systematic uncertainties assigned to the energy scale in the mass reconstruction.

A. Exotic-spin study with the $H \to ZZ \to 4\ell$ channel

In the case of the spin-one studies, the hypothesis testing is performed for a discrete set of values of the parameter f_{b2}. The input observables are $(\mathcal{D}_{\mathrm{bkg}}, \mathcal{D}_{1^-}, \mathcal{D}_{1^+})$. It has been demonstrated in the context of this study that the distributions of these observables are not sensitive to the phase between the b_1 and b_2 coupling parameters in Eq. (8), and therefore the results of the f_{b2} scan are valid for any value of the phase term in the interference. The spin-one hypothesis is tested for two scenarios, $q\bar{q}$ production and using only decay information. The latter requires the input observables $(\mathcal{D}^{\mathrm{dec}}_{\mathrm{bkg}}, \mathcal{D}^{\mathrm{dec}}_{1^-}, \mathcal{D}^{\mathrm{dec}}_{1^+})$.

Figure 5 (left) shows the distribution of the test statistic $q = -2\ln(\mathcal{L}_{J^P}/\mathcal{L}_{0^+})$ for a SM Higgs boson and for the $J^P = 1^+$ hypothesis. The expected and observed separations of spin-one models from the test statistic distributions are summarized in Table VII and in Fig. 6. The expected separation between the alternative signal hypotheses is quoted for two cases. In the first case, the expected SM

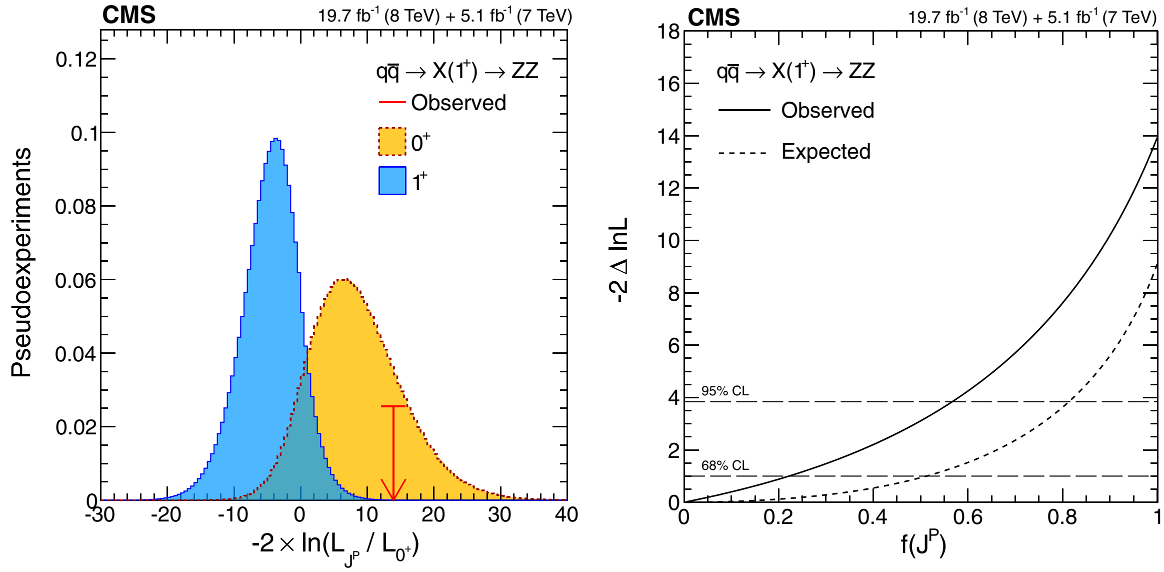

FIG. 5 (color online). (left) Distributions of the test statistic $q = -2\ln(\mathcal{L}_{J^P}/\mathcal{L}_{0^+})$ for the $J^P = 1^+$ hypothesis of $q\bar{q} \to X(1^+) \to ZZ$ tested against the SM Higgs boson hypothesis (0^+). The expectation for the SM Higgs boson is represented by the yellow histogram on the right and the alternative J^P hypothesis by the blue histogram on the left. The red arrow indicates the observed q value. (right) Observed value of $-2\Delta\ln\mathcal{L}$ as a function of $f(J^P)$ and the expectation in the SM for the $q\bar{q} \to X(1^+) \to ZZ$ alternative J^P model.

Higgs boson signal strength and the alternative signal cross section are the ones obtained in the fit to the data. The second case assumes the nominal SM Higgs boson signal strength (defined as $\mu = 1$), while the cross section for the alternative signal hypothesis is taken to be the same as for the SM Higgs boson (the $2e2\mu$ channel at 8 TeV is taken as a reference). Since the observed signal strength is very close to unity, the two results for the expected separations are also similar.

Figure 5 (right) also shows an example of the likelihood scan, $-2\Delta\ln\mathcal{L}$, as a function of $f(J^P)$ for the $q\bar{q}$ produced 1^+ model, where the fractional cross section of a second overlapping but noninterfering resonance $f(J^P)$ is defined in Eq. (16). The expected and observed measurements of the noninterfering fractions are also summarized in Table VII and in Fig. 7. The production cross-section fractions are represented by $f(J^P)$ and therefore require knowledge of the reconstruction

TABLE VII. List of spin-one models tested in the $X \to ZZ$ analysis. The expected separation is quoted for two scenarios, for the signal production cross section obtained from the fit to data for each hypothesis and using the SM expectation ($\mu = 1$). The observed separation shows the consistency of the observation with the SM Higgs boson model or the alternative J^P model, from which the CL_s value is derived. The $f(J^P)$ constraints are quoted, where the decay-only measurements are valid for any production mechanism and are performed using the efficiency of the $q\bar{q} \to X \to ZZ$ selection.

$f_{b2}(J^P)$ Model	J^P Production	Expected ($\mu = 1$)	Observed 0^+	Observed J^P	CL_s	$f(J^P)$ 95% C.L. Observed (Expected)	$f(J^P)$ Best fit
$0.0(1^-)$	$q\bar{q}$	2.9σ (2.8σ)	-1.4σ	$+5.0\sigma$	$<0.001\%$	<0.46 (0.78)	$0.00^{+0.16}_{-0.00}$
0.2	$q\bar{q}$	2.6σ (2.6σ)	-1.4σ	$+4.6\sigma$	0.002%	<0.49 (0.81)	$0.00^{+0.17}_{-0.00}$
0.4	$q\bar{q}$	2.5σ (2.4σ)	-1.3σ	$+4.4\sigma$	0.005%	<0.51 (0.83)	$0.00^{+0.19}_{-0.00}$
0.6	$q\bar{q}$	2.4σ (2.4σ)	-1.2σ	$+4.1\sigma$	0.015%	<0.53 (0.83)	$0.00^{+0.20}_{-0.00}$
0.8	$q\bar{q}$	2.4σ (2.4σ)	-1.0σ	$+4.0\sigma$	0.021%	<0.55 (0.83)	$0.00^{+0.21}_{-0.00}$
$1.0(1^+)$	$q\bar{q}$	2.4σ (2.4σ)	-0.8σ	$+3.8\sigma$	0.031%	<0.57 (0.81)	$0.00^{+0.22}_{-0.00}$
$0.0(1^-)$	any	2.9σ (2.7σ)	-2.0σ	$>5.0\sigma$	$<0.001\%$	<0.37 (0.79)	$0.00^{+0.12}_{-0.00}$
0.2	any	2.7σ (2.5σ)	-2.2σ	$>5.0\sigma$	$<0.001\%$	<0.38 (0.82)	$0.00^{+0.12}_{-0.00}$
0.4	any	2.5σ (2.4σ)	-2.3σ	$>5.0\sigma$	$<0.001\%$	<0.39 (0.84)	$0.00^{+0.13}_{-0.00}$
0.6	any	2.5σ (2.3σ)	-2.4σ	$>5.0\sigma$	$<0.001\%$	<0.39 (0.86)	$0.00^{+0.13}_{-0.00}$
0.8	any	2.4σ (2.3σ)	-2.3σ	$>5.0\sigma$	$<0.001\%$	<0.40 (0.86)	$0.00^{+0.13}_{-0.00}$
$1.0(1^+)$	any	2.5σ (2.3σ)	-2.3σ	$>5.0\sigma$	$<0.001\%$	<0.41 (0.85)	$0.00^{+0.13}_{-0.00}$

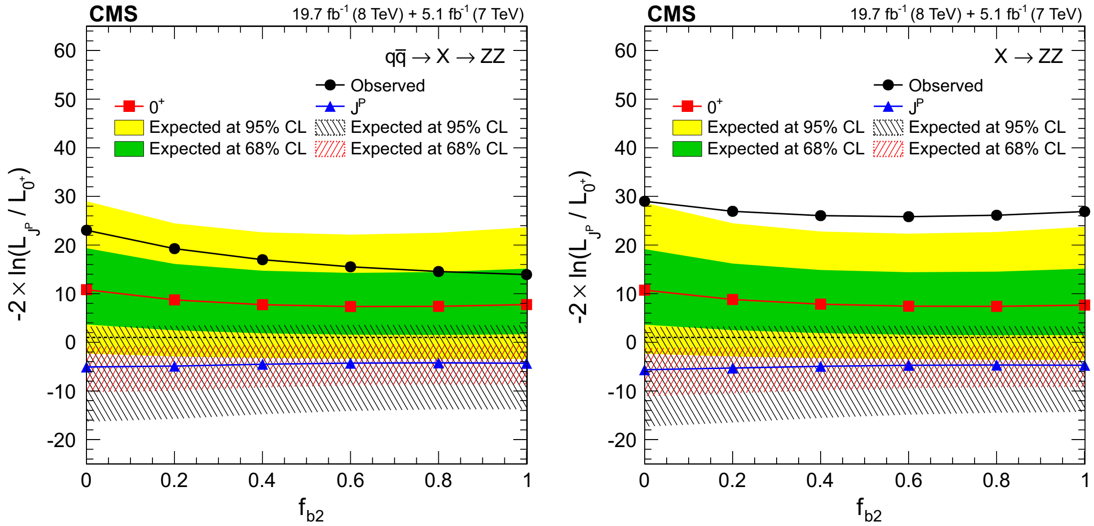

FIG. 6 (color online). Distributions of the test statistic $q = -2\ln(\mathcal{L}_{J^P}/\mathcal{L}_{0^+})$ as a function of f_{b2} for the spin-one J^P models tested against the SM Higgs boson hypothesis in the $q\bar{q} \to X \to ZZ$ (left) and decay-only $X \to ZZ$ (right) analyses. The median expectation for the SM Higgs boson is represented by the red squares with the green (68% C.L.) and yellow (95% C.L.) solid color regions and for the alternative J^P hypotheses by the blue triangles with the red (68% C.L.) and blue (95% C.L.) hatched regions. The observed values are indicated by the black dots.

efficiency for the interpretation of the measured yields. In the case of the production-independent scenarios of spin-one models, the $f(J^P)$ results are extracted using the reconstruction efficiency of the $q\bar{q} \to X$ process. The values of $-2\Delta\ln\mathcal{L} = 1$ and 3.84 represent the 68% and 95% C.L., respectively.

All spin-one tests are consistent with the expectation for the SM Higgs boson. While the decay-only analysis uses less information and is expected to provide weaker constraints, the fluctuations in the observed data lead to stronger constraints for spin-one models. The least restrictive result corresponds to the 1^+ model in the $q\bar{q}$ production test with a CL_s value of 0.031%.

Any arbitrary spin-one model for the resonance observed in the $X \to ZZ \to 4\ell$ decay mode with any mixture of parity-even and parity-odd interactions and any production mechanism is excluded at a CL of 99.97% or higher.

In the case of the spin-two studies, hypothesis testing is performed for ten models and three scenarios: gg, $q\bar{q}$ production, and using only decay information. Two input observables are used since interference between the different amplitude components is not considered. Several models have been tested in Ref. [12], and here those results are repeated for completeness. They cover all the lowest order terms in the amplitude without considering mixing of different contributions.

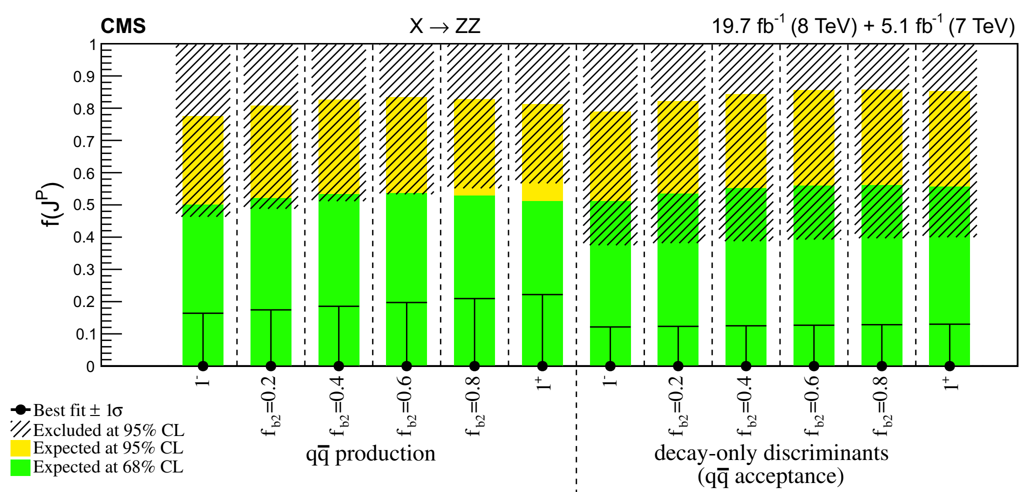

FIG. 7 (color online). Summary of the $f(J^P)$ constraints as a function of f_{b2} from Table VII, where the decay-only measurements are performed using the efficiency of the $q\bar{q} \to X \to ZZ$ selection. The expected 68% and 95% C.L. regions are shown as green and yellow bands. The observed constraints at 68% and 95% C.L. are shown as the points with error bars and the excluded hatched regions.

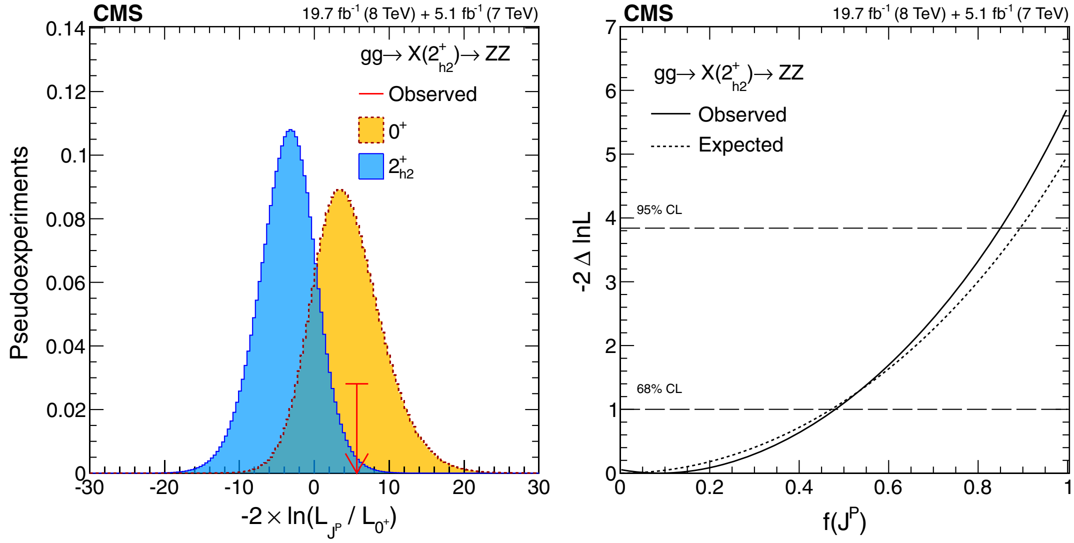

FIG. 8 (color online). (left) Distributions of the test statistic $q = -2\ln(\mathcal{L}_{J^P}/\mathcal{L}_{0^+})$ for the $J^P = 2^+_{h2}$ hypothesis of $gg \to X(2^+_{h2}) \to ZZ$ tested against the SM Higgs boson hypothesis (0^+). The expectation for the SM Higgs boson is represented by the yellow histogram on the right and the alternative J^P hypothesis by the blue histogram on the left. The red arrow indicates the observed q value. (right) Observed value of $-2\Delta\ln\mathcal{L}$ as a function of $f(J^P)$ and the expectation in the SM for the $gg \to X(2^+_{h2}) \to ZZ$ alternative J^P model.

An example distribution of the test statistic and observed value in the case of the SM Higgs boson and the spin-two hypothesis 2^+_{h2} is shown in Fig. 8 (left). The expected and observed separation from the test statistic distributions for all the spin-two models considered is summarized in Table VIII and in Fig. 9. The 2^+_{h2} model is the least restricted one (see Table VIII): $CL_s = 0.74\%$ for any production mechanism. The observed noninterfering fraction measurements are summarized in Table VIII and in Fig. 10. In the case of production-independent scenarios, the $f(J^P)$ results are extracted using the $gg \to X$ efficiency. Figure 8 (right) shows the likelihood scan for the 2^+_{h2} hypothesis as a function of $f(J^P)$.

The data disfavor all the spin-two $X \to ZZ \to 4\ell$ hypotheses tested in favor of the SM hypothesis $J^P = 0^+$ with $1 - CL_s$ values larger than 99% C.L. when only decay information is used (Table VIII).

B. Exotic-spin study with the $H \to WW \to \ell\nu\ell\nu$ channel

Similar to the $X \to ZZ \to 4\ell$ study above, ten spin-two hypotheses, listed in Table II, and three spin-one hypotheses, including a mixed case with $f^{WW}_{b2} = 0.5$, are tested using the $X \to WW \to \ell\nu\ell\nu$ decay. Examples of distributions of the test statistic, $q = -2\ln(\mathcal{L}_{J^P}/\mathcal{L}_{0^+})$, for the SM Higgs boson and alternative spin-one and spin-two models are shown in Figs. 11 and 12 (left). Examples of the likelihood scans, $-2\Delta\ln\mathcal{L}$, as a function of $f(J^P)$ are also shown in Figs. 11 and 12 (right).

The expected and observed separation of the test statistic for the various models are summarized in Table IX for the spin-one models and in Table X for the spin-two models. The expected separation between the SM Higgs boson and each alternative spin-one or spin-two hypothesis is larger than 1 standard deviation in most cases, reaching 3 standard deviations for several models.

The spin-one J^P hypothesis is tested against the SM Higgs boson for several values of f^{WW}_{b2}. The results are shown in Fig. 13 (left) and summarized in Table IX. As in the $X \to ZZ \to 4\ell$ study, the 1^+ model is found to be the least restricted.

The summary of the spin-two results is presented in Fig. 14 and Table X. In the case of the spin-two studies, the results for the different scenarios are estimated assuming different production fractions from $f(q\bar{q}) = 0$, representing the pure $gg \to X$ process, to $f(q\bar{q}) = 1$, representing the pure $q\bar{q} \to X$ process. A scan of the $f(q\bar{q})$ fraction is performed in each case, with an example of the scan for the 2^+_{h2} model shown in Fig. 13 (right). The results with pure gluon fusion production $f(q\bar{q}) = 0$ are found to be the least restricted in each case. The observed noninterfering fraction measurements are summarized in Fig. 15.

In all cases the data favor the SM hypothesis over the alternative spin-one or spin-two hypotheses.

C. Combined exotic-spin results with the $H \to ZZ$ and WW channels

The results of testing the spin-one and spin-two hypotheses obtained by considering the $X \to ZZ \to 4\ell$ and

TABLE VIII. List of spin-two models tested in the $X \to ZZ$ analysis. The expected separation is quoted for two scenarios, for the signal production cross section obtained from the fit to data for each hypothesis, and using the SM expectation ($\mu = 1$). The observed separation shows the consistency of the observation with the SM Higgs boson or an alternative J^P model, from which the CL_s value is derived. The $f(J^P)$ constraints are quoted, where the decay-only measurements are valid for any production mechanism and are performed using the efficiency of the $gg \to X \to ZZ$ selection. Results from Ref. [12] are explicitly noted.

J^P Model	J^P Production	Expected ($\mu = 1$)	Observed 0^+	Observed J^P	CL_s	$f(J^P)$ 95% C.L. Observed (Expected)	$f(J^P)$ Best fit
2^+_m [12]	gg	$1.9\sigma\,(1.8\sigma)$	-1.1σ	$+3.0\sigma$	0.90%	< 0.71 (1.00)	$0.00^{+0.30}_{-0.00}$
2^+_{h2}	gg	$2.0\sigma\,(2.1\sigma)$	-0.3σ	$+2.4\sigma$	2.0%	< 0.85 (0.89)	$0.09^{+0.39}_{-0.09}$
2^+_{h3}	gg	$3.2\sigma\,(3.4\sigma)$	$+0.3\sigma$	$+3.0\sigma$	0.17%	< 0.72 (0.58)	$0.13^{+0.29}_{-0.13}$
2^+_h [12]	gg	$3.8\sigma\,(4.0\sigma)$	$+1.8\sigma$	$+2.0\sigma$	2.3%	< 1.00 (0.48)	$0.48^{+0.28}_{-0.29}$
2^+_b [12]	gg	$1.6\sigma\,(1.8\sigma)$	-1.4σ	$+3.4\sigma$	0.50%	< 0.64 (1.00)	$0.00^{+0.24}_{-0.00}$
2^+_{h6}	gg	$3.4\sigma\,(3.7\sigma)$	-0.6σ	$+4.9\sigma$	$< 0.001\%$	< 0.38 (0.58)	$0.00^{+0.13}_{-0.00}$
2^+_{h7}	gg	$3.8\sigma\,(4.5\sigma)$	-0.3σ	$+4.5\sigma$	$< 0.001\%$	< 0.44 (0.43)	$0.00^{+0.19}_{-0.00}$
2^-_h [12]	gg	$4.2\sigma\,(4.5\sigma)$	$+1.0\sigma$	$+3.2\sigma$	0.090%	< 0.77 (0.44)	$0.29^{+0.26}_{-0.23}$
2^-_{h9}	gg	$2.5\sigma\,(2.6\sigma)$	-1.1σ	$+4.0\sigma$	0.029%	< 0.46 (0.76)	$0.00^{+0.15}_{-0.00}$
2^-_{h10}	gg	$4.2\sigma\,(4.3\sigma)$	-0.1σ	$+4.8\sigma$	$< 0.001\%$	< 0.57 (0.50)	$0.06^{+0.27}_{-0.06}$
2^+_m [12]	$q\bar{q}$	$1.7\sigma\,(1.7\sigma)$	-1.7σ	$+3.8\sigma$	0.17%	< 0.56 (0.99)	$0.00^{+0.19}_{-0.00}$
2^+_{h2}	$q\bar{q}$	$2.2\sigma\,(2.2\sigma)$	-0.8σ	$+3.3\sigma$	0.26%	< 0.61 (0.86)	$0.00^{+0.23}_{-0.00}$
2^+_{h3}	$q\bar{q}$	$3.1\sigma\,(3.0\sigma)$	$+0.2\sigma$	$+3.0\sigma$	0.21%	< 0.81 (0.70)	$0.13^{+0.40}_{-0.13}$
2^+_h	$q\bar{q}$	$4.0\sigma\,(3.9\sigma)$	$+0.2\sigma$	$+3.9\sigma$	0.008%	< 0.71 (0.53)	$0.21^{+0.28}_{-0.21}$
2^+_b	$q\bar{q}$	$1.7\sigma\,(1.7\sigma)$	-1.9σ	$+4.1\sigma$	0.062%	< 0.45 (1.00)	$0.00^{+0.14}_{-0.00}$
2^+_{h6}	$q\bar{q}$	$3.4\sigma\,(3.3\sigma)$	-0.2σ	$+4.0\sigma$	0.008%	< 0.74 (0.71)	$0.04^{+0.45}_{-0.04}$
2^+_{h7}	$q\bar{q}$	$4.1\sigma\,(3.9\sigma)$	$+0.4\sigma$	$+3.8\sigma$	0.010%	< 0.77 (0.55)	$0.35^{+0.23}_{-0.28}$
2^-_h	$q\bar{q}$	$4.3\sigma\,(4.4\sigma)$	$+0.0\sigma$	$+4.6\sigma$	$< 0.001\%$	< 0.57 (0.48)	$0.01^{+0.31}_{-0.01}$
2^-_{h9}	$q\bar{q}$	$2.4\sigma\,(2.2\sigma)$	$+0.5\sigma$	$+2.0\sigma$	3.1%	< 0.99 (0.86)	$0.31^{+0.43}_{-0.31}$
2^-_{h10}	$q\bar{q}$	$4.0\sigma\,(3.9\sigma)$	$+0.4\sigma$	$+4.0\sigma$	0.006%	< 0.75 (0.59)	$0.30^{+0.26}_{-0.30}$
2^+_m [12]	any	$1.5\sigma\,(1.5\sigma)$	-1.6σ	$+3.4\sigma$	0.71%	< 0.63 (1.00)	$0.00^{+0.22}_{-0.00}$
2^+_{h2}	any	$1.9\sigma\,(2.0\sigma)$	-0.9σ	$+3.0\sigma$	0.74%	< 0.66 (0.95)	$0.00^{+0.27}_{-0.00}$
2^+_{h3}	any	$3.0\sigma\,(3.1\sigma)$	$+0.0\sigma$	$+3.1\sigma$	0.18%	< 0.69 (0.64)	$0.00^{+0.35}_{-0.00}$
2^+_h	any	$3.8\sigma\,(4.0\sigma)$	$+0.3\sigma$	$+3.6\sigma$	0.025%	< 0.64 (0.49)	$0.07^{+0.30}_{-0.07}$
2^+_b	any	$1.7\sigma\,(1.7\sigma)$	-1.6σ	$+3.6\sigma$	0.29%	< 0.55 (1.00)	$0.00^{+0.19}_{-0.00}$
2^+_{h6}	any	$3.3\sigma\,(3.4\sigma)$	-0.3σ	$+4.2\sigma$	0.003%	< 0.54 (0.62)	$0.00^{+0.23}_{-0.00}$
2^+_{h7}	any	$4.0\sigma\,(4.2\sigma)$	$+0.6\sigma$	$+3.5\sigma$	0.032%	< 0.70 (0.47)	$0.17^{+0.28}_{-0.17}$
2^-_h	any	$4.2\sigma\,(4.6\sigma)$	-0.2σ	$+4.8\sigma$	$< 0.001\%$	< 0.48 (0.43)	$0.04^{+0.21}_{-0.04}$
2^-_{h9}	any	$2.2\sigma\,(2.1\sigma)$	-0.6σ	$+2.9\sigma$	0.57%	< 0.69 (0.89)	$0.00^{+0.27}_{-0.00}$
2^-_{h10}	any	$3.9\sigma\,(4.0\sigma)$	$+0.1\sigma$	$+4.3\sigma$	0.002%	< 0.61 (0.54)	$0.08^{+0.30}_{-0.08}$

$X \to WW \to \ell\nu\ell\nu$ decay channels together are presented in this section. The assumption made is that the same tensor structure for the interactions appears in both XZZ and XWW couplings, as outlined for spin-two models in Table II.

Since only isolated tensor structure terms, and not the interference between them, are tested, the relationship between the absolute strengths of those couplings is not important and is not used in the analysis. Therefore, the combined spin-one exclusion of pure 1^- and 1^+ states is tested, and for spin-two models the ten hypotheses listed in Table II are tested. The combination of the $f(J^P)$ results is not considered here because the relative strength between the two channels is left unconstrained and the fractions remain independent measurements.

The $q\bar{q}$ production mechanism is tested for spin-one and spin-two models, and gluon fusion is tested for spin-two models. The combination of an arbitrary admixture of the $q\bar{q}$ and gluon production mechanisms is also tested. These results are based on the channels presented in Secs. V A and V B. For several of the models some production mechanisms have been tested already [11,12,14].

In the spin-one studies, an example of the distribution of the test statistic and observed value in the case of the SM Higgs boson along with the spin-one 1^+ hypothesis is shown in Fig. 16. The expected and observed separations

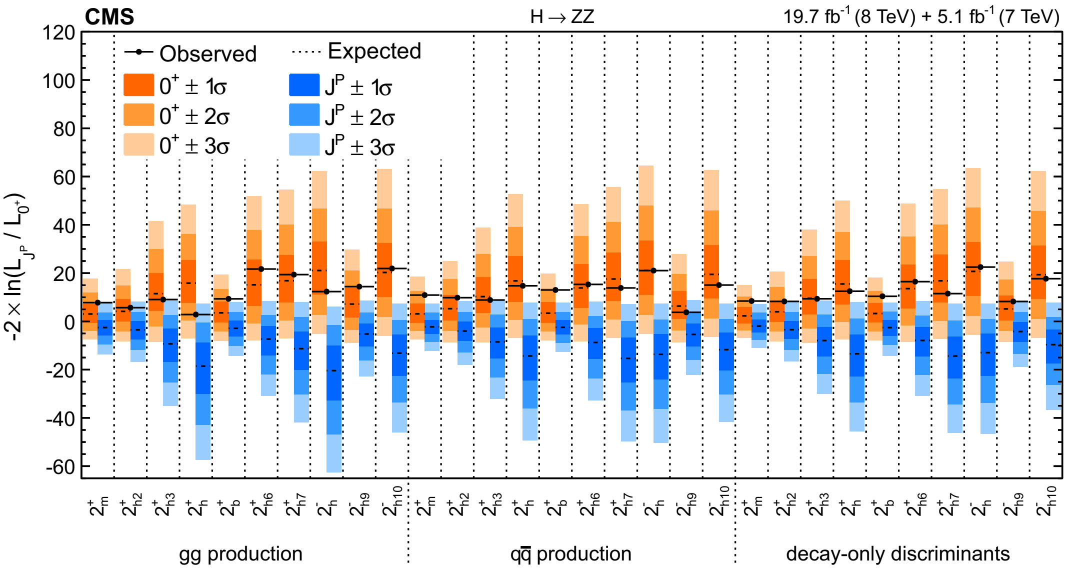

FIG. 9 (color online). Distributions of the test statistic $q = -2\ln(\mathcal{L}_{J^P}/\mathcal{L}_{0^+})$ for the spin-two J^P models tested against the SM Higgs boson hypothesis in the $X \to ZZ$ analyses. The expected median and the 68.3%, 95.4%, and 99.7% C.L. regions for the SM Higgs boson (orange, the left for each model) and for the alternative J^P hypotheses (blue, right) are shown. The observed q values are indicated by the black dots.

from the test statistic distributions are summarized in Table XI. In the case of the spin-two studies, the distributions of the test statistic and observed value in the case of the SM Higgs boson along with the spin-two hypotheses $gg \to X(2^+_{h2})$ and $gg \to X(2^+_m)$ are shown in Figs. 16 (bottom) and 17 (left). All the spin-one and spin-two models tested in the combination are summarized in Fig. 18.

The expected separations between the test statistic distributions for all the models considered are summarized in Table XI. In all cases, the expected separation between the alternative signal hypotheses is quoted for the case where the expected SM Higgs boson signal strength and the alternative signal cross sections are obtained in the fit of the data. The signal strengths in the $X \to ZZ$ and $X \to WW$ channels are fit independently. The expected separation is also quoted for the case where the events are generated with the SM expectation for the signal cross section ($\mu = 1$).

These tests are performed for several choices of the ratio of the two production rates $f(q\bar{q})$. The analysis, which uses information from the $X \to ZZ \to 4\ell$ decay channel, is performed in a production-independent way, unless

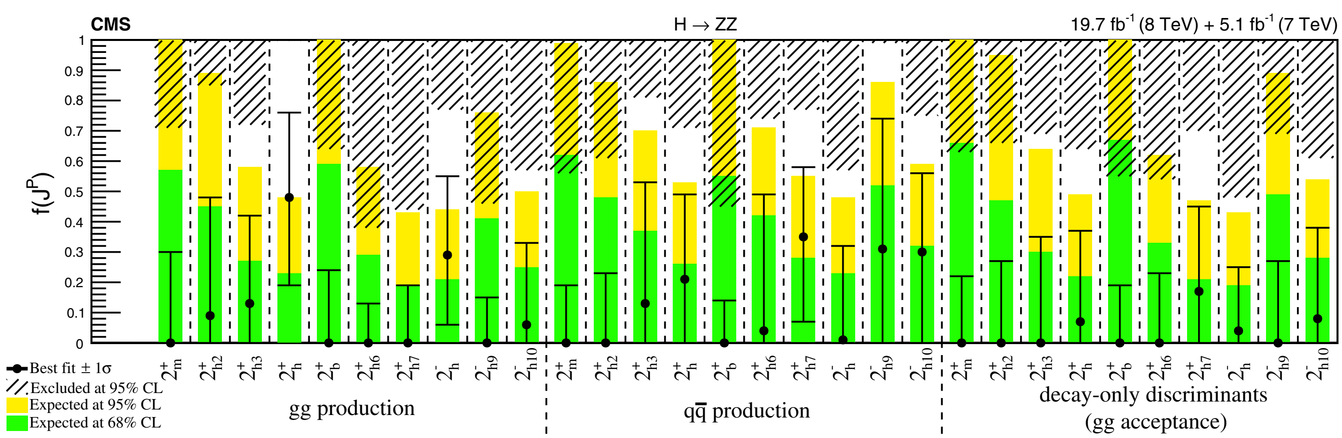

FIG. 10 (color online). Summary of the $f(J^P)$ constraints for the spin-two models from Table VIII, where the decay-only measurements are performed using the efficiency of the $gg \to X \to ZZ$ selection. The expected 68% and 95% C.L. regions are shown as the green and yellow bands. The observed constraints at 68% and 95% C.L. are shown as the points with error bars and the excluded hatched regions.

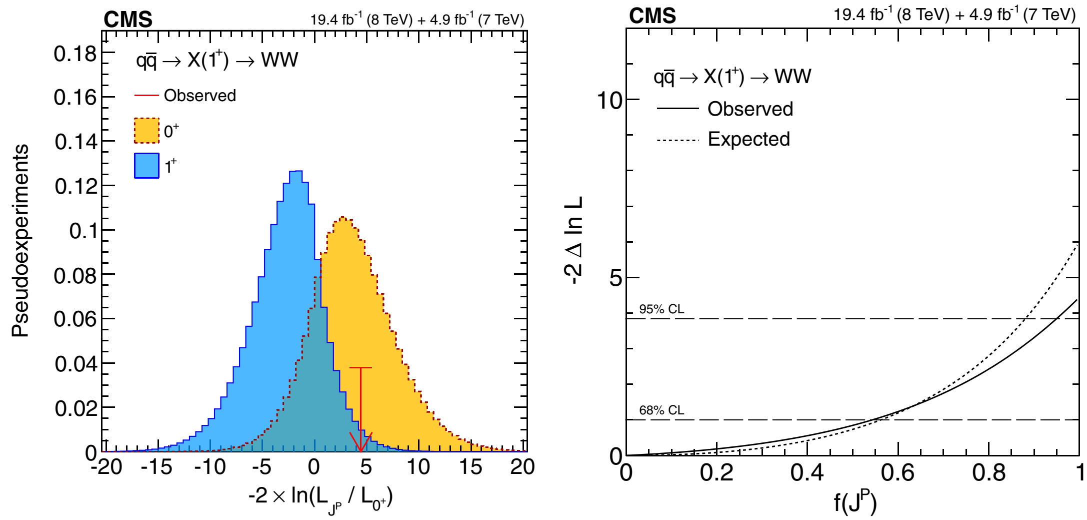

FIG. 11 (color online). (left) Distributions of the test statistic $q = -2\ln(\mathcal{L}_{J^P}/\mathcal{L}_{0^+})$ for the $J^P = 1^+$ hypothesis of $q\bar{q} \to X(1^+) \to WW$ against the SM Higgs boson hypothesis (0^+). The expectation for the SM Higgs boson is represented by the yellow histogram on the right and the alternative J^P hypothesis by the blue histogram on the left. The red arrow indicates the observed q value. (right) Observed value of $-2\Delta\ln\mathcal{L}$ as a function of $f(J^P)$ and the expectation in the SM for the $q\bar{q} \to X(1^+) \to WW$ alternative J^P model.

$f(q\bar{q}) = 0$ or 1. Part of the analysis, which is based on the $X \to WW \to \ell\nu\ell\nu$ decay channel, tests several choices of the $f(q\bar{q})$ ratio explicitly. An example of such a test is shown in Fig. 17 (right). For the combined $X \to ZZ$ and WW analysis, as in the case of the $X \to WW$ analysis, the results with gluon fusion ($f(q\bar{q}) = 0$) and with $q\bar{q}$ production ($f(q\bar{q}) = 1$) exhibit the largest and the smallest observed separation when compared to any other value in the scan of $0 < f(q\bar{q}) < 1$. The data disfavor all the spin-one and spin-two hypotheses tested in favor of the SM hypothesis $J^P = 0^+$ with $1 - CL_s$ values larger than 98% C.L. (Table XI).

D. Combined exotic-spin results with the $H \to ZZ$, WW, and $\gamma\gamma$ channels

In this analysis, the $X \to \gamma\gamma$ decay channel is studied only in the context of the exotic spin-two 2^+_m hypothesis. Several spin-two scenarios in Table II are only defined for

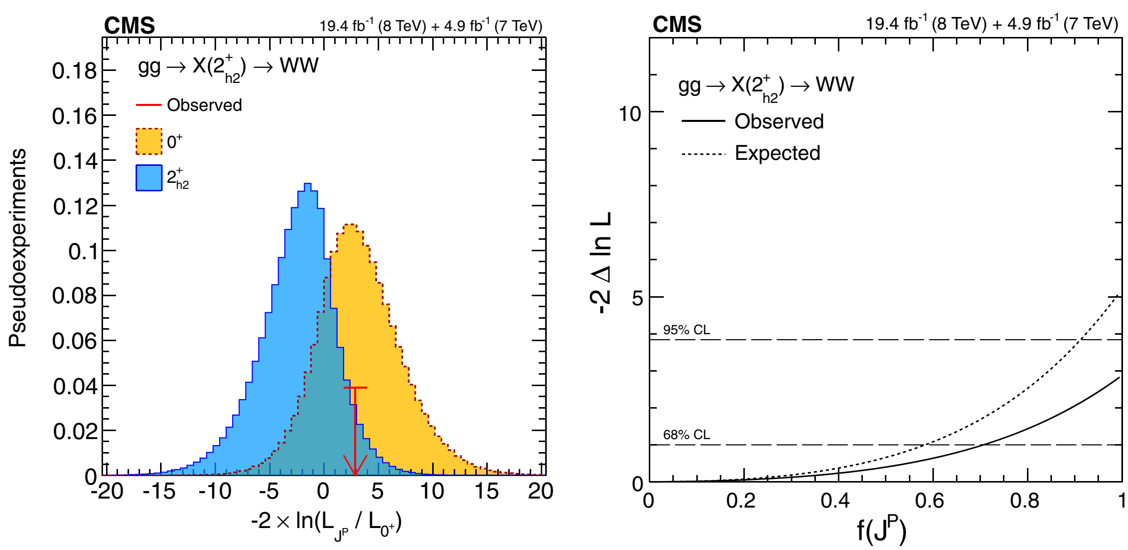

FIG. 12 (color online). (left) Distributions of the test statistic $q = -2\ln(\mathcal{L}_{J^P}/\mathcal{L}_{0^+})$ for the $J^P = 2^+_{h2}$ hypothesis of $gg \to X(2^+_{h2}) \to WW$ against the SM Higgs boson hypothesis (0^+). The expectation for the SM Higgs boson is represented by the yellow histogram on the right and the alternative J^P hypothesis by the blue histogram on the left. The red arrow indicates the observed q value. (right) Observed value of $-2\Delta\ln\mathcal{L}$ as a function of $f(J^P)$ and the expectation in the SM for the $gg \to X(2^+_{h2}) \to WW$ alternative J^P model.

TABLE IX. List of spin-one models tested in the $X \to WW$ analysis. The expected separation is quoted for two scenarios, for the signal production cross section obtained from the fit to data for each hypothesis, and using the SM expectation ($\mu = 1$). The observed separation shows the consistency of the observation with the SM Higgs boson model or the alternative J^P model, from which a CL_s value is derived. The constraints on the noninterfering J^P fraction are quoted in the last two columns.

$f_{b2}^{WW}(J^P)$ Model	J^P Production	Expected ($\mu = 1$)	Observed 0^+	Observed J^P	CL_s	$f(J^P)$ 95% C.L. Observed (Expected)	$f(J^P)$ Best fit
$0.0(1^-)$	$q\bar{q}$	$2.2\sigma\,(3.3\sigma)$	-0.1σ	$+2.5\sigma$	1.5%	< 0.88 (0.81)	$0.00^{+0.55}_{-0.00}$
0.5	$q\bar{q}$	$2.0\sigma\,(3.0\sigma)$	-0.2σ	$+2.2\sigma$	3.1%	< 0.93 (0.86)	$0.00^{+0.57}_{-0.00}$
$1.0(1^+)$	$q\bar{q}$	$1.8\sigma\,(2.7\sigma)$	-0.3σ	$+2.1\sigma$	4.1%	< 0.95 (0.88)	$0.00^{+0.54}_{-0.00}$

couplings to massive vector bosons and are not defined for $X \to \gamma\gamma$. Several of the remaining higher-dimension operators in the spin-two scenario are not considered here. However, the direct model-independent analysis of the $\cos\theta^*$ distribution can be performed [15,29]. The spin-one scenario of a resonance decaying to a two-photon final state is forbidden [67,68], and all spin-zero scenarios have an identical isotropic two-photon distribution in the rest frame of the boson. Therefore, the spin-zero and spin-one scenarios are not considered.

The individual 2_m^+ hypothesis test results in each channel were presented earlier [12,14,15] and the combined results are shown in Table XII. In Fig. 19 examples of the test statistic, $q = -2\ln(\mathcal{L}_{J^P}/\mathcal{L}_{0^+})$, are shown for various fractions of the $q\bar{q}$ production mechanism $f(q\bar{q})$. As a result, the 2_m^+ model is excluded with a 99.87% C.L. or higher for any combination of the gg and $q\bar{q}$ production mechanisms.

VI. STUDY OF SPIN-ZERO HVV COUPLINGS

Given the exclusion of the exotic spin-one and spin-two scenarios presented in Sec. V, detailed studies of HVV interactions under the assumption that the new boson is a

TABLE X. List of spin-two models tested in the $X \to WW$ analysis. The expected separation is quoted for two scenarios, for the signal production cross section obtained from the fit to data for each hypothesis, and using the SM expectation ($\mu = 1$). The observed separation shows the consistency of the observation with the SM Higgs boson or an alternative J^P model, from which the CL_s value is derived. The constraints on the noninterfering J^P fraction are quoted in the last two columns. Results from Ref. [14] are explicitly noted.

J^P Model	J^P Production	Expected ($\mu = 1$)	Observed 0^+	Observed J^P	CL_s	$f(J^P)$ 95% C.L. Observed (Expected)	$f(J^P)$ Best fit
2_m^+ [14]	gg	$1.8\sigma\,(2.9\sigma)$	$+0.6\sigma$	$+1.2\sigma$	16%	< 1.00 (0.87)	$0.50^{+0.42}_{-0.50}$
2_{h2}^+	gg	$1.7\sigma\,(2.6\sigma)$	0.0σ	$+1.6\sigma$	10%	< 1.00 (0.91)	$0.00^{+0.71}_{-0.00}$
2_{h3}^+	gg	$1.9\sigma\,(2.8\sigma)$	$+0.1\sigma$	$+1.9\sigma$	5.2%	< 0.99 (0.82)	$0.00^{+0.62}_{-0.00}$
2_h^+	gg	$0.7\sigma\,(1.3\sigma)$	$+0.1\sigma$	$+0.6\sigma$	52%	< 1.00 (1.00)	$0.13^{+0.87}_{-0.13}$
2_b^+	gg	$1.8\sigma\,(2.7\sigma)$	$+0.1\sigma$	$+1.7\sigma$	8.6%	< 1.00 (0.89)	$0.03^{+0.68}_{-0.03}$
2_{h6}^+	gg	$2.5\sigma\,(3.4\sigma)$	$+0.0\sigma$	$+2.6\sigma$	0.88%	< 0.81 (0.69)	$0.00^{+0.50}_{-0.00}$
2_{h7}^+	gg	$1.8\sigma\,(2.5\sigma)$	$+0.2\sigma$	$+1.7\sigma$	8.1%	< 1.00 (0.85)	$0.01^{+0.64}_{-0.01}$
2_h^-	gg	$1.2\sigma\,(2.3\sigma)$	-0.1σ	$+1.4\sigma$	19%	< 1.00 (1.00)	$0.00^{+0.78}_{-0.00}$
2_{h9}^-	gg	$1.4\sigma\,(2.5\sigma)$	-0.2σ	$+1.6\sigma$	12%	< 1.00 (1.00)	$0.00^{+0.66}_{-0.00}$
2_{h10}^-	gg	$2.0\sigma\,(3.3\sigma)$	$+0.4\sigma$	$+1.6\sigma$	7.8%	< 1.00 (0.85)	$0.36^{+0.46}_{-0.36}$
2_m^+ [14]	$q\bar{q}$	$2.7\sigma\,(3.9\sigma)$	-0.2σ	$+3.1\sigma$	0.25%	< 0.76 (0.68)	$0.00^{+0.45}_{-0.00}$
2_{h2}^+	$q\bar{q}$	$2.6\sigma\,(3.7\sigma)$	-0.4σ	$+3.3\sigma$	0.16%	< 0.66 (0.70)	$0.00^{+0.32}_{-0.00}$
2_{h3}^+	$q\bar{q}$	$2.3\sigma\,(3.3\sigma)$	-0.4σ	$+2.9\sigma$	0.56%	< 0.76 (0.75)	$0.00^{+0.40}_{-0.00}$
2_h^+	$q\bar{q}$	$1.6\sigma\,(2.3\sigma)$	-0.1σ	$+1.7\sigma$	8.8%	< 1.00 (0.95)	$0.00^{+0.67}_{-0.00}$
2_b^+	$q\bar{q}$	$2.8\sigma\,(3.8\sigma)$	-0.2σ	$+3.2\sigma$	0.18%	< 0.71 (0.68)	$0.00^{+0.38}_{-0.00}$
2_{h6}^+	$q\bar{q}$	$2.8\sigma\,(3.7\sigma)$	0.0σ	$+2.9\sigma$	0.41%	< 0.80 (0.70)	$0.00^{+0.52}_{-0.00}$
2_{h7}^+	$q\bar{q}$	$2.2\sigma\,(3.1\sigma)$	-0.2σ	$+2.5\sigma$	1.6%	< 0.85 (0.80)	$0.00^{+0.48}_{-0.00}$
2_h^-	$q\bar{q}$	$2.0\sigma\,(2.9\sigma)$	$+0.1\sigma$	$+1.9\sigma$	5.1%	< 1.00 (0.87)	$0.01^{+0.67}_{-0.01}$
2_{h9}^-	$q\bar{q}$	$2.0\sigma\,(2.9\sigma)$	$+0.2\sigma$	$+1.8\sigma$	6.2%	< 1.00 (0.86)	$0.10^{+0.64}_{-0.10}$
2_{h10}^-	$q\bar{q}$	$2.6\sigma\,(3.6\sigma)$	$+0.1\sigma$	$+2.5\sigma$	1.1%	< 0.90 (0.78)	$0.07^{+0.58}_{-0.07}$

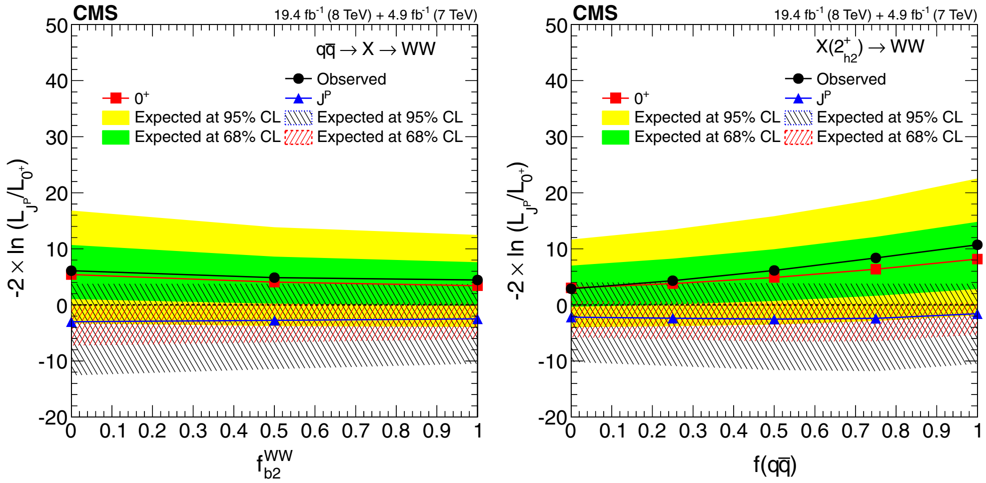

FIG. 13 (color online). (left) Distributions of the test statistic $q = -2\ln(\mathcal{L}_{J^P}/\mathcal{L}_{0^+})$ as a function of f_{b2}^{WW} for the hypothesis of the spin-one J^P models against the SM Higgs boson hypothesis in the $q\bar{q} \to X \to WW$ analysis. (right) Distribution of the test statistic $q = -2\ln(\mathcal{L}_{J^P}/\mathcal{L}_{0^+})$ as a function of $f(q\bar{q})$ for the 2^+_{h2} hypothesis against the SM Higgs boson hypothesis in the $H \to WW$ analysis. The median expectation for the SM Higgs boson is represented by the red squares with the green (68% C.L.) and yellow (95% C.L.) solid color regions and for the alternative J^P hypotheses by the blue triangles with the red (68% C.L.) and blue (95% C.L.) hatched regions. The observed values are indicated by the black dots.

spin-zero resonance are performed. The results are obtained following the techniques presented in Sec. IV.

First, constraints are applied on the presence of only one anomalous term in the HVV amplitude where the couplings are considered to be real. A summary of such results is presented in Table XIII and Fig. 20. The details of these and other measurements are presented in the following subsections, with further measurements considering simultaneously up to four fractions and phase parameters in several cases. The combination of the HZZ and HWW coupling measurements provides further constraints on the HVV interactions. All results are obtained with the template method, and the f_{a2} and f_{a3} measurements in HZZ interactions are also validated with the multidimensional distribution method.

A. Study of HZZ couplings with the $H \to ZZ \to 4\ell$ channel

The study of the anomalous HVV couplings starts with the test of three contributions to the HZZ interaction as

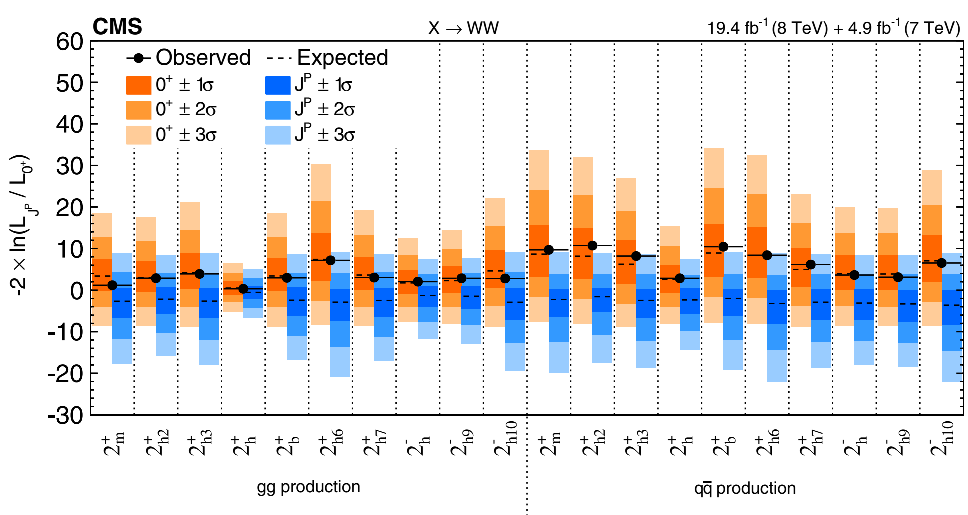

FIG. 14 (color online). Distribution of the test statistic $q = -2\ln(\mathcal{L}_{J^P}/\mathcal{L}_{0^+})$ for the spin-two J^P models tested against the SM Higgs boson hypothesis in the $X \to WW$ analyses. The expected median and the 68.3%, 95.4%, and 99.7% C.L. regions for the SM Higgs boson (orange, the left for each model) and for the alternative J^P hypotheses (blue, right) are shown. The observed q values are indicated by the black dots.

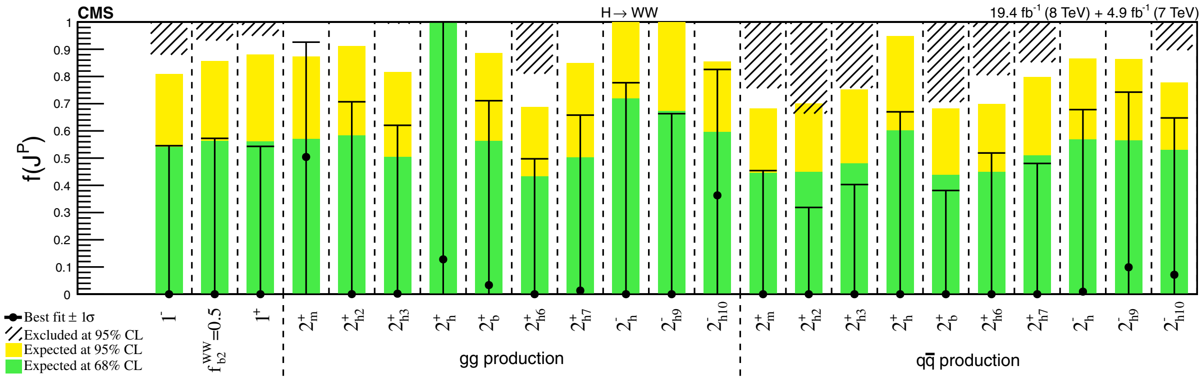

FIG. 15 (color online). Summary of the $f(J^P)$ constraints for the spin-one and spin-two models from Tables IX and X in the $X \to WW$ analyses. The expected 68% and 95% C.L. regions are shown as the green and yellow bands. The observed constraints at 68% and 95% C.L. are shown as the points with error bars and the excluded hatched regions.

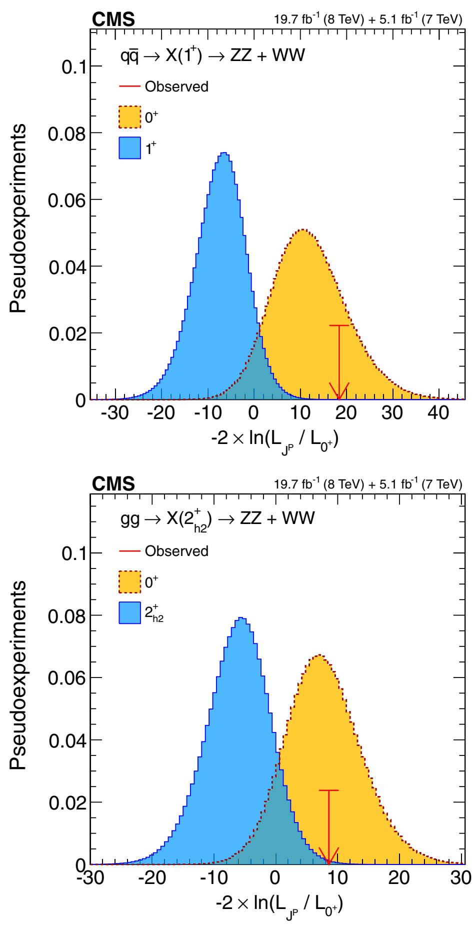

FIG. 16 (color online). Distributions of the test statistic $q = -2\ln(\mathcal{L}_{J^P}/\mathcal{L}_{0^+})$ in the combination of the $X \to ZZ$ and WW channels for the hypotheses of $q\bar{q} \to X(1^+)$ (top) and $gg \to X(2^+_{h2})$ (bottom) tested against the SM Higgs boson hypothesis. The expectation for the SM Higgs boson is represented by the yellow histogram on the bottom of each plot and the alternative J^P hypothesis by the blue histogram on the top. The red arrow indicates the observed q value.

shown in Eq. (1). Only real couplings are considered in this test, $\phi_{ai} = 0$ or π, where ϕ_{ai} generically refers to the phase of the coupling in question, such as $\phi_{\Lambda 1}$, ϕ_{a2}, or ϕ_{a3}. Since the expansion of terms in Eq. (1) is considered for small anomalous contributions, all other parameters are set to zero when the anomalous couplings of interest are considered. These constraints of real couplings and zero contribution from other terms are relaxed in further tests discussed below. In the template approach, the three sets of observables in each fit are given in Table VI. The only exception is in the $f_{\Lambda 1}$ measurement, where the usual interference discriminant does not provide additional information and instead the third observable is $\mathcal{D}_{0h+}$ to minimize the number of configurations also used for other studies. Since $\mathcal{D}_{0h+}$ does not bring additional information for this measurement, it is not reflected in Table VI.

The results of the likelihood function scan for the three parameters, $f_{ai}\cos\phi_{ai}$, are shown in Fig. 21 (left), where the $\cos\phi_{ai}$ term allows for a signed quantity with $\cos\phi_{ai} = -1$ or $+1$. The 68% and 95% C.L. intervals are shown in Table XIII. Using the transformation in Eq. (5), these results can be interpreted for the coupling parameters used in Eq. (1), as shown in Table XIV. Strong destructive interference of the SM and anomalous contributions at $f_{\Lambda 1}\cos(\phi_{\Lambda 1}) \sim +0.5$ or $f_{a2}\cos(\phi_{a2}) \sim -0.5$ leads to very different kinematic distributions and exclusions with high confidence levels. Additional features with multiple likelihood function maxima observed in the $f_{\Lambda 1}$ likelihood scan are due to the superposition of measurements in the $4e/4\mu$ and $2e2\mu$ channels, which have different maxima due to the interference between the leptons.

Next, two parameters f_{ai} and ϕ_{ai} are considered at the same time. For example, if the coupling is known to be either positive or negative, such a scenario is considered in Table XV. In this case, constraints are set on f_{ai} for a given phase value. More generally, one can allow ϕ_{ai} to be

TABLE XI. List of spin-one and spin-two models tested in the combination of the $X \to ZZ$ and $X \to WW$ channels. The combined expected separation is quoted for two scenarios, for the signal production cross section obtained from the fit to data for each hypothesis and using the SM expectation ($\mu = 1$). For comparison, the former expectations are also quoted for the individual channels as in Tables VII–X. The observed separation shows the consistency of the observation with the SM Higgs boson model or an alternative J^P model, from which the CL_s value is derived.

J^P Model	J^P Production	Expected $X \to ZZ$	Expected $X \to WW$	Expected ($\mu = 1$)	Observed 0^+	Observed J^P	CL_s
1^-	$q\bar{q}$	2.9σ	2.2σ	3.6σ (4.6σ)	-1.2σ	$+4.9\sigma$	$< 0.001\%$
1^+	$q\bar{q}$	2.4σ	1.8σ	3.0σ (3.8σ)	-0.8σ	$+4.3\sigma$	0.004%
2_m^+	gg	1.9σ	1.8σ	2.4σ (3.4σ)	-0.4σ	$+2.9\sigma$	0.53%
2_{h2}^+	gg	2.0σ	1.7σ	2.5σ (3.3σ)	-0.2σ	$+2.8\sigma$	0.52%
2_{h3}^+	gg	3.2σ	1.6σ	3.7σ (4.3σ)	$+0.4\sigma$	$+3.5\sigma$	0.031%
2_h^+	gg	3.8σ	0.7σ	3.8σ (4.2σ)	$+1.7\sigma$	$+2.1\sigma$	1.9%
2_b^+	gg	1.6σ	1.8σ	2.4σ (3.2σ)	-0.9σ	$+3.4\sigma$	0.16%
2_{h6}^+	gg	3.4σ	2.5σ	4.2σ (4.9σ)	-0.5σ	$> 5\sigma$	$< 0.001\%$
2_{h7}^+	gg	3.8σ	1.8σ	4.2σ (5.0σ)	-0.1σ	$+4.7\sigma$	$< 0.001\%$
2_h^-	gg	4.2σ	1.2σ	4.3σ (5.0σ)	$+1.0\sigma$	$+3.4\sigma$	0.039%
2_{h9}^-	gg	2.5σ	1.4σ	2.8σ (3.5σ)	-1.0σ	$+4.2\sigma$	0.009%
2_{h10}^-	gg	4.2σ	2.0σ	4.6σ (5.3σ)	$+0.1\sigma$	$+4.9\sigma$	$< 0.001\%$
2_m^+	$q\bar{q}$	1.7σ	2.7σ	3.1σ (4.3σ)	-1.0σ	$+4.5\sigma$	0.002%
2_{h2}^+	$q\bar{q}$	2.2σ	2.6σ	3.3σ (4.3σ)	-0.8σ	$+4.4\sigma$	0.002%
2_{h3}^+	$q\bar{q}$	3.1σ	2.6σ	3.8σ (4.5σ)	0.0σ	$+4.1\sigma$	0.005%
2_h^+	$q\bar{q}$	4.0σ	1.6σ	4.3σ (4.5σ)	$+0.2\sigma$	$+4.3\sigma$	0.002%
2_b^+	$q\bar{q}$	1.7σ	2.8σ	3.1σ (4.2σ)	-1.3σ	$+4.8\sigma$	$< 0.001\%$
2_{h6}^+	$q\bar{q}$	3.4σ	2.8σ	4.3σ (5.0σ)	-0.1σ	$+4.8\sigma$	$< 0.001\%$
2_{h7}^+	$q\bar{q}$	4.1σ	2.2σ	4.6σ (5.0σ)	$+0.3\sigma$	$+4.5\sigma$	$< 0.001\%$
2_h^-	$q\bar{q}$	4.3σ	2.0σ	4.7σ (5.2σ)	$+0.1\sigma$	$+5.0\sigma$	$< 0.001\%$
2_{h9}^-	$q\bar{q}$	2.4σ	2.0σ	3.1σ (3.8σ)	$+0.5\sigma$	$+2.7\sigma$	0.55%
2_{h10}^-	$q\bar{q}$	4.0σ	2.6σ	4.7σ (5.3σ)	$+0.5\sigma$	$+4.6\sigma$	$< 0.001\%$

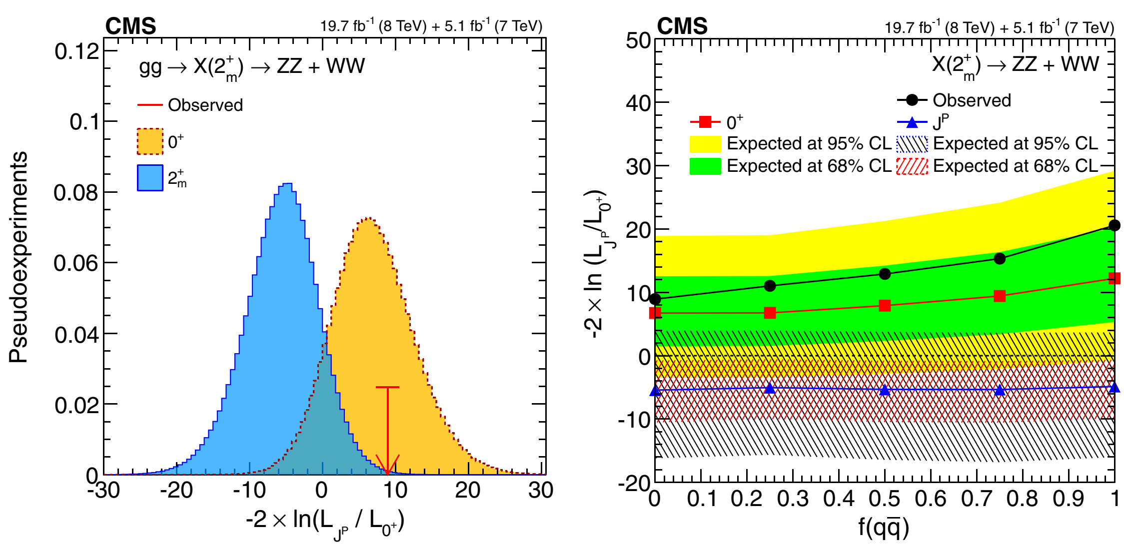

FIG. 17 (color online). (left) Distributions of the test statistic $q = -2\ln(\mathcal{L}_{J^P}/\mathcal{L}_{0^+})$ in the combination of the $X \to ZZ$ and WW channels for the hypothesis of $gg \to X(2_m^+)$ tested against the SM Higgs boson hypothesis. The expectation for the SM Higgs boson is represented by the yellow histogram on the right and the alternative J^P hypothesis by the blue histogram on the left. The red arrow indicates the observed q value. (right) Distribution of q as a function of $f(q\bar{q})$ for the 2_m^+ hypothesis against the SM Higgs boson hypothesis in the $X \to ZZ$ and WW channels. The median expectation for the SM Higgs boson is represented with the solid green (68% C.L.) and yellow (95% C.L.) regions. The alternative 2_m^+ hypotheses are represented by the blue triangles with the red (68% C.L.) and blue (95% C.L.) hatched regions. The observed values are indicated by the black dots.

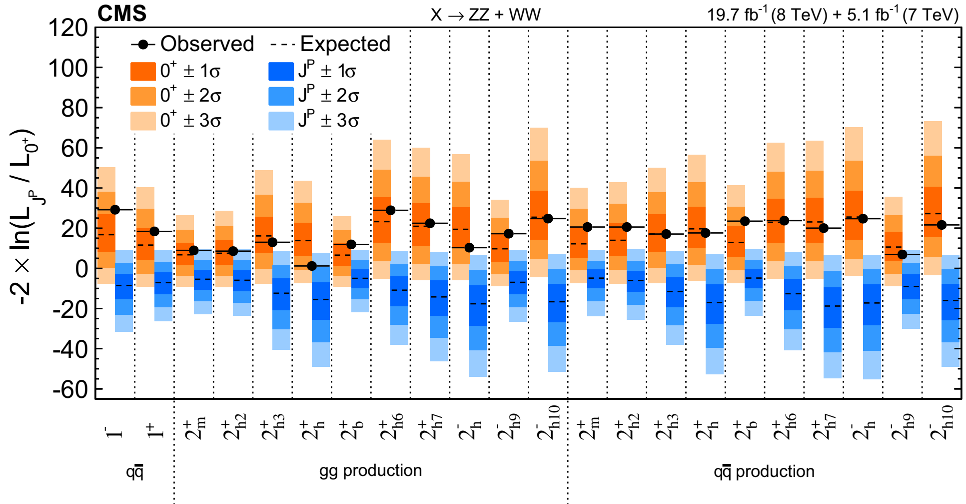

FIG. 18 (color online). Distributions of the test statistic $q = -2\ln(\mathcal{L}_{J^P}/\mathcal{L}_{0^+})$ for the spin-one and spin-two J^P models tested against the SM Higgs boson hypothesis in the combined $X \to ZZ$ and WW analyses. The expected median and the 68.3%, 95.4%, and 99.7% C.L. regions for the SM Higgs boson (orange, the left for each model) and for the alternative J^P hypotheses (blue, right) are shown. The observed q values are indicated by the black dots.

unconstrained, that is, to have any value between $-\pi$ and $+\pi$ with a generally complex coupling. Such a fit is performed for $f_{\Lambda 1}$ and f_{a2} using the same configuration, but with additional $\phi_{\Lambda 1}$ and ϕ_{a2} parameters in Eq. (21). The results with ϕ_{ai} unconstrained (any) are shown in Table XV as well. The f_{a3} measurement with ϕ_{a3} unconstrained is performed with a different technique and is presented in Ref. [12], where the $\mathcal{D}_{CP}$ observable is removed from the fit and the result becomes insensitive to the phase of the amplitude. This technique is adopted due to its simpler implementation and equivalent performance.

The next step in generalizing the constraints is to consider two anomalous contributions at the same time, both with and without the constraints that the couplings are real. Therefore, up to four parameters are considered at the same time: f_{ai}, ϕ_{ai}, f_{aj}, and ϕ_{aj}. Constraints on one parameter, when other parameters are left unconstrained in the full allowed parameter space, with $0 \le f_{ai} \le 1$, are presented in Table XV. Even though the expansion with only three anomalous contributions in Eq. (1) becomes incomplete when large values of $f_{ai} \sim 1$ are considered, this is still a valuable test of the consistency of the data with the SM. All of the above results, with phases fixed or unconstrained and with other anomalous couplings unconstrained, are shown in Fig. 21 (right). Some observed f_{ai} constraints appear to be tighter when compared to the one-parameter fits shown in Fig. 21 (left). This happens because the values of other profiled parameters are away from the SM expectation at the minimum of $-2\ln\mathcal{L}$, though still consistent with the SM. The expected constraints are always weaker with additional free parameters.

The above one-parameter measurements, with other couplings also considered to be unconstrained, are obtained from the fit configurations used for the two-parameter measurements shown in Fig. 22. Both options are considered, either with or without the assumption that the couplings are real. To keep the number of observables to the maximum of three, in the template approach, the following discriminants are used to set the

TABLE XII. Results of the study of the 2^+_m model for the combination of the $X \to ZZ$, WW, and $\gamma\gamma$ decay channels. The expected separation is quoted for the three channels separately and for the combination with the signal strength for each hypothesis determined from the fit to data independently in each channel. Also shown in parentheses is the expectation with the SM signal cross section ($\mu = 1$). The observed separation shows the consistency of the observation with the SM 0^+ model or J^P model and corresponds to the scenario where the signal strength is floating in the fit to data.

J^P Model	J^P Production	Expected $X \to ZZ$	Expected $X \to WW$	Expected $X \to \gamma\gamma$	Expected ($\mu = 1$)	Observed 0^+	Observed J^P	CL_s
2^+_m	gg	1.9σ	1.8σ	1.6σ	3.0σ (3.7σ)	-0.2σ	$+3.3\sigma$	0.13%
2^+_m	$q\bar{q}$	1.7σ	2.7σ	1.2σ	3.3σ (4.4σ)	-0.9σ	$+4.7\sigma$	0.001%

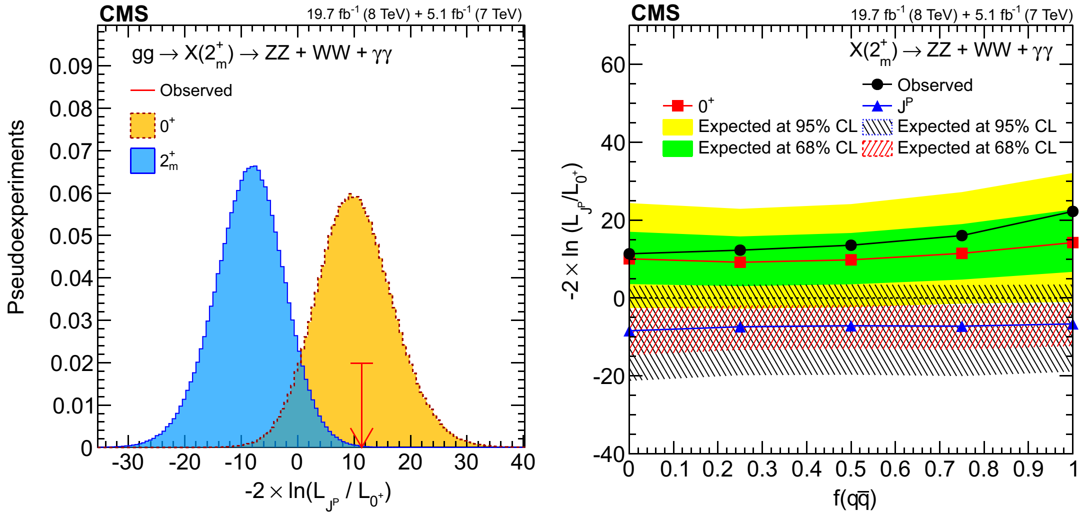

FIG. 19 (color online). (left) Distributions of the test statistic $q = -2\ln(\mathcal{L}_{J^P}/\mathcal{L}_{0^+})$ in the combination of the $X \to ZZ, WW$, and $\gamma\gamma$ channels for the hypothesis of $gg \to X(2^+_m)$ tested against the SM Higgs boson hypothesis (0^+). The expectation for the SM Higgs boson is represented by the yellow histogram on the right and the alternative J^P hypothesis by the blue histogram on the left. The red arrow indicates the observed q value. (right) Distributions of the test statistic $q = -2\ln(\mathcal{L}_{J^P}/\mathcal{L}_{0^+})$ as a function of $f(q\bar{q})$ for the hypotheses of the 2^+_m model tested against the SM Higgs boson hypothesis in the $X \to ZZ, WW$, and $\gamma\gamma$ channels. The median expectation for the SM Higgs boson is represented with the solid green (68% C.L.) and yellow (95% C.L.) regions. The alternative 2^+_m hypotheses are represented by the blue triangles with the red (68% C.L.) and blue (95% C.L.) hatched regions. The observed values are indicated by the black dots.

constraints, ($\mathcal{D}_{\rm bkg}$, $\mathcal{D}_{\Lambda1}$, $\mathcal{D}_{0h+}$), ($\mathcal{D}_{\rm bkg}$, $\mathcal{D}_{\Lambda1}$, $\mathcal{D}_{0-}$), and ($\mathcal{D}_{\rm bkg}$, $\mathcal{D}_{0-}$ or $\mathcal{D}_{0h+}$), for the measurements of $f_{\Lambda1}$ vs. f_{a2}, $f_{\Lambda1}$ vs. f_{a3}, and f_{a2} vs. f_{a3}, respectively. The left set of plots in Fig. 22 shows constraints on two real couplings, and the right set of plots in Fig. 22 shows constraints on two couplings that are allowed to have any complex phase. Similarly to the one-parameter constraints, the allowed 95% C.L. regions are formally defined using the profile likelihood function ($-2\Delta\ln\mathcal{L} = 5.99$). The results in Table XV are obtained from these two-parameter likelihood scans by profiling one parameter.

TABLE XIII. Summary of allowed 68% C.L. (central values with uncertainties) and 95% C.L. (ranges in square brackets) intervals on anomalous coupling parameters in HVV interactions under the assumption that all the coupling ratios are real ($\phi^{VV}_{ai} = 0$ or π). The ranges are truncated at the physical boundaries of $f^{VV}_{ai} = 1$. The last column indicates the observed (expected) confidence level of a pure anomalous coupling corresponding to $f^{VV}_{ai} = 1$ when compared to the SM expectation $f^{VV}_{ai} = 0$. The expected results are quoted for the SM signal production cross section ($\mu = 1$). The results are obtained with the template method.

Parameter	Observed	Expected	$f^{VV}_{ai} = 1$
$f_{\Lambda1}\cos(\phi_{\Lambda1})$	$0.22^{+0.10}_{-0.16}$ $[-0.25, 0.37]$	$0.00^{+0.16}_{-0.87}$ $[-1.00, 0.27]\cup[0.92, 1.00]$	1.1% (16%)
$f_{a2}\cos(\phi_{a2})$	$0.00^{+0.41}_{-0.06}$ $[-0.66, -0.57]\cup[-0.15, 1.00]$	$0.00^{+0.38}_{-0.08}$ $[-0.18, 1.00]$	5.2% (5.0%)
$f_{a3}\cos(\phi_{a3})$	$0.00^{+0.14}_{-0.11}$ $[-0.40, 0.43]$	$0.00^{+0.33}_{-0.33}$ $[-0.70, 0.70]$	0.02% (0.41%)
$f^{WW}_{\Lambda1}\cos(\phi^{WW}_{\Lambda1})$	$0.21^{+0.18}_{-1.21}$ $[-1.00, 1.00]$	$0.00^{+0.34}_{-1.00}$ $[-1.00, 0.41]\cup[0.49, 1.00]$	78% (67%)
$f^{WW}_{a2}\cos(\phi^{WW}_{a2})$	$-0.02^{+1.02}_{-0.16}$ $[-1.00, -0.54]\cup[-0.29, 1.00]$	$0.00^{+1.00}_{-0.12}$ $[-1.00, -0.58]\cup[-0.22, 1.00]$	42% (46%)
$f^{WW}_{a3}\cos(\phi^{WW}_{a3})$	$-0.03^{+1.03}_{-0.97}$ $[-1.00, 1.00]$	$0.00^{+1.00}_{-1.00}$ $[-1.00, 1.00]$	34% (49%)
$f^{Z\gamma}_{\Lambda1}\cos(\phi^{Z\gamma}_{\Lambda1})$	$-0.27^{+0.34}_{-0.49}$ $[-1.00, 1.00]$	$0.00^{+0.83}_{-0.53}$ $[-1.00, 1.00]$	26% (16%)
$f^{Z\gamma}_{a2}\cos(\phi^{Z\gamma}_{a2})$	$0.00^{+0.14}_{-0.20}$ $[-0.49, 0.46]$	$0.00^{+0.51}_{-0.51}$ $[-0.78, 0.79]$	$< 0.01\%$ (0.01%)
$f^{Z\gamma}_{a3}\cos(\phi^{Z\gamma}_{a3})$	$0.02^{+0.21}_{-0.13}$ $[-0.40, 0.51]$	$0.00^{+0.51}_{-0.51}$ $[-0.75, 0.75]$	$< 0.01\%(< 0.01\%)$
$f^{\gamma\gamma}_{a2}\cos(\phi^{\gamma\gamma}_{a2})$	$0.12^{+0.20}_{-0.11}$ $[-0.04, +0.51]$	$0.00^{+0.11}_{-0.09}$ $[-0.32, 0.34]$	$< 0.01\%(< 0.01\%)$
$f^{\gamma\gamma}_{a3}\cos(\phi^{\gamma\gamma}_{a3})$	$-0.02^{+0.06}_{-0.13}$ $[-0.35, 0.32]$	$0.00^{+0.15}_{-0.11}$ $[-0.37, 0.40]$	$< 0.01\%(< 0.01\%)$

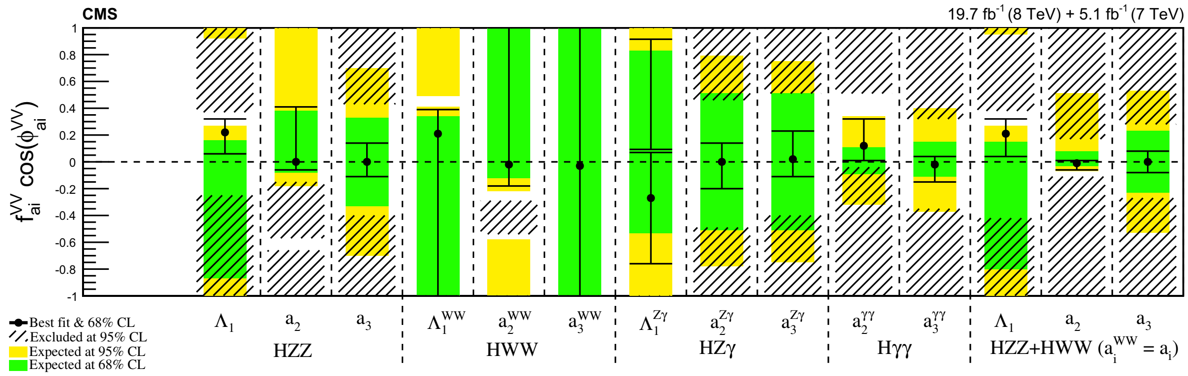

FIG. 20 (color online). Summary of allowed confidence level intervals on anomalous coupling parameters in HVV interactions under the assumption that all the coupling ratios are real ($\phi_{ai}^{VV} = 0$ or π). The expected 68% and 95% C.L. regions are shown as the green and yellow bands. The observed constraints at 68% and 95% C.L. are shown as the points with errors and the excluded hatched regions. In the case of the $f_{\Lambda 1}^{Z\gamma}$ measurement, there are two minima and two 68% C.L. intervals, while only one global minimum is indicated with a point. The combination of the HZZ and HWW measurements is presented, assuming the symmetry $a_i = a_i^{WW}$, including $R_{ai} = 0.5$.

Overall, all anomalous HZZ couplings are found to be consistent with zero, which is also consistent with the expectation from the SM where these couplings are expected to be very small, well below the current sensitivity.

B. Validation of the HZZ measurements

It has been shown that the template method with a small set of optimal observables and the multidimensional distribution method are expected to produce equivalent results [31]. Nonetheless, this is validated explicitly with a

TABLE XIV. Summary of the allowed 95% C.L. intervals on the anomalous couplings in HZZ interactions using results in Table XIII. The coupling ratios are assumed to be real [including $\cos(\phi_{\Lambda_1}) = 0$ or π].

Parameter	Observed	Expected
$(\Lambda_1\sqrt{\lvert a_1\rvert})\cos(\phi_{\Lambda_1})$	$[-\infty, -119\text{ GeV}] \cup [104\text{ GeV}, \infty]$	$[-\infty, 50\text{ GeV}] \cup [116\text{ GeV}, \infty]$
a_2/a_1	$[-2.28, -1.88] \cup [-0.69, \infty]$	$[-0.77, \infty]$
a_3/a_1	$[-2.05, 2.19]$	$[-3.85, 3.85]$

TABLE XV. Summary of the allowed 68% C.L. (central values with uncertainties) and 95% C.L. (ranges in square brackets) intervals on anomalous coupling parameters in the HZZ interactions under the condition of a given phase of the coupling (0 or π) or when the phase or other parameters are unconstrained (any value allowed). Results are presented with the template method and expectations are quoted in parentheses following the observed values. The results for f_{a3} with ϕ_{a3} unconstrained are from Ref. [12].

Measurement	$f_{\Lambda 1}$	f_{a2}	f_{a3}
$\phi_{ai} = 0$	$0.22^{+0.10}_{-0.16}$ [0.00, 0.37]	$0.00^{+0.42}_{-0.00}$ [0.00, 1.00]	$0.00^{+0.14}_{-0.00}$ [0.00, 0.43]
	($0.00^{+0.16}_{-0.00}$ [0.00, 0.27] ∪ [0.92, 1.00])	($0.00^{+0.35}_{-0.00}$ [0.00, 1.00])	($0.00^{+0.33}_{-0.00}$ [0.00, 0.70])
$\phi_{ai} = \pi$	$0.00^{+0.08}_{-0.00}$ [0.00, 0.82]	$0.00^{+0.06}_{-0.00}$ [0.00, 0.15] ∪ [0.56, 0.68]	$0.00^{+0.11}_{-0.00}$ [0.00, 0.40]
	($0.00^{+0.87}_{-0.00}$ [0.00, 1.00])	($0.00^{+0.08}_{-0.00}$ [0.00, 0.18] ∪ [0.62, 0.73])	($0.00^{+0.32}_{-0.00}$ [0.00, 0.70])
any ϕ_{ai}	$0.39^{+0.16}_{-0.31}$ [0.00, 0.57]	$0.32^{+0.28}_{-0.32}$ [0.00, 1.00]	$0.00^{+0.17}_{-0.00}$ [0.00, 0.47]
	($0.00^{+0.85}_{-0.00}$ [0.00, 1.00])	($0.00^{+0.59}_{-0.00}$ [0.00, 1.00])	($0.00^{+0.40}_{-0.00}$ [0.00, 0.74])
any $\phi_{ai}, f_{\Lambda 1}, \phi_{\Lambda 1}$		$0.11^{+0.16}_{-0.11}$ [0.00, 0.65]	$0.00^{+0.02}_{-0.00}$ [0.00, 0.19]
		($0.00^{+0.72}_{-0.00}$ [0.00, 1.00])	($0.00^{+0.52}_{-0.00}$ [0.00, 0.84])
any $\phi_{ai}, f_{a2}, \phi_{a2}$	$0.28^{+0.21}_{-0.15}$ [0.00, 0.63]		$0.00^{+0.15}_{-0.00}$ [0.00, 0.54]
	($0.00^{+0.85}_{-0.00}$ [0.00, 1.00])		($0.00^{+0.42}_{-0.00}$ [0.00, 0.81])
any $\phi_{ai}, f_{a3}, \phi_{a3}$	$0.42^{+0.09}_{-0.33}$ [0.00, 0.57]	$0.28^{+0.29}_{-0.28}$ [0.00, 0.97]	
	($0.00^{+0.86}_{-0.00}$ [0.00, 1.00])	($0.00^{+0.59}_{-0.00}$ [0.00, 1.00])	

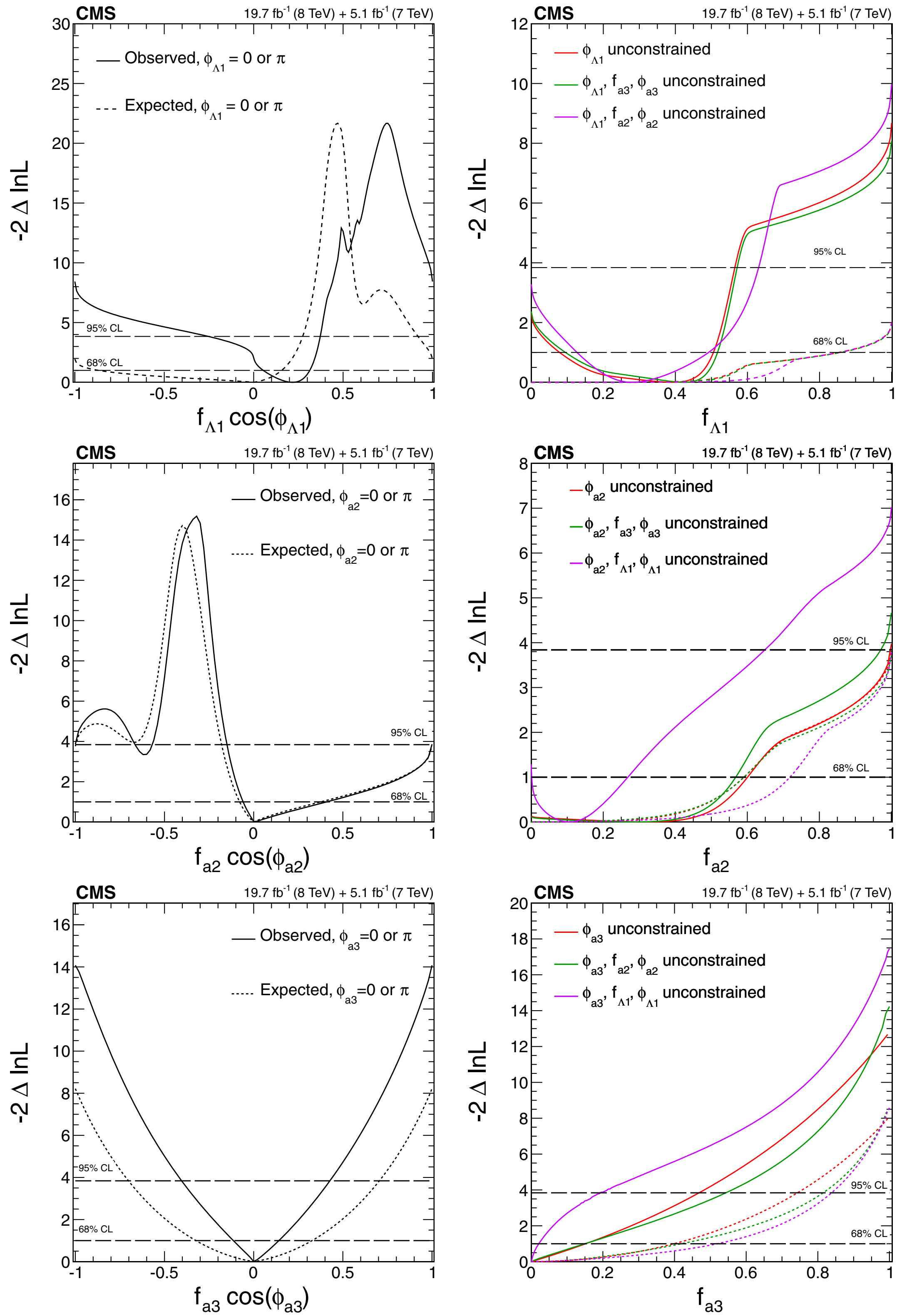

FIG. 21 (color online). Expected (dashed line) and observed (solid line) likelihood scans using the template method for the effective fractions $f_{\Lambda 1}$, f_{a2}, f_{a3} (from top to bottom) describing HZZ interactions. Plots on the left show the results when the couplings studied are constrained to be real and all other couplings are fixed to the SM predictions. The $\cos\phi_{ai}$ term allows a signed quantity where $\cos\phi_{ai} = -1$ or $+1$. Plots on the right show the results where the phases of the anomalous couplings and additional HZZ couplings are left unconstrained, as indicated in the legend. The f_{a3} result with ϕ_{a3} unconstrained (in the bottom-right plot) is from Ref. [12].

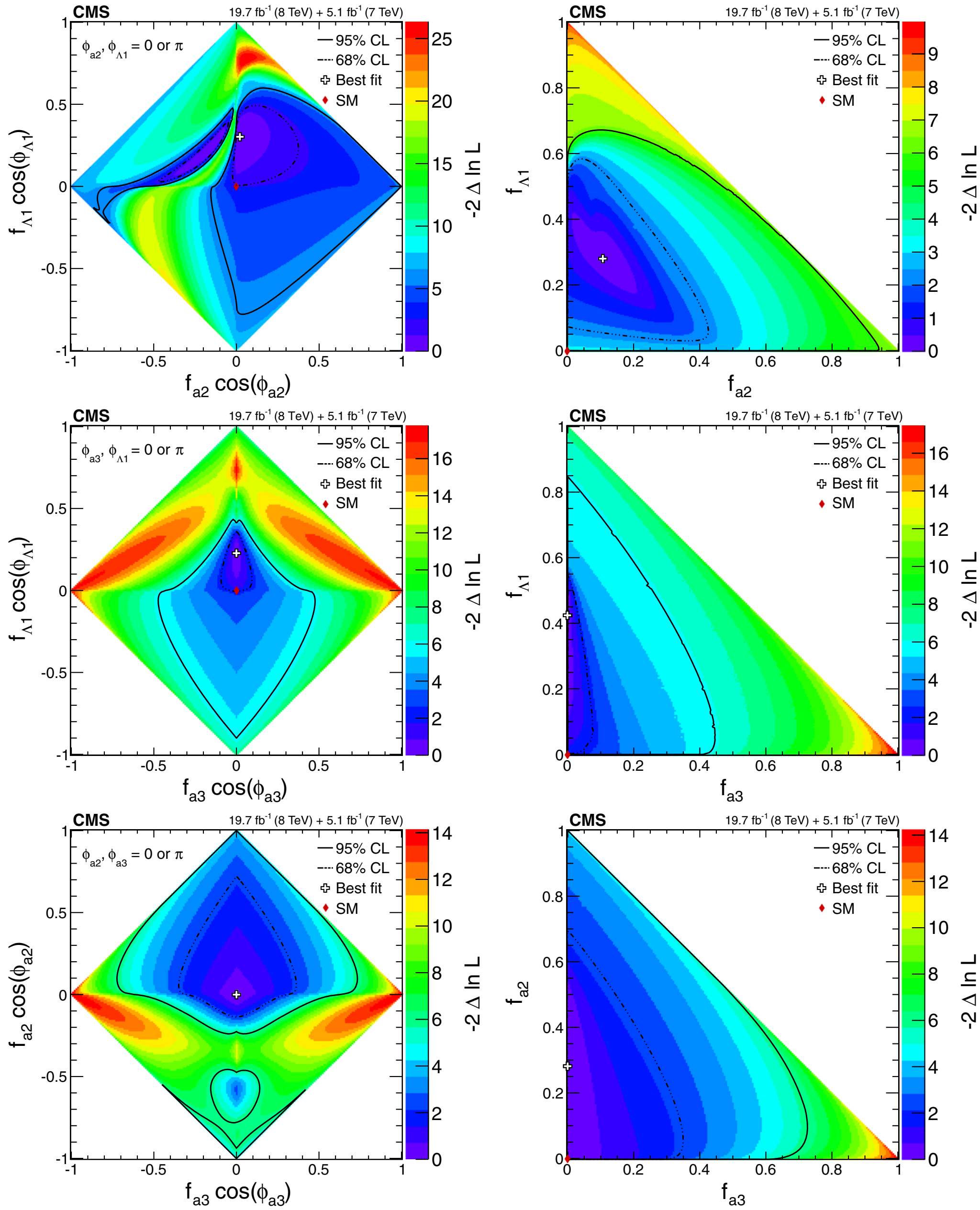

FIG. 22 (color online). Observed likelihood scans using the template method for pairs of effective fractions $f_{\Lambda 1}$ vs. f_{a2}, $f_{\Lambda 1}$ vs. f_{a3}, and f_{a2} vs. f_{a3} (from top to bottom) describing HZZ interactions. Plots on the left show the results when the couplings studied are constrained to be real and all other couplings are fixed to the SM predictions. Plots on the right show the results when the phases of the anomalous couplings are left unconstrained. The SM expectations correspond to points (0,0) and the best fit values are shown with the crosses. The confidence level intervals are indicated by the corresponding $-2\Delta \ln \mathcal{L}$ contours.

subset of the above HZZ measurements. The multidimensional distribution method has been applied to the study of the f_{a2} and f_{a3} parameters, as shown in Table XVI. Figure 23 shows the expected and observed likelihood scans for the effective fractions f_{a2} and f_{a3} under the assumption of real couplings for both the template and multidimensional distribution methods. The two methods have a compatible expected performance and the differences are within the systematic uncertainties of the

TABLE XVI. Summary of the allowed 95% C.L. intervals on the anomalous coupling parameters in HZZ interactions under the assumption that all the coupling ratios are real ($\phi_{ai} = 0$ or π) using the multidimensional distribution method. These results cross-check those presented in Table XIII.

Parameter	Observed	Expected
$f_{a2}\cos(\phi_{a2})$	$[-0.14, 1.00]$	$[-0.18, 0.97]$
$f_{a3}\cos(\phi_{a3})$	$[-0.44, 0.40]$	$[-0.67, 0.67]$

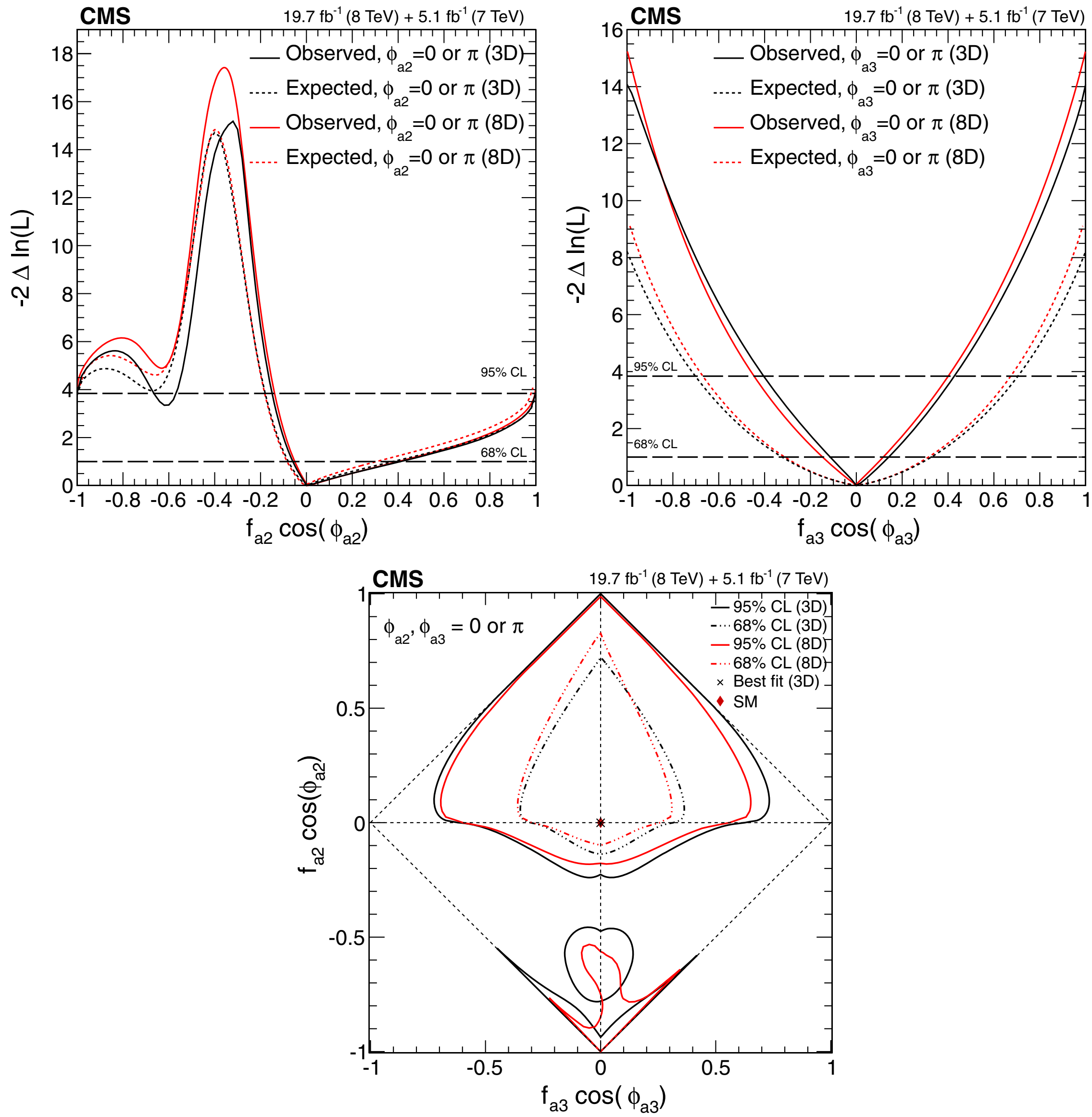

FIG. 23 (color online). Expected (dashed line) and observed (solid line) likelihood scans for f_{a2} (top left) and f_{a3} (top right), and observed likelihood scan for the f_{a2} vs. f_{a3} fractions (bottom), obtained using the template method (3D, black line) and the multidimensional distribution method (8D, red line) in the study of anomalous HZZ interactions. The couplings are constrained to be real.

methods. The observed constraints are not expected to produce identical results because of the incomplete overlap of the data, which is due to the slightly different selection requirement on $m_{4\ell}$. Also, statistical variations occur because of the different parametrization of observables. The two methods provide consistent results.

C. Study of $HZ\gamma$ and $H\gamma\gamma$ couplings with the $H \to VV \to 4\ell$ channel

In the following, constraints on anomalous $HZ\gamma$ and $H\gamma\gamma$ interactions are obtained using the $H \to VV \to 4\ell$ data. Five anomalous couplings are considered, following Eq. (1) and Table VI, where the three observables for each measurement are listed. Only real couplings, $\phi_{ai} = 0$ or π, are considered in this test. The results of the likelihood function scan for the three parameters, $f_{ai} \cos\phi_{ai}$, are shown in Fig. 24, following the same formalism presented for the HZZ couplings in Sec. VI A. The 68% and 95% C.L. intervals are shown in Table XIII. In the case of the $f_{\Lambda1}^{Z\gamma}$ measurement, there are two minima and only one central value with its 68% C.L. interval shown in Table XIII, while both 68% C.L. intervals are presented in Fig. 20.

Using the transformation in Eq. (5), these results can be interpreted in terms of the coupling parameters used in Eq. (1) as shown in Table XVII. The ratio

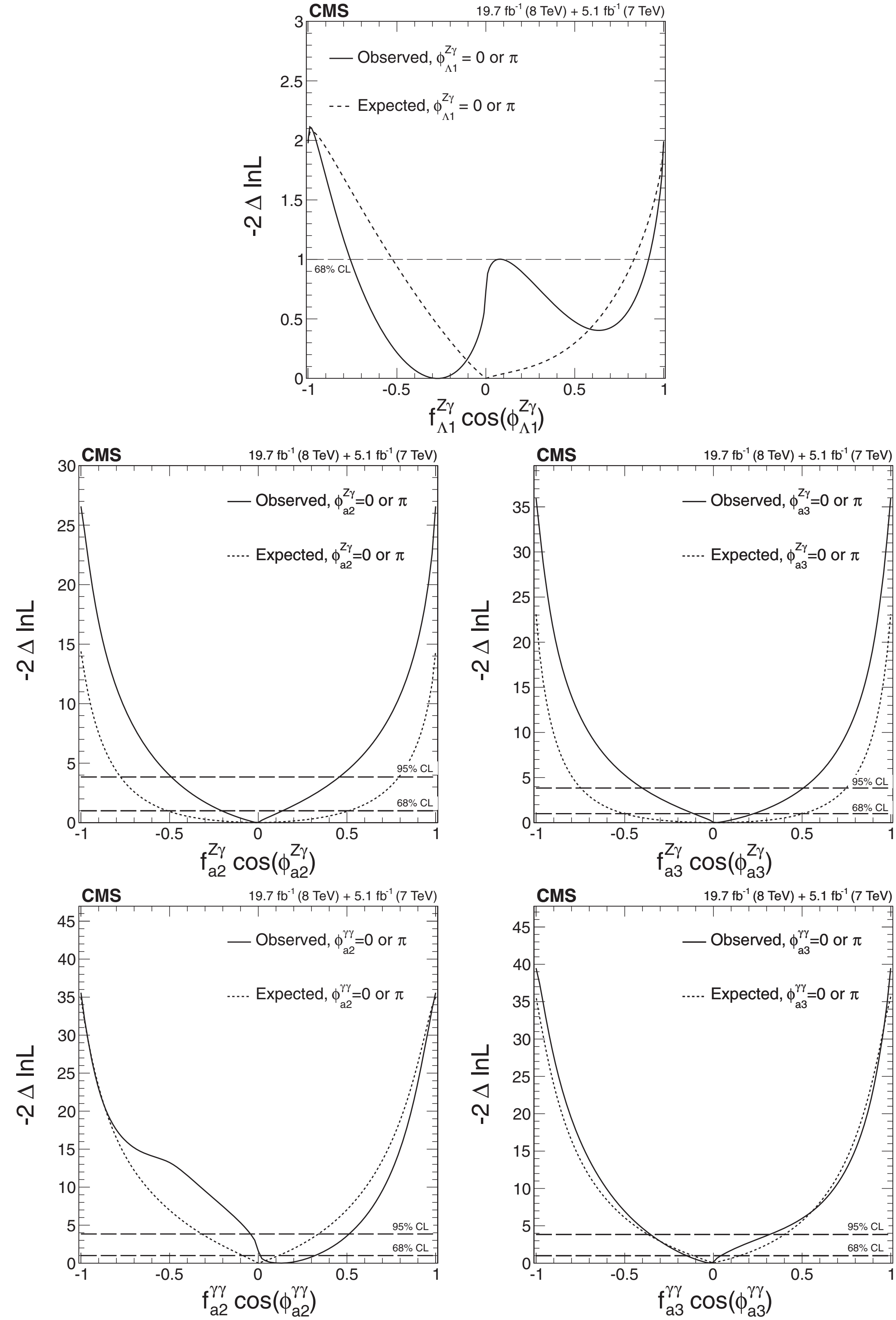

FIG. 24. Expected (dashed line) and observed (solid line) likelihood scans using the template method for the effective fractions $f^{Z\gamma}_{\Lambda1}$ (top), $f^{Z\gamma}_{a2}$ (middle left), $f^{Z\gamma}_{a3}$ (middle right), $f^{\gamma\gamma}_{a2}$ (bottom left), and $f^{\gamma\gamma}_{a3}$ (bottom right). The couplings studied are constrained to be real and all other couplings are fixed to the SM predictions. The $\cos\phi^{VV}_{ai}$ term allows a signed quantity where $\cos\phi^{VV}_{ai} = -1$ or $+1$.

TABLE XVII. Summary of the allowed 95% C.L. intervals on the anomalous couplings in $HZ\gamma$ and $H\gamma\gamma$ interactions using results obtained with the template method in Table XIII. The coupling ratios are assumed to be real [$\cos(\phi_{ai}^{VV}) = 0$ or π].

Parameter	Observed	Expected
$(\Lambda_1^{Z\gamma}\sqrt{\lvert a_1\rvert})\cos(\phi_{\Lambda_1}^{Z\gamma})$	$[-\infty, +\infty]$	$[-\infty, +\infty]$
$a_2^{Z\gamma}/a_1$	$[-0.046, 0.044]$	$[-0.089, 0.092]$
$a_3^{Z\gamma}/a_1$	$[-0.042, 0.053]$	$[-0.090, 0.090]$
$a_2^{\gamma\gamma}/a_1$	$[-0.011, 0.054]$	$[-0.036, 0.038]$
$a_3^{\gamma\gamma}/a_1$	$[-0.039, 0.037]$	$[-0.041, 0.044]$
$(\sigma_2^{Z\gamma}/\sigma_{\mathrm{SM}}^{Z\gamma})(2a_2^{Z\gamma}/a_1)^2\cos(\phi_{a2}^{Z\gamma})$	$[-1.7, 1.6]\times 10^2$	$[-6.5, 6.9]\times 10^2$
$(\sigma_3^{Z\gamma}/\sigma_{\mathrm{SM}}^{Z\gamma})(2a_3^{Z\gamma}/a_1)^2\cos(\phi_{a2}^{Z\gamma})$	$[-1.2, 1.9]\times 10^2$	$[-5.5, 5.5]\times 10^2$
$(\sigma_2^{\gamma\gamma}/\sigma_{\mathrm{SM}}^{\gamma\gamma})(2a_2^{\gamma\gamma}/a_1)^2\cos(\phi_{a2}^{\gamma\gamma})$	$[-0.3, 7.3]\times 10^2$	$[-3.3, 3.6]\times 10^2$
$(\sigma_3^{\gamma\gamma}/\sigma_{\mathrm{SM}}^{\gamma\gamma})(2a_3^{\gamma\gamma}/a_1)^2\cos(\phi_{a3}^{\gamma\gamma})$	$[-3.8, 3.3]\times 10^2$	$[-4.1, 4.7]\times 10^2$

$(\sigma_i^{V\gamma}/\sigma_{\mathrm{SM}}^{V\gamma})(2a_i^{V\gamma}/a_1)^2$ approximates the ratio $\mu = \sigma/\sigma_{\mathrm{SM}}$ of the measured and expected SM cross sections for a Higgs boson decay $H \to V\gamma$. The ratio $(2/a_1)^2$ scales this measurement with respect to the $H \to ZZ$ coupling and is expected to be 1.0 in the SM. As can be seen in Table XVII, the constraints presented on these ratios (<170 for $|a_2^{Z\gamma}|$ or <730 for $|a_2^{\gamma\gamma}|$ at 95% C.L.) are about 1 or 3 orders of magnitude higher than from the analyses of the direct $H \to Z\gamma$ ($\mu < 9.5$ at 95% C.L. [19]) or $H \to \gamma\gamma$ ($\mu = 1.14^{+0.26}_{-0.23}$ at 68% C.L. [15]) decays with on-shell photons, respectively. Therefore, the constraints presented on $f_{a2}^{Z\gamma}, f_{a3}^{Z\gamma}, f_{a2}^{\gamma\gamma}, f_{a3}^{\gamma\gamma}$ are not competitive compared with the direct cross-section measurements in $H \to Z\gamma$ or $\gamma\gamma$ decays. However, eventually with sufficiently large integrated luminosity, it might be possible to measure $f_{a2}^{V\gamma}$ and $f_{a3}^{V\gamma}$ separately in the $H \to VV \to 4\ell$ decay, allowing for measurements of the CP properties in these couplings [56,64]. The $H \to Z\gamma$ or $\gamma\gamma$ measurements with on-shell photons are sensitive only to the sum of the two cross-section fractions $f_{a2}^{V\gamma}$ and $f_{a3}^{V\gamma}$ and therefore cannot distinguish the two. Moreover, the $f_{\Lambda 1}^{Z\gamma}$ measurement is not possible with on-shell photons.

As in the case of the HZZ couplings, anomalous $HZ\gamma$ and $H\gamma\gamma$ couplings are found to be consistent with zero, as expected in the SM with the current precision. Since the measurement of the $HZ\gamma$ and $H\gamma\gamma$ couplings in the $H \to VV \to 4\ell$ decay is not yet competitive with the on-shell measurements, further investigation of several parameters simultaneously is not considered with the current data.

D. Study of HWW couplings with the $H \to WW \to \ell\nu\ell\nu$ channel

Constraints on anomalous HWW interactions are obtained using the $H \to WW \to \ell\nu\ell\nu$ final state. Three measurements are performed using the template method with the two observables, m_{T} and $m_{\ell\ell}$, as summarized in Table VI. Only real couplings, $\phi_{ai}^{WW} = 0$ or π, are considered. The results of the likelihood function scan for the three parameters, $f_{ai}^{WW}\cos\phi_{ai}^{WW}$, are shown in Fig. 25, following the HZZ approach presented in Sec. VI A. The 68% and 95% C.L. intervals are shown in Table XIII. Using the transformation in Eq. (5), these results could be interpreted for the coupling parameters used in Eq. (1) as shown in Table XVIII.

Similarly to the HZZ case, strong destructive interference of the SM and anomalous contributions at $f_{\Lambda 1}^{WW}\cos(\phi_{\Lambda 1}^{WW}) \sim +0.5$ or $f_{a2}^{WW}\cos(\phi_{a2}^{WW}) \sim -0.5$ leads to very different kinematic distributions and exclusions with high confidence levels. Since the measurement of the HWW anomalous couplings with the $H \to WW \to \ell\nu\ell\nu$ decay is not expected to provide strong constraints with the current data, a deeper investigation of several parameters simultaneously is not considered here. On the other hand, the combination of the HZZ and HWW measurements is expected to provide an improvement in the precision of the HVV couplings with certain symmetry considerations.

E. Combination of HZZ and HWW results

Further improvement on the HVV anomalous coupling constraints can be obtained from the combination of the $H \to ZZ \to 4\ell$ and $H \to WW \to \ell\nu\ell\nu$ analyses by employing symmetry considerations between the HZZ and HWW interactions. Two scenarios are considered. In the first, custodial symmetry is assumed, leading to $a_1^{WW} = a_1$. The second scenario assumes no relationship between the two couplings. In both cases, a combined likelihood scan of f_{ai} is performed for the full range of $-1 \le R_{ai} \le +1$. For a given value of R_{ai} in Eq. (6), the f_{ai} and f_{ai}^{WW} values are related by Eq. (7) and constraints on a single parameter can be obtained.

For the combination where custodial symmetry is assumed, the yield in the $H \to WW \to \ell\nu\ell\nu$ channel is related to the yield in the $H \to ZZ \to 4\ell$ channel, which leads to stronger constraints. This yield relationship is possible if either the fraction of VBF and VH production is known or reconstruction efficiency for these and gluon fusion production mechanisms is the same. The latter is

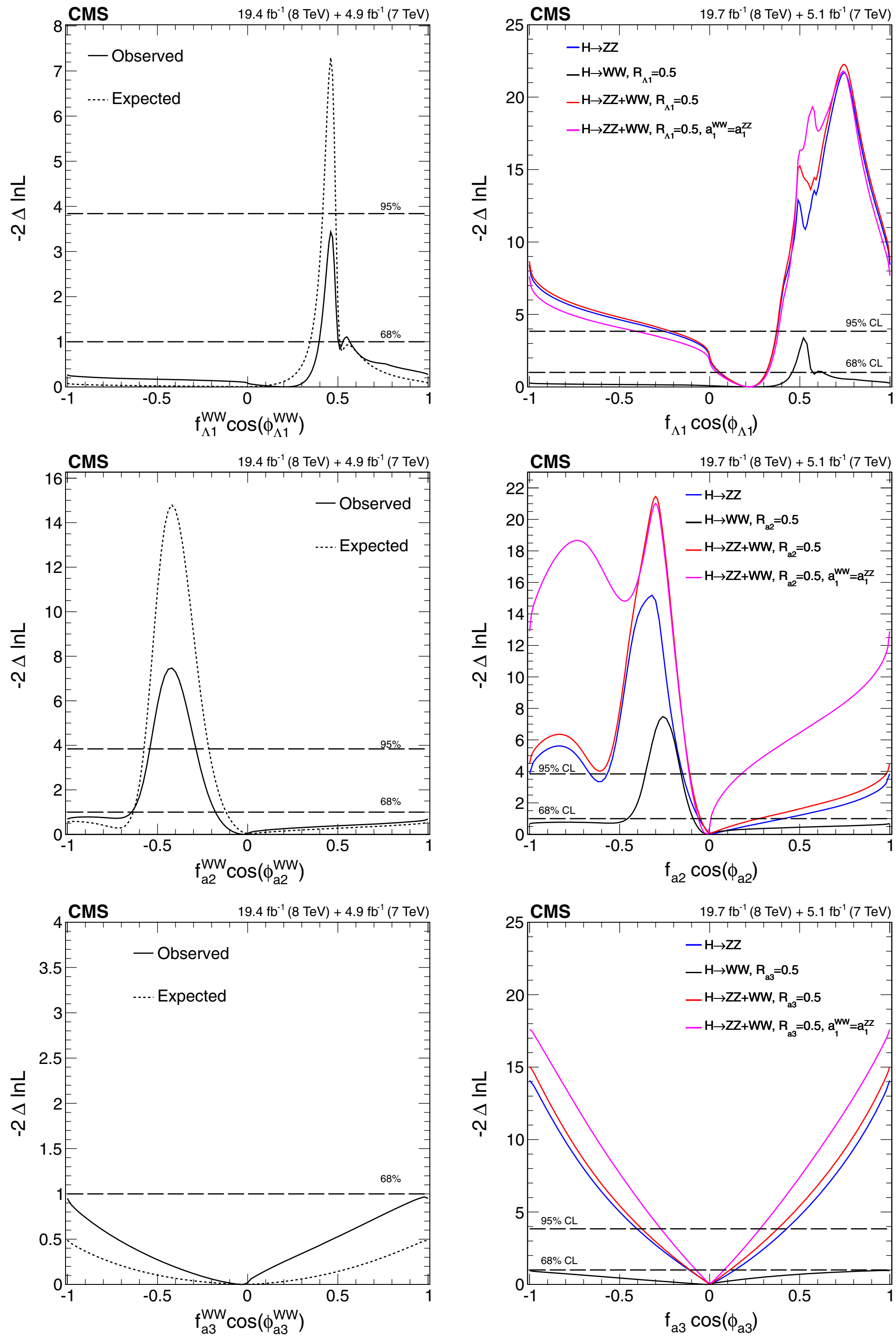

FIG. 25 (color online). Expected (dashed line) and observed (solid line) likelihood scans for effective fractions $f_{\Lambda1}$ (top), f_{a2} (middle), f_{a3} (bottom). The couplings studied are constrained to be real and all other anomalous couplings are fixed to the SM predictions. The $\cos\phi_{ai}$ term allows a signed quantity where $\cos\phi_{ai} = -1$ or $+1$. Plots on the left show the results of the $H \to WW \to \ell\nu\ell\nu$ analysis expressed in terms of the HWW couplings. Plots on the right show the combined $H \to WW$ and $H \to ZZ$ result in terms of the HZZ couplings for $R_{ai} = 0.5$. Measurements are shown for each channel separately, and two types of combinations are present: using $a_1^{WW} = a_1$ (red line) and without such a constraint (magenta line).

TABLE XVIII. Summary of the allowed 95% C.L. intervals on the anomalous couplings in HWW interactions using results obtained with the template method in Table XIII. The coupling ratios are assumed to be real [including $\cos(\phi_{\Lambda_1}^{WW}) = 0$ or π].

Parameter	Observed	Expected
$(\Lambda_1^{WW}\sqrt{\lvert a_1^{WW}\rvert})\cos(\phi_{\Lambda_1}^{WW})$	$[-\infty, +\infty]$	$[-\infty, 87\ \mathrm{GeV}] \cup [93\ \mathrm{GeV}, +\infty]$
a_2^{WW}/a_1^{WW}	$[-\infty, -1.22] \cup [-0.71, +\infty]$	$[-\infty, -1.30] \cup [-0.59, +\infty]$
a_3^{WW}/a_1^{WW}	$[-\infty, +\infty]$	$[-\infty, +\infty]$

TABLE XIX. Summary of allowed 68% C.L. (central values with uncertainties) and 95% C.L. (ranges in square brackets) intervals on anomalous coupling parameters in HVV interactions in the combinations of HZZ and HWW measurements assuming the symmetry $a_i = a_i^{WW}$, including $R_{ai} = 0.5$, and real coupling ratios ($\phi_{ai}^{VV} = 0$ or π). The last column indicates the observed (expected) confidence level of a pure anomalous coupling corresponding to $f_{ai}^{VV} = 1$ when compared to the SM expectation $f_{ai}^{VV} = 0$. The results are obtained with the template method.

Parameter	Observed	Expected	$f_{ai}^{VV} = 1$
$f_{\Lambda 1}\cos(\phi_{\Lambda 1})$	$0.21^{+0.11}_{-0.17}$ $[-0.42, 0.38]$	$0.00^{+0.15}_{-0.80}$ $[-1, 0.27] \cup [0.95, 1]$	0.56% (13%)
$f_{a2}\cos(\phi_{a2})$	$-0.01^{+0.02}_{-0.05}$ $[-0.11, 0.17]$	$0.00^{+0.08}_{-0.03}$ $[-0.07, 0.51]$	0.03% (0.25%)
$f_{a3}\cos(\phi_{a3})$	$0.00^{+0.08}_{-0.08}$ $[-0.27, 0.28]$	$0.00^{+0.23}_{-0.23}$ $[-0.53, 0.53]$	$<$ 0.01% (0.08%)

TABLE XX. Summary of the allowed 95% C.L. intervals on the anomalous couplings in HVV interactions in the combinations of HZZ and HWW measurements in Table XIX assuming the symmetry $a_i = a_i^{WW}$, including $R_{ai} = 0.5$, and real coupling ratios ($\phi_{ai}^{VV} = 0$ or π).

Parameter	Observed	Expected
$(\Lambda_1\sqrt{\lvert a_1\rvert})\cos(\phi_{\Lambda_1})$	$[-\infty, -100\ \mathrm{GeV}] \cup [103\ \mathrm{GeV}, \infty]$	$[-\infty, 43\ \mathrm{GeV}] \cup [116\ \mathrm{GeV}, \infty]$
a_2/a_1	$[-0.58, 0.76]$	$[-0.45, 1.67]$
a_3/a_1	$[-1.54, 1.57]$	$[-2.65, 2.65]$

known to be somewhat different in the $H \to WW \to \ell\nu\ell\nu$ channel due to the selection being sensitive to the associated jets (see Table IV). The fraction of VBF and VH production has been found to be small and consistent with the SM expectation of 12% [21]. However, this constraint is performed under the assumption of the SM kinematics of associated particles. While it is possible to obtain similar constraints on associated Higgs boson production with anomalous couplings, that analysis is beyond the scope of this paper. Therefore, we assume that the gluon fusion production dominates and the fraction of VBF and VH production is not larger than expected in the SM. This leads to potential uncertainty on the yield relationship of about 3%, which we neglect. Should the fraction of VBF and VH production be different, the corresponding limits could be recalculated.

An example of the combination under the assumption $R_{ai} = 0.5$ ($r_{ai} = 1$) is shown in Fig. 25 and Table XIX, where the effect of using the information on the relative yield can be seen. Both combination scenarios are shown. When the $H \to ZZ \to 4\ell$ and $H \to WW \to \ell\nu\ell\nu$ signal yields are left independent, custodial symmetry is not assumed. The increase in expected signal yield towards $f_{ai} = \pm 1$ is greater in the $H \to WW$ channel compared to the $H \to ZZ$ channel, leading to additional discriminating power when the yields are related. For example, the enhancement relative to the SM is a factor of 2.4 for $f_{a2} = \pm 1$. Since the number of events observed in the $H \to ZZ \to 4\ell$ and $H \to WW \to \ell\nu\ell\nu$ channels is compatible with the SM, this enhancement of 2.4 is not compatible with the SM and the $f_{a2} = \pm 1$ scenario is strongly excluded from the consideration of the yields alone. The combined analysis uses both yield and kinematic information in an optimal way. Using the transformation in Eq. (5), these results could be interpreted for the coupling parameters used in Eq. (1) as shown in Table XX.

To present the results in a model-independent way, conditional likelihood scans of f_{ai}, for a particular R_{ai} value, are performed. In this way, the confidence intervals of f_{ai} are obtained for a given value of R_{ai}. These results are presented in Fig. 26, and show features that arise from the combination of the $H \to ZZ$ and WW channels, but with larger exclusion power in some areas of the parameter space.

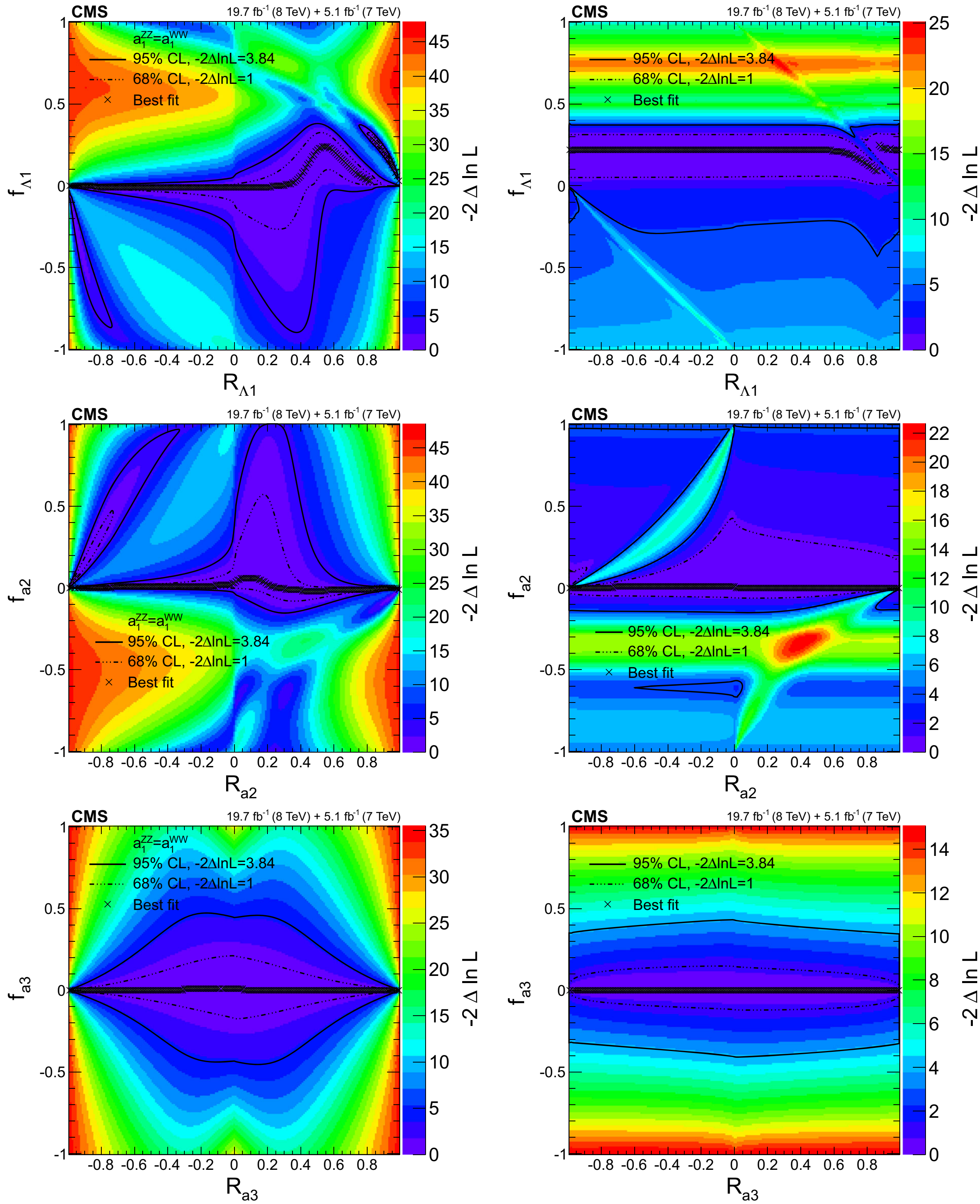

FIG. 26 (color online). Observed conditional likelihood scans of $f_{\Lambda 1}$ (top), f_{a2} (middle), f_{a3} (bottom) for a given R_{ai} value from the combined analysis of the $H \to WW$ and $H \to ZZ$ channels using the template method. The results are shown with custodial symmetry $a_1 = a_1^{WW}$ (left) and without such an assumption (right). Each cross indicates the minimum value of $-2\Delta \ln \mathcal{L}$ and the contours indicate the one-parameter confidence intervals of f_{ai} for a given value of R_{ai}.

VII. SUMMARY

In this paper, a comprehensive study of the spin-parity properties of the recently discovered H boson and of the tensor structure of its interactions with electroweak gauge bosons is presented using the $H \to ZZ$, $Z\gamma^*$, $\gamma^*\gamma^* \to 4\ell$, $H \to WW \to \ell\nu\ell\nu$, and $H \to \gamma\gamma$ decay modes. The results are based on the 2011 and 2012 data from pp collisions recorded with the CMS detector at the LHC, and they correspond to an integrated luminosity of up to 5.1 fb^{-1} at a center-of-mass energy of 7 TeV and up to 19.7 fb^{-1} at 8 TeV.

The phenomenological formulation for the interactions of a spin-zero, -one, or -two boson with the SM particles is based on a scattering amplitude or, equivalently, an effective field theory Lagrangian, with operators up to dimension five. The dedicated simulation and matrix element likelihood approach for the analysis of the kinematics of H boson production and decay in different topologies are based on this formulation. A maximum likelihood fit of the signal and background distributions provides constraints on the anomalous couplings of the H boson.

The study focuses on testing for the presence of anomalous effects in HZZ and HWW interactions under spin-zero, -one, and -two hypotheses. The combination of the $H \to ZZ$ and $H \to WW$ measurements leads to tighter constraints on the H boson spin-parity and anomalous HVV interactions. The combination with the $H \to \gamma\gamma$ measurements also allows tighter constraints in the spin-two case. The $HZ\gamma$ and $H\gamma\gamma$ interactions are probed for the first time using the 4ℓ final state.

The exotic-spin study covers the analysis of mixed-parity spin-one states and ten spin-two hypotheses under the assumption of production either via gluon fusion or quark-antiquark annihilation, or without such an assumption. The spin-one hypotheses are excluded at a greater than 99.999% C.L. in the ZZ and WW modes, while in the $\gamma\gamma$ mode they are excluded by the Landau-Yang theorem. The spin-two boson with gravitylike minimal couplings is excluded at a 99.87% C.L., and the other spin-two hypotheses tested are excluded at a 99% C.L. or higher.

Given the exclusion of the spin-one and spin-two scenarios, constraints are set on the contribution of eleven anomalous couplings to the HZZ, $HZ\gamma$, $H\gamma\gamma$, and HWW interactions of a spin-zero H boson, as summarized in Table XIII. Among these is the measurement of the f_{a3} parameter, which is defined as the fractional pseudoscalar cross section in the $H \to ZZ$ channel. The constraint is $f_{a3} < 0.43$ (0.40) at a 95% C.L. for the positive (negative) phase of the pseudoscalar coupling with respect to the dominant SM-like coupling and $f_{a3} = 1$ exclusion of a pure pseudoscalar hypothesis at a 99.98% C.L.

All observations are consistent with the expectations for a scalar SM-like Higgs boson. It is not presently established that the interactions of the observed state conserve C-parity or CP-parity. However, under the assumption that both quantities are conserved, our measurements require the quantum numbers of the new state to be $J^{PC} = 0^{++}$. The positive P-parity follows from the f_{a3}^{VV} measurements in the $H \to ZZ$, $Z\gamma^*$, $\gamma^*\gamma^* \to 4\ell$, and $H \to WW \to \ell\nu\ell\nu$ decays and the positive C-parity follows from observation of the $H \to \gamma\gamma$ decay. Further measurements probing the tensor structure of the HVV and $Hf\bar{f}$ interactions can test the assumption of CP invariance.

ACKNOWLEDGMENTS

We thank Markus Schulze for optimizing the JHUGen Monte Carlo simulation program for this analysis. We congratulate our colleagues in the CERN accelerator departments for the excellent performance of the LHC and thank the technical and administrative staffs at CERN and at other CMS institutes for their contributions to the success of the CMS effort. In addition, we gratefully acknowledge the computing centers and personnel of the Worldwide LHC Computing Grid for delivering so effectively the computing infrastructure essential to our analyses. Finally, we acknowledge the enduring support for the construction and operation of the LHC and the CMS detector provided by the following funding agencies: the Austrian Federal Ministry of Science, Research and Economy and the Austrian Science Fund; the Belgian Fonds de la Recherche Scientifique, and Fonds voor Wetenschappelijk Onderzoek; the Brazilian Funding Agencies (CNPq, CAPES, FAPERJ, and FAPESP); the Bulgarian Ministry of Education and Science; CERN; the Chinese Academy of Sciences, Ministry of Science and Technology, and National Natural Science Foundation of China; the Colombian Funding Agency (COLCIENCIAS); the Croatian Ministry of Science, Education and Sport, and the Croatian Science Foundation; the Research Promotion Foundation, Cyprus; the Ministry of Education and Research, Estonian Research Council via IUT23-4 and IUT23-6 and European Regional Development Fund, Estonia; the Academy of Finland, Finnish Ministry of Education and Culture, and Helsinki Institute of Physics; the Institut National de Physique Nucléaire et de Physique des Particules/CNRS, and Commissariat à l'Énergie Atomique et aux Énergies Alternatives/CEA, France; the Bundesministerium für Bildung und Forschung, Deutsche Forschungsgemeinschaft, and Helmholtz-Gemeinschaft Deutscher Forschungszentren, Germany; the General Secretariat for Research and Technology, Greece; the National Scientific Research Foundation, and National Innovation Office, Hungary; the Department of Atomic Energy and the Department of Science and Technology, India; the Institute for Studies in Theoretical Physics and Mathematics, Iran; the Science Foundation, Ireland; the Istituto Nazionale di Fisica Nucleare, Italy; the Ministry of Science, ICT and Future Planning, and National Research Foundation (NRF), Republic of Korea; the Lithuanian Academy of Sciences; the Ministry of Education, and

University of Malaya (Malaysia); the Mexican Funding Agencies (CINVESTAV, CONACYT, SEP, and UASLP-FAI); the Ministry of Business, Innovation and Employment, New Zealand; the Pakistan Atomic Energy Commission; the Ministry of Science and Higher Education and the National Science Centre, Poland; the Fundação para a Ciência e a Tecnologia, Portugal; JINR, Dubna; the Ministry of Education and Science of the Russian Federation, the Federal Agency of Atomic Energy of the Russian Federation, Russian Academy of Sciences, and the Russian Foundation for Basic Research; the Ministry of Education, Science and Technological Development of Serbia; the Secretaría de Estado de Investigación, Desarrollo e Innovación and Programa Consolider-Ingenio 2010, Spain; the Swiss Funding Agencies (ETH Board, ETH Zurich, PSI, SNF, UniZH, Canton Zurich, and SER); the Ministry of Science and Technology, Taipei; the Thailand Center of Excellence in Physics, the Institute for the Promotion of Teaching Science and Technology of Thailand, Special Task Force for Activating Research and the National Science and Technology Development Agency of Thailand; the Scientific and Technical Research Council of Turkey, and Turkish Atomic Energy Authority; the National Academy of Sciences of Ukraine, and State Fund for Fundamental Researches, Ukraine; the Science and Technology Facilities Council, UK; the US Department of Energy, and the US National Science Foundation. Individuals have received support from the Marie-Curie programme and the European Research Council and EPLANET (European Union); the Leventis Foundation; the A. P. Sloan Foundation; the Alexander von Humboldt Foundation; the Belgian Federal Science Policy Office; the Fonds pour la Formation à la Recherche dans l'Industrie et dans l'Agriculture (FRIA-Belgium); the Agentschap voor Innovatie door Wetenschap en Technologie (IWT-Belgium); the Ministry of Education, Youth and Sports (MEYS) of the Czech Republic; the Council of Science and Industrial Research, India; the HOMING PLUS programme of Foundation for Polish Science, cofinanced from European Union, Regional Development Fund; the Compagnia di San Paolo (Torino); the Consorzio per la Fisica (Trieste); MIUR Project No. 20108T4XTM (Italy); the Thalis and Aristeia programmes cofinanced by EU-ESF and the Greek NSRF; and the National Priorities Research Program by Qatar National Research Fund.

[1] ATLAS Collaboration, Observation of a new particle in the search for the standard model Higgs boson with the ATLAS detector at the LHC, Phys. Lett. B **716**, 1 (2012).

[2] CMS Collaboration, Observation of a new boson at a mass of 125 GeV with the CMS experiment at the LHC, Phys. Lett. B **716**, 30 (2012).

[3] CMS Collaboration, Observation of a new boson with mass near 125 GeV in pp collisions at $\sqrt{s} = 7$ and 8 TeV, J. High Energy Phys. 06 (2013) 081.

[4] S. L. Glashow, Partial-symmetries of weak interactions, Nucl. Phys. **22**, 579 (1961).

[5] F. Englert and R. Brout, Broken Symmetry and the Mass of Gauge Vector Mesons, Phys. Rev. Lett. **13**, 321 (1964).

[6] P. W. Higgs, Broken symmetries, massless particles and gauge fields, Phys. Lett. **12**, 132 (1964).

[7] P. W. Higgs, Broken Symmetries and the Masses of Gauge Bosons, Phys. Rev. Lett. **13**, 508 (1964).

[8] G. S. Guralnik, C. R. Hagen, and T. W. B. Kibble, Global Conservation Laws and Massless Particles, Phys. Rev. Lett. **13**, 585 (1964).

[9] S. Weinberg, A Model of Leptons, Phys. Rev. Lett. **19**, 1264 (1967).

[10] A. Salam, Weak and Electromagnetic Interactions, in *Elementary Particle Physics: Relativistic Groups and Analyticity*, edited by N. Svartholm (Almqvist & Wiksell, Stockholm, 1968), p. 367, Proceedings of the Eighth Nobel Symposium.

[11] CMS Collaboration, On the Mass and Spin-Parity of the Higgs Boson Candidate via Its Decays to Z Boson Pairs, Phys. Rev. Lett. **110**, 081803 (2013).

[12] CMS Collaboration, Measurement of the properties of a Higgs boson in the four-lepton final state, Phys. Rev. D **89**, 092007 (2014).

[13] CMS Collaboration, Constraints on the Higgs boson Width from off-shell production and decay to Z-boson pairs, Phys. Lett. B **736**, 64 (2014).

[14] CMS Collaboration, Measurement of Higgs boson production and properties in the WW decay channel with leptonic final states, J. High Energy Phys. 01 (2014) 096.

[15] CMS Collaboration, Observation of the diphoton decay of the Higgs boson and measurement of its properties, Eur. Phys. J. C **74**, 3076 (2014).

[16] CMS Collaboration, Search for the standard model Higgs boson produced in association with a W or a Z boson and decaying to bottom quarks, Phys. Rev. D **89**, 012003 (2014).

[17] CMS Collaboration, Evidence for the 125 GeV Higgs boson decaying to a pair of τ leptons, J. High Energy Phys. 05 (2014) 104.

[18] CMS Collaboration, Search for the standard model Higgs boson produced in association with a top-quark pair in pp collisions at the LHC, J. High Energy Phys. 05 (2013) 145.

[19] CMS Collaboration, Search for a Higgs boson decaying into a Z and a photon in pp collisions at $\sqrt{s} = 7$ and 8 TeV, Phys. Lett. B **726**, 587 (2013).

[20] CMS Collaboration, Search for invisible decays of Higgs bosons in the vector boson fusion and associated ZH production modes, Eur. Phys. J. C **74**, 2980 (2014).

[21] CMS Collaboration, Precise determination of the mass of the Higgs boson and tests of compatibility of its couplings with the standard model predictions using proton collisions at 7 and 8 TeV, arXiv:1412.8662.

[22] ATLAS Collaboration, Evidence for the spin-0 nature of the Higgs boson using ATLAS data, Phys. Lett. B **726**, 120 (2013).

[23] ATLAS Collaboration, Measurements of Higgs boson production and couplings in Diboson final states with the ATLAS detector at the LHC, Phys. Lett. B **726**, 88 (2013).

[24] ATLAS Collaboration, Measurement of the Higgs boson mass from the $H \to \gamma\gamma$ and $H \to ZZ^* \to 4\ell$ channels with the ATLAS detector using 25 fb^{-1} of pp collision data, Phys. Rev. D **90**, 052004 (2014).

[25] ATLAS Collaboration, Search for Higgs boson decays to a photon and a Z boson in pp collisions at $\sqrt{s} = 7$ and 8 TeV with the ATLAS detector, Phys. Lett. B **732**, 8 (2014).

[26] ATLAS Collaboration, Search for Invisible Decays of a Higgs Boson Produced in Association with a Z Boson in ATLAS, Phys. Rev. Lett. **112**, 201802 (2014).

[27] ATLAS Collaboration, Measurement of Higgs boson production in the diphoton decay channel in pp collisions at center-of-mass energies of 7 and 8 TeV with the ATLAS detector, Phys. Rev. D **90**, 112015 (2014).

[28] Y. Gao, A. V. Gritsan, Z. Guo, K. Melnikov, M. Schulze, and N. V. Tran, Spin determination of single-produced resonances at Hadron colliders, Phys. Rev. D **81**, 075022 (2010).

[29] S. Bolognesi, Y. Gao, A. V. Gritsan, K. Melnikov, M. Schulze, N. V. Tran, and A. Whitbeck, Spin and parity of a single-produced resonance at the LHC, Phys. Rev. D **86**, 095031 (2012).

[30] Y. Chen, N. Tran, and R. Vega-Morales, Scrutinizing the Higgs signal and background in the $2e2\mu$ golden channel, J. High Energy Phys. 01 (2013) 182.

[31] I. Anderson, S. Bolognesi, F. Caola, Y. Gao, A. V. Gritsan, C. B. Martin, K. Melnikov, M. Schulze, N. V. Tran, A. Whitbeck, and Y. Zhou, Constraining anomalous HVV interactions at proton and lepton colliders, Phys. Rev. D **89**, 035007 (2014).

[32] M. Chen, T. Cheng, J. S. Gainer, A. Korytov, K. T. Matchev, P. Milenovic, G. Mitselmakher, M. Park, A. Rinkevicius, and M. Snowball, Role of interference in unraveling the ZZ couplings of the newly discovered boson at the LHC, Phys. Rev. D **89**, 034002 (2014).

[33] Y. Chen, E. Di Marco, J. Lykken, M. Spiropulu, R. Vega-Morales, and S. Xie, 8D likelihood effective Higgs couplings extraction framework in the golden channel, J. High Energy Phys. 01 (2015) 125.

[34] J. R. Dell'Aquila and C. A. Nelson, Simple tests for CP or P violation by sequential decays: $V_1 V_2$ modes with decays into $\bar{\ell}_A \ell_B$ and/or $\bar{q}_A q_B$, Phys. Rev. D **33**, 101 (1986).

[35] C. A. Nelson, Correlation between decay planes in Higgs boson decays into W pair (into Z pair), Phys. Rev. D **37**, 1220 (1988).

[36] A. Soni and R. M. Xu, Probing CP violation via Higgs decays to four leptons, Phys. Rev. D **48**, 5259 (1993).

[37] D. Chang, W.-Y. Keung, and I. Phillips, CP odd correlation in the decay of neutral Higgs boson into ZZ, W^+W^-, or $t\bar{t}$, Phys. Rev. D **48**, 3225 (1993).

[38] V. D. Barger, K.-m. Cheung, A. Djouadi, B. A. Kniehl, and P. M. Zerwas, Higgs bosons: Intermediate mass range at $e^+ e^-$ colliders, Phys. Rev. D **49**, 79 (1994).

[39] T. Arens and L. M. Sehgal, Energy spectra and energy correlations in the decay $H \to ZZ \to \mu^+\mu^-\mu^+\mu^-$, Z. Phys. C **66**, 89 (1995).

[40] T. Han and J. Jiang, CP violating ZZH coupling at e^+e^- linear colliders, Phys. Rev. D **63**, 096007 (2001).

[41] T. Plehn, D. L. Rainwater, and D. Zeppenfeld, Determining the Structure of Higgs Couplings at the LHC, Phys. Rev. Lett. **88**, 051801 (2002).

[42] S. Y. Choi, D. J. Miller, M. M. Mühlleitner, and P. M. Zerwas, Identifying the higgs spin and parity in decays to Z pairs, Phys. Lett. B **553**, 61 (2003).

[43] C. P. Buszello, I. Fleck, P. Marquard, and J. J. van der Bij, Prospective analysis of spin- and CP-sensitive variables in $H \to ZZ \to l_1^+ l_1^- l_2^+ l_2^-$ at the LHC, Eur. Phys. J. C **32**, 209 (2004).

[44] E. Accomando *et al.*, Workshop on CP studies and non-standard Higgs physics, arXiv:hep-ph/0608079.

[45] R. M. Godbole, D. J. Miller, and M. M. Mühlleitner, Aspects of CP violation in the H ZZ coupling at the LHC, J. High Energy Phys. 12 (2007) 031.

[46] O. Antipin and A. Soni, Towards establishing the spin of warped gravitons, J. High Energy Phys. 10 (2008) 018.

[47] W.-Y. Keung, I. Low, and J. Shu, Landau-Yang Theorem and Decays of a Z Boson into Two Z Bosons, Phys. Rev. Lett. **101**, 091802 (2008).

[48] K. Hagiwara, Q. Li, and K. Mawatari, Jet angular correlation in vector-boson fusion processes at hadron colliders, J. High Energy Phys. 07 (2009) 101.

[49] A. De Rújula, J. Lykken, M. Pierini, C. Rogan, and M. Spiropulu, Higgs look-alikes at the LHC, Phys. Rev. D **82**, 013003 (2010).

[50] N. D. Christensen, T. Han, and Y. Li, Testing CP violation in ZZH interactions at the LHC, Phys. Lett. B **693**, 28 (2010).

[51] J. S. Gainer, K. Kumar, I. Low, and R. Vega-Morales, Improving the sensitivity of Higgs boson searches in the golden channel, J. High Energy Phys. 11 (2011) 027.

[52] J. Ellis, D. S. Hwang, V. Sanz, and T. You, A fast track towards the 'Higgs' spin and parity, J. High Energy Phys. 11 (2012) 134.

[53] J. S. Gainer, J. Lykken, K. T. Matchev, S. Mrenna, and M. Park, Geolocating the Higgs Boson Candidate at the LHC, Phys. Rev. Lett. **111**, 041801 (2013).

[54] P. Artoisenet, P. de Aquino, F. Demartin, R. Frederix, S. Frixione, F. Maltoni, M. K. Mandal, P. Mathews, K. Mawatari, V. Ravindran, S. Seth, P. Torrielli, and M. Zaro, A framework for Higgs characterisation, J. High Energy Phys. 11 (2013) 043.

[55] Y. Chen and R. Vega-Morales, Extracting effective Higgs couplings in the golden channel, J. High Energy Phys. 04 (2014) 057.

[56] Y. Chen, R. Harnik, and R. Vega-Morales, Probing the Higgs Couplings to Photons in $h \to 4\ell$ at the LHC, Phys. Rev. Lett. **113**, 191801 (2014).

[57] J. S. Gainer, J. Lykken, K. T. Matchev, S. Mrenna, and M. Park, Beyond geolocating: constraining higher dimensional operators in $H \to 4\ell$ with off-shell production and more, Phys. Rev. D **91**, 035011 (2015).

[58] N. P. Samios, R. Plano, A. Prodell, M. Schwartz, and J. Steinberger, Parity of the neutral pion and the decay $\pi^0 \to 2e^+ + 2e^-$, Phys. Rev. **126**, 1844 (1962).

[59] N. Cabibbo and A. Maksymowicz, Angular correlations in K_{e4} decays and determination of low-energy π-π phase shifts, Phys. Rev. **137**, B438 (1965); **168**, 1926(E) (1968).

[60] G. Kramer and W. F. Palmer, Branching ratios and CP asymmetries in the decay $B \to VV$, Phys. Rev. D **45**, 193 (1992).

[61] E. Abouzaid *et al.* (KTeV Collaboration), Determination of the Parity of the Neutral Pion via the Four-Electron Decay, Phys. Rev. Lett. **100**, 182001 (2008).

[62] B. Aubert *et al.* (*BABAR* Collaboration), Time-dependent and time-integrated angular analysis of $B \to \phi K_s \pi^0$ and $B \to \phi K^+ \pi^-$, Phys. Rev. D **78**, 092008 (2008).

[63] I. Low, J. Lykken, and G. Shaughnessy, Have we observed the Higgs (imposter)? Phys. Rev. D **86**, 093012 (2012).

[64] S. Dawson *et al.*, Higgs working group report of the Snowmass 2013 community planning study, arXiv:1310.8361.

[65] I. Low and J. Lykken, Revealing the electroweak properties of a new scalar resonance, J. High Energy Phys. 10 (2010) 053.

[66] P. Sikivie, L. Susskind, M. B. Voloshin, and V. I. Zakharov, Isospin breaking in technicolor models, Nucl. Phys. **B173**, 189 (1980).

[67] L. D. Landau, On the angular momentum of a two-photon system, Dokladi na Bulgarskata akademiia na naukite **60**, 207 (1948).

[68] C. N. Yang, Selection rules for the dematerialization of a particle into two photons, Phys. Rev. **77**, 242 (1950).

[69] L. Randall and R. Sundrum, An Alternative to Compactification, Phys. Rev. Lett. **83**, 4690 (1999).

[70] L. Randall and R. Sundrum, A Large Mass Hierarchy from a Small Extra Dimension, Phys. Rev. Lett. **83**, 3370 (1999).

[71] K. Agashe, H. Davoudiasl, G. Perez, and A. Soni, Warped gravitons at the CERN LHC and beyond, Phys. Rev. D **76**, 036006 (2007).

[72] N. Kauer and G. Passarino, Inadequacy of zero-width approximation for a light Higgs boson signal, J. High Energy Phys. 08 (2012) 116.

[73] F. Caola and K. Melnikov, Constraining the Higgs boson width with ZZ production at the LHC, Phys. Rev. D **88**, 054024 (2013).

[74] K. A. Olive *et al.* (Particle Data Group), Review of particle physics, Chin. Phys. C **38**, 090001 (2014).

[75] C. Cawlfield *et al.* (CLEO Collaboration), Experimental study of $\chi_b(2\mathrm{P}) \to \pi\pi\chi_b(1\mathrm{P})$, Phys. Rev. D **73**, 012003 (2006).

[76] S. G. Karshenboim, Precision study of positronium: Testing bound state QED theory, Int. J. Mod. Phys. A **19**, 3879 (2004).

[77] CMS Collaboration, The CMS experiment at the CERN LHC, J. Instrum. **3**, S08004 (2008).

[78] CMS Collaboration, Measurement of Inclusive W and Z Boson Production Cross Sections in pp Collisions at $\sqrt{s} = 8$ TeV, Phys. Rev. Lett. **112**, 191802 (2014).

[79] CMS Collaboration, CMS luminosity based on pixel cluster counting - summer 2013 update, CMS Physics Analysis Summary Report No. CMS-PAS-LUM-13-001, 2013, http://cds.cern.ch/record/1598864/.

[80] S. Frixione, P. Nason, and C. Oleari, Matching NLO QCD computations with parton shower simulations: The POWHEG method, J. High Energy Phys. 11 (2007) 070.

[81] E. Bagnaschi, G. Degrassi, P. Slavich, and A. Vicini, Higgs production via gluon fusion in the POWHEG approach in the SM and in the MSSM, J. High Energy Phys. 02 (2012) 088.

[82] P. Nason and C. Oleari, NLO Higgs boson production via vector-boson fusion matched with shower in POWHEG, J. High Energy Phys. 02 (2010) 037.

[83] T. Sjöstrand, S. Mrenna, and P. Skands, PYTHIA 6.4 physics and manual, J. High Energy Phys. 05 (2006) 026.

[84] S. Agostinelli *et al.* (GEANT4), GEANT4—A simulation toolkit, Nucl. Instrum. Methods Phys. Res., Sect. A **506**, 250 (2003).

[85] T. Binoth, N. Kauer, and P. Mertsch, Gluon-induced QCD corrections to $pp \to ZZ \to \ell\bar{\ell}\ell'\bar{\ell}'$, in Proceedings of the XVI International Workshop on Deep-Inelastic Scattering and Related Topics (DIS'07), arXiv:0807.0024.

[86] J. M. Campbell and R. K. Ellis, MCFM for the Tevatron and the LHC, Nucl. Phys. B, Proc. Suppl. **205–206**, 10 (2010).

[87] J. M. Campbell, R. K. Ellis, and C. Williams, Vector boson pair production at the LHC, J. High Energy Phys. 07 (2011) 018.

[88] J. M. Campbell, R. K. Ellis, and C. Williams, Bounding the Higgs width at the LHC using full analytic results for $gg \to e^- e^+ \mu^- \mu^+$, J. High Energy Phys. 04 (2014) 060.

[89] J. Alwall, M. Herquet, F. Maltoni, O. Mattelaer, and T. Stelzer, MadGraph 5: Going beyond, J. High Energy Phys. 06 (2011) 128.

[90] T. Binoth, M. Ciccolini, N. Kauer, and M. Krämer, Gluon-induced W-boson pair production at the LHC, J. High Energy Phys. 12 (2006) 046.

[91] A. Ballestrero, A. Belhouari, G. Bevilacqua, V. Kashkan, and E. Maina, PHANTOM: A Monte Carlo event generator for six parton final states at high energy colliders, Comput. Phys. Commun. **180**, 401 (2009).

[92] S. Jadach, J. H. Kuhn, and Z. Wąs, TAUOLA—A library of Monte Carlo programs to simulate decays of polarized tau leptons, Comput. Phys. Commun. **64**, 275 (1991).

[93] CMS Collaboration, Particle-flow event reconstruction in CMS and performance for jets, taus, and MET, CMS Physics Analysis Summary Report No. CMS-PAS-PFT-09-001, 2009, http://cdsweb.cern.ch/record/1194487.

[94] CMS Collaboration, Commissioning of the particle-flow event reconstruction with the first LHC collisions recorded in the CMS detector, CMS Physics Analysis Summary Report No. CMS-PAS-PFT-10-001, 2010, https://cds.cern.ch/record/1247373/.

[95] CMS Collaboration, Performance of CMS muon reconstruction in pp collision events at $\sqrt{s} = 7$ TeV, J. Instrum. **7**, P10002 (2012).

[96] M. Cacciari, G. P. Salam, and G. Soyez, The anti-k_t jet clustering algorithm, J. High Energy Phys. 04 (2008) 063.

[97] M. Cacciari, G. P. Salam, and G. Soyez, FastJet user manual, Eur. Phys. J. C **72**, 1896 (2012).

[98] P. Avery, D. Bourilkov, M. Chen, T. Cheng, A. Drozdetskiy, J. S. Gainer, A. Korytov, K. T. Matchev, P. Milenovic, G. Mitselmakher, M. Park, A. Rinkevicius, and M. Snowball, Precision studies of the Higgs boson decay channel $H \to ZZ^* \to 4\ell$ with MEKD, Phys. Rev. D **87**, 055006 (2013).

[99] N. D. Christensen and C. Duhr, FeynRules—Feynman rules made easy, Comput. Phys. Commun. **180**, 1614 (2009).

[100] M. Rosenblatt, Remarks on some nonparametric estimates of a density function, Ann. Math. Stat. **27**, 832 (1956).

[101] E. Parzen, On estimation of a probability density function and mode, Ann. Math. Stat. **33**, 1065 (1962).

[102] S. S. Wilks, The large-sample distribution of the likelihood ratio for testing composite hypotheses, Ann. Math. Stat. **9**, 60 (1938).

[103] A. L. Read, Presentation of search results: The CL_s technique, J. Phys. G **28**, 2693 (2002).

[104] T. Junk, Confidence level computation for combining searches with small statistics, Nucl. Instrum. Methods Phys. Res., Sect. A **434**, 435 (1999).

[105] S. Heinemeyer *et al.*, Handbook of LHC Higgs cross sections: 3. Higgs properties, CERN Report No. CERN-2013-004, 2013.

[106] CMS Collaboration, Measurement of the weak mixing angle with the Drell-Yan process in proton-proton collisions at the LHC, Phys. Rev. D **84**, 112002 (2011).

[107] CMS Collaboration, Observation of Z decays to four leptons with the CMS detector at the LHC, J. High Energy Phys. 12 (2012) 034.

V. Khachatryan,[1] A. M. Sirunyan,[1] A. Tumasyan,[1] W. Adam,[2] T. Bergauer,[2] M. Dragicevic,[2] J. Erö,[2] M. Friedl,[2] R. Frühwirth,[2,b] V. M. Ghete,[2] C. Hartl,[2] N. Hörmann,[2] J. Hrubec,[2] M. Jeitler,[2,b] W. Kiesenhofer,[2] V. Knünz,[2] M. Krammer,[2,b] I. Krätschmer,[2] D. Liko,[2] I. Mikulec,[2] D. Rabady,[2,c] B. Rahbaran,[2] H. Rohringer,[2] R. Schöfbeck,[2] J. Strauss,[2] W. Treberer-Treberspurg,[2] W. Waltenberger,[2] C.-E. Wulz,[2,b] V. Mossolov,[3] N. Shumeiko,[3] J. Suarez Gonzalez,[3] S. Alderweireldt,[4] S. Bansal,[4] T. Cornelis,[4] E. A. De Wolf,[4] X. Janssen,[4] A. Knutsson,[4] J. Lauwers,[4] S. Luyckx,[4] S. Ochesanu,[4] R. Rougny,[4] M. Van De Klundert,[4] H. Van Haevermaet,[4] P. Van Mechelen,[4] N. Van Remortel,[4] A. Van Spilbeeck,[4] F. Blekman,[5] S. Blyweert,[5] J. D'Hondt,[5] N. Daci,[5] N. Heracleous,[5] J. Keaveney,[5] S. Lowette,[5] M. Maes,[5] A. Olbrechts,[5] Q. Python,[5] D. Strom,[5] S. Tavernier,[5] W. Van Doninck,[5] P. Van Mulders,[5] G. P. Van Onsem,[5] I. Villella,[5] C. Caillol,[6] B. Clerbaux,[6] G. De Lentdecker,[6] D. Dobur,[6] L. Favart,[6] A. P. R. Gay,[6] A. Grebenyuk,[6] A. Léonard,[6] A. Mohammadi,[6] L. Perniè,[6,c] A. Randle-conde,[6] T. Reis,[6] T. Seva,[6] L. Thomas,[6] C. Vander Velde,[6] P. Vanlaer,[6] J. Wang,[6] F. Zenoni,[6] V. Adler,[7] K. Beernaert,[7] L. Benucci,[7] A. Cimmino,[7] S. Costantini,[7] S. Crucy,[7] S. Dildick,[7] A. Fagot,[7] G. Garcia,[7] J. Mccartin,[7] A. A. Ocampo Rios,[7] D. Ryckbosch,[7] S. Salva Diblen,[7] M. Sigamani,[7] N. Strobbe,[7] F. Thyssen,[7] M. Tytgat,[7] E. Yazgan,[7] N. Zaganidis,[7] S. Basegmez,[8] C. Beluffi,[8,d] G. Bruno,[8] R. Castello,[8] A. Caudron,[8] L. Ceard,[8] G. G. Da Silveira,[8] C. Delaere,[8] T. du Pree,[8] D. Favart,[8] L. Forthomme,[8] A. Giammanco,[8,e] J. Hollar,[8] A. Jafari,[8] P. Jez,[8] M. Komm,[8] V. Lemaitre,[8] C. Nuttens,[8] L. Perrini,[8] A. Pin,[8] K. Piotrzkowski,[8] A. Popov,[8,f] L. Quertenmont,[8] M. Selvaggi,[8] M. Vidal Marono,[8] J. M. Vizan Garcia,[8] N. Beliy,[9] T. Caebergs,[9] E. Daubie,[9] G. H. Hammad,[9] W. L. Aldá Júnior,[10] G. A. Alves,[10] L. Brito,[10] M. Correa Martins Junior,[10] T. Dos Reis Martins,[10] J. Molina,[10] C. Mora Herrera,[10] M. E. Pol,[10] P. Rebello Teles,[10] W. Carvalho,[11] J. Chinellato,[11,g] A. Custódio,[11] E. M. Da Costa,[11] D. De Jesus Damiao,[11] C. De Oliveira Martins,[11] S. Fonseca De Souza,[11] H. Malbouisson,[11] D. Matos Figueiredo,[11] L. Mundim,[11] H. Nogima,[11] W. L. Prado Da Silva,[11] J. Santaolalla,[11] A. Santoro,[11] A. Sznajder,[11] E. J. Tonelli Manganote,[11,g] A. Vilela Pereira,[11] C. A. Bernardes,[12b] S. Dogra,[12a] T. R. Fernandez Perez Tomei,[12a] E. M. Gregores,[12b] P. G. Mercadante,[12b] S. F. Novaes,[12a] Sandra S. Padula,[12a] A. Aleksandrov,[13] V. Genchev,[13,c] R. Hadjiiska,[13] P. Iaydjiev,[13] A. Marinov,[13] S. Piperov,[13] M. Rodozov,[13] G. Sultanov,[13] M. Vutova,[13] A. Dimitrov,[14] I. Glushkov,[14] L. Litov,[14] B. Pavlov,[14] P. Petkov,[14] J. G. Bian,[15] G. M. Chen,[15] H. S. Chen,[15] M. Chen,[15] T. Cheng,[15] R. Du,[15] C. H. Jiang,[15] R. Plestina,[15,h] F. Romeo,[15] J. Tao,[15] Z. Wang,[15] C. Asawatangtrakuldee,[16] Y. Ban,[16] Q. Li,[16] S. Liu,[16] Y. Mao,[16] S. J. Qian,[16] D. Wang,[16] Z. Xu,[16] W. Zou,[16] C. Avila,[17] A. Cabrera,[17] L. F. Chaparro Sierra,[17] C. Florez,[17] J. P. Gomez,[17] B. Gomez Moreno,[17] J. C. Sanabria,[17] N. Godinovic,[18] D. Lelas,[18] D. Polic,[18] I. Puljak,[18] Z. Antunovic,[19] M. Kovac,[19] V. Brigljevic,[20] K. Kadija,[20] J. Luetic,[20] D. Mekterovic,[20] L. Sudic,[20] A. Attikis,[21] G. Mavromanolakis,[21] J. Mousa,[21] C. Nicolaou,[21] F. Ptochos,[21] P. A. Razis,[21] M. Bodlak,[22] M. Finger,[22] M. Finger Jr.,[22,i] Y. Assran,[23,j] A. Ellithi Kamel,[23,k] M. A. Mahmoud,[23,l] A. Radi,[23,m,n] M. Kadastik,[24] M. Murumaa,[24] M. Raidal,[24] A. Tiko,[24] P. Eerola,[25] G. Fedi,[25] M. Voutilainen,[25] J. Härkönen,[26] V. Karimäki,[26] R. Kinnunen,[26] M. J. Kortelainen,[26] T. Lampén,[26] K. Lassila-Perini,[26] S. Lehti,[26] T. Lindén,[26] P. Luukka,[26] T. Mäenpää,[26]

T. Peltola,[26] E. Tuominen,[26] J. Tuominiemi,[26] E. Tuovinen,[26] L. Wendland,[26] J. Talvitie,[27] T. Tuuva,[27] M. Besancon,[28] F. Couderc,[28] M. Dejardin,[28] D. Denegri,[28] B. Fabbro,[28] J. L. Faure,[28] C. Favaro,[28] F. Ferri,[28] S. Ganjour,[28] A. Givernaud,[28] P. Gras,[28] G. Hamel de Monchenault,[28] P. Jarry,[28] E. Locci,[28] J. Malcles,[28] J. Rander,[28] A. Rosowsky,[28] M. Titov,[28] S. Baffioni,[29] F. Beaudette,[29] P. Busson,[29] C. Charlot,[29] T. Dahms,[29] M. Dalchenko,[29] L. Dobrzynski,[29] N. Filipovic,[29] A. Florent,[29] R. Granier de Cassagnac,[29] L. Mastrolorenzo,[29] P. Miné,[29] I. N. Naranjo,[29] M. Nguyen,[29] C. Ochando,[29] G. Ortona,[29] P. Paganini,[29] S. Regnard,[29] R. Salerno,[29] J. B. Sauvan,[29] Y. Sirois,[29] C. Veelken,[29] Y. Yilmaz,[29] A. Zabi,[29] J.-L. Agram,[30,o] J. Andrea,[30] A. Aubin,[30] D. Bloch,[30] J.-M. Brom,[30] E. C. Chabert,[30] C. Collard,[30] E. Conte,[30,o] J.-C. Fontaine,[30,o] D. Gelé,[30] U. Goerlach,[30] C. Goetzmann,[30] A.-C. Le Bihan,[30] K. Skovpen,[30] P. Van Hove,[30] S. Gadrat,[31] S. Beauceron,[32] N. Beaupere,[32] C. Bernet,[32,h] G. Boudoul,[32,c] E. Bouvier,[32] S. Brochet,[32] C. A. Carrillo Montoya,[32] J. Chasserat,[32] R. Chierici,[32] D. Contardo,[32,c] P. Depasse,[32] H. El Mamouni,[32] J. Fan,[32] J. Fay,[32] S. Gascon,[32] M. Gouzevitch,[32] B. Ille,[32] T. Kurca,[32] M. Lethuillier,[32] L. Mirabito,[32] S. Perries,[32] J. D. Ruiz Alvarez,[32] D. Sabes,[32] L. Sgandurra,[32] V. Sordini,[32] M. Vander Donckt,[32] P. Verdier,[32] S. Viret,[32] H. Xiao,[32] Z. Tsamalaidze,[33,i] C. Autermann,[34] S. Beranek,[34] M. Bontenackels,[34] M. Edelhoff,[34] L. Feld,[34] A. Heister,[34] O. Hindrichs,[34] K. Klein,[34] A. Ostapchuk,[34] M. Preuten,[34] F. Raupach,[34] J. Sammet,[34] S. Schael,[34] J. F. Schulte,[34] H. Weber,[34] B. Wittmer,[34] V. Zhukov,[34,f] M. Ata,[35] M. Brodski,[35] E. Dietz-Laursonn,[35] D. Duchardt,[35] M. Erdmann,[35] R. Fischer,[35] A. Güth,[35] T. Hebbeker,[35] C. Heidemann,[35] K. Hoepfner,[35] D. Klingebiel,[35] S. Knutzen,[35] P. Kreuzer,[35] M. Merschmeyer,[35] A. Meyer,[35] P. Millet,[35] M. Olschewski,[35] K. Padeken,[35] P. Papacz,[35] H. Reithler,[35] S. A. Schmitz,[35] L. Sonnenschein,[35] D. Teyssier,[35] S. Thüer,[35] M. Weber,[35] V. Cherepanov,[36] Y. Erdogan,[36] G. Flügge,[36] H. Geenen,[36] M. Geisler,[36] W. Haj Ahmad,[36] F. Hoehle,[36] B. Kargoll,[36] T. Kress,[36] Y. Kuessel,[36] A. Künsken,[36] J. Lingemann,[36,c] A. Nowack,[36] I. M. Nugent,[36] O. Pooth,[36] A. Stahl,[36] M. Aldaya Martin,[37] I. Asin,[37] N. Bartosik,[37] J. Behr,[37] U. Behrens,[37] A. J. Bell,[37] A. Bethani,[37] K. Borras,[37] A. Burgmeier,[37] A. Cakir,[37] L. Calligaris,[37] A. Campbell,[37] S. Choudhury,[37] F. Costanza,[37] C. Diez Pardos,[37] G. Dolinska,[37] S. Dooling,[37] T. Dorland,[37] G. Eckerlin,[37] D. Eckstein,[37] T. Eichhorn,[37] G. Flucke,[37] J. Garay Garcia,[37] A. Geiser,[37] P. Gunnellini,[37] J. Hauk,[37] M. Hempel,[37,p] H. Jung,[37] A. Kalogeropoulos,[37] M. Kasemann,[37] P. Katsas,[37] J. Kieseler,[37] C. Kleinwort,[37] I. Korol,[37] D. Krücker,[37] W. Lange,[37] J. Leonard,[37] K. Lipka,[37] A. Lobanov,[37] W. Lohmann,[37,p] B. Lutz,[37] R. Mankel,[37] I. Marfin,[37,p] I.-A. Melzer-Pellmann,[37] A. B. Meyer,[37] G. Mittag,[37] J. Mnich,[37] A. Mussgiller,[37] S. Naumann-Emme,[37] A. Nayak,[37] E. Ntomari,[37] H. Perrey,[37] D. Pitzl,[37] R. Placakyte,[37] A. Raspereza,[37] P. M. Ribeiro Cipriano,[37] B. Roland,[37] E. Ron,[37] M. Ö. Sahin,[37] J. Salfeld-Nebgen,[37] P. Saxena,[37] T. Schoerner-Sadenius,[37] M. Schröder,[37] C. Seitz,[37] S. Spannagel,[37] A. D. R. Vargas Trevino,[37] R. Walsh,[37] C. Wissing,[37] V. Blobel,[38] M. Centis Vignali,[38] A. R. Draeger,[38] J. Erfle,[38] E. Garutti,[38] K. Goebel,[38] M. Görner,[38] J. Haller,[38] M. Hoffmann,[38] R. S. Höing,[38] A. Junkes,[38] H. Kirschenmann,[38] R. Klanner,[38] R. Kogler,[38] J. Lange,[38] T. Lapsien,[38] T. Lenz,[38] I. Marchesini,[38] J. Ott,[38] T. Peiffer,[38] A. Perieanu,[38] N. Pietsch,[38] J. Poehlsen,[38] T. Poehlsen,[38] D. Rathjens,[38] C. Sander,[38] H. Schettler,[38] P. Schleper,[38] E. Schlieckau,[38] A. Schmidt,[38] M. Seidel,[38] V. Sola,[38] H. Stadie,[38] G. Steinbrück,[38] D. Troendle,[38] E. Usai,[38] L. Vanelderen,[38] A. Vanhoefer,[38] C. Barth,[39] C. Baus,[39] J. Berger,[39] C. Böser,[39] E. Butz,[39] T. Chwalek,[39] W. De Boer,[39] A. Descroix,[39] A. Dierlamm,[39] M. Feindt,[39] F. Frensch,[39] M. Giffels,[39] A. Gilbert,[39] F. Hartmann,[39,c] T. Hauth,[39] U. Husemann,[39] I. Katkov,[39,f] A. Kornmayer,[39,c] E. Kuznetsova,[39] P. Lobelle Pardo,[39] M. U. Mozer,[39] T. Müller,[39] Th. Müller,[39] A. Nürnberg,[39] G. Quast,[39] K. Rabbertz,[39] S. Röcker,[39] H. J. Simonis,[39] F. M. Stober,[39] R. Ulrich,[39] J. Wagner-Kuhr,[39] S. Wayand,[39] T. Weiler,[39] R. Wolf,[39] G. Anagnostou,[40] G. Daskalakis,[40] T. Geralis,[40] V. A. Giakoumopoulou,[40] A. Kyriakis,[40] D. Loukas,[40] A. Markou,[40] C. Markou,[40] A. Psallidas,[40] I. Topsis-Giotis,[40] A. Agapitos,[41] S. Kesisoglou,[41] A. Panagiotou,[41] N. Saoulidou,[41] E. Stiliaris,[41] X. Aslanoglou,[42] I. Evangelou,[42] G. Flouris,[42] C. Foudas,[42] P. Kokkas,[42] N. Manthos,[42] I. Papadopoulos,[42] E. Paradas,[42] J. Strologas,[42] G. Bencze,[43] C. Hajdu,[43] P. Hidas,[43] D. Horvath,[43,q] F. Sikler,[43] V. Veszpremi,[43] G. Vesztergombi,[43,r] A. J. Zsigmond,[43] N. Beni,[44] S. Czellar,[44] J. Karancsi,[44,s] J. Molnar,[44] J. Palinkas,[44] Z. Szillasi,[44] A. Makovec,[45] P. Raics,[45] Z. L. Trocsanyi,[45] B. Ujvari,[45] S. K. Swain,[46] S. B. Beri,[47] V. Bhatnagar,[47] R. Gupta,[47] U. Bhawandeep,[47] A. K. Kalsi,[47] M. Kaur,[47] R. Kumar,[47] M. Mittal,[47] N. Nishu,[47] J. B. Singh,[47] Ashok Kumar,[48] Arun Kumar,[48] S. Ahuja,[48] A. Bhardwaj,[48] B. C. Choudhary,[48] A. Kumar,[48] S. Malhotra,[48] M. Naimuddin,[48] K. Ranjan,[48] V. Sharma,[48] S. Banerjee,[49] S. Bhattacharya,[49] K. Chatterjee,[49] S. Dutta,[49] B. Gomber,[49] Sa. Jain,[49] Sh. Jain,[49] R. Khurana,[49] A. Modak,[49] S. Mukherjee,[49] D. Roy,[49] S. Sarkar,[49] M. Sharan,[49] A. Abdulsalam,[50] D. Dutta,[50] V. Kumar,[50] A. K. Mohanty,[50,c] L. M. Pant,[50] P. Shukla,[50] A. Topkar,[50] T. Aziz,[51] S. Banerjee,[51] S. Bhowmik,[51,t] R. M. Chatterjee,[51] R. K. Dewanjee,[51] S. Dugad,[51] S. Ganguly,[51] S. Ghosh,[51] M. Guchait,[51] A. Gurtu,[51,u] G. Kole,[51] S. Kumar,[51] M. Maity,[51,t] G. Majumder,[51] K. Mazumdar,[51] G. B. Mohanty,[51] B. Parida,[51]

K. Sudhakar,[51] N. Wickramage,[51,v] H. Bakhshiansohi,[52] H. Behnamian,[52] S. M. Etesami,[52,w] A. Fahim,[52,x] R. Goldouzian,[52] M. Khakzad,[52] M. Mohammadi Najafabadi,[52] M. Naseri,[52] S. Paktinat Mehdiabadi,[52] F. Rezaei Hosseinabadi,[52] B. Safarzadeh,[52,y] M. Zeinali,[52] M. Felcini,[53] M. Grunewald,[53] M. Abbrescia,[54a,54b] C. Calabria,[54a,54b] S. S. Chhibra,[54a,54b] A. Colaleo,[54a] D. Creanza,[54a,54c] N. De Filippis,[54a,54c] M. De Palma,[54a,54b] L. Fiore,[54a] G. Iaselli,[54a,54c] G. Maggi,[54a,54c] M. Maggi,[54a] S. My,[54a,54c] S. Nuzzo,[54a,54b] A. Pompili,[54a,54b] G. Pugliese,[54a,54c] R. Radogna,[54a,54b,c] G. Selvaggi,[54a,54b] A. Sharma,[54a] L. Silvestris,[54a,c] R. Venditti,[54a,54b] P. Verwilligen,[54a] G. Abbiendi,[55a] A. C. Benvenuti,[55a] D. Bonacorsi,[55a,55b] S. Braibant-Giacomelli,[55a,55b] L. Brigliadori,[55a,55b] R. Campanini,[55a,55b] P. Capiluppi,[55a,55b] A. Castro,[55a,55b] F. R. Cavallo,[55a] G. Codispoti,[55a,55b] M. Cuffiani,[55a,55b] G. M. Dallavalle,[55a] F. Fabbri,[55a] A. Fanfani,[55a,55b] D. Fasanella,[55a,55b] P. Giacomelli,[55a] C. Grandi,[55a] L. Guiducci,[55a,55b] S. Marcellini,[55a] G. Masetti,[55a] A. Montanari,[55a] F. L. Navarria,[55a,55b] A. Perrotta,[55a] F. Primavera,[55a,55b] A. M. Rossi,[55a,55b] T. Rovelli,[55a,55b] G. P. Siroli,[55a,55b] N. Tosi,[55a,55b] R. Travaglini,[55a,55b] S. Albergo,[56a,56b] G. Cappello,[56a] M. Chiorboli,[56a,56b] S. Costa,[56a,56b] F. Giordano,[56a,c] R. Potenza,[56a,56b] A. Tricomi,[56a,56b] C. Tuve,[56a,56b] G. Barbagli,[57a] V. Ciulli,[57a,57b] C. Civinini,[57a] R. D'Alessandro,[57a,57b] E. Focardi,[57a,57b] E. Gallo,[57a] S. Gonzi,[57a,57b] V. Gori,[57a,57b] P. Lenzi,[57a,57b] M. Meschini,[57a] S. Paoletti,[57a] G. Sguazzoni,[57a] A. Tropiano,[57a,57b] L. Benussi,[58] S. Bianco,[58] F. Fabbri,[58] D. Piccolo,[58] R. Ferretti,[59a,59b] F. Ferro,[59a] M. Lo Vetere,[59a,59b] E. Robutti,[59a] S. Tosi,[59a,59b] M. E. Dinardo,[60a,60b] S. Fiorendi,[60a,60b] S. Gennai,[60a,c] R. Gerosa,[60a,60b,c] A. Ghezzi,[60a,60b] P. Govoni,[60a,60b] M. T. Lucchini,[60a,60b,c] S. Malvezzi,[60a] R. A. Manzoni,[60a,60b] A. Martelli,[60a,60b] B. Marzocchi,[60a,60b,c] D. Menasce,[60a] L. Moroni,[60a] M. Paganoni,[60a,60b] D. Pedrini,[60a] S. Ragazzi,[60a,60b] N. Redaelli,[60a] T. Tabarelli de Fatis,[60a,60b] S. Buontempo,[61a] N. Cavallo,[61a,61c] S. Di Guida,[61a,61d,c] F. Fabozzi,[61a,61c] A. O. M. Iorio,[61a,61b] L. Lista,[61a] S. Meola,[61a,61d,c] M. Merola,[61a] P. Paolucci,[61a,c] P. Azzi,[62a] N. Bacchetta,[62a] D. Bisello,[62a,62b] A. Branca,[62a,62b] R. Carlin,[62a,62b] P. Checchia,[62a] M. Dall'Osso,[62a,62b] T. Dorigo,[62a] U. Dosselli,[62a] M. Galanti,[62a,62b] F. Gasparini,[62a,62b] U. Gasparini,[62a,62b] A. Gozzelino,[62a] K. Kanishchev,[62a,62c] S. Lacaprara,[62a] M. Margoni,[62a,62b] A. T. Meneguzzo,[62a,62b] J. Pazzini,[62a,62b] N. Pozzobon,[62a,62b] P. Ronchese,[62a,62b] F. Simonetto,[62a,62b] E. Torassa,[62a] M. Tosi,[62a,62b] P. Zotto,[62a,62b] A. Zucchetta,[62a,62b] G. Zumerle,[62a,62b] M. Gabusi,[63a,63b] S. P. Ratti,[63a,63b] V. Re,[63a] C. Riccardi,[63a,63b] P. Salvini,[63a] P. Vitulo,[63a,63b] M. Biasini,[64a,64b] G. M. Bilei,[64a] D. Ciangottini,[64a,64b,c] L. Fanò,[64a,64b] P. Lariccia,[64a,64b] G. Mantovani,[64a,64b] M. Menichelli,[64a] A. Saha,[64a] A. Santocchia,[64a,64b] A. Spiezia,[64a,64b,c] K. Androsov,[65a,z] P. Azzurri,[65a] G. Bagliesi,[65a] J. Bernardini,[65a] T. Boccali,[65a] G. Broccolo,[65a,65c] R. Castaldi,[65a] M. A. Ciocci,[65a,z] R. Dell'Orso,[65a] S. Donato,[65a,65c,c] F. Fiori,[65a,65c] L. Foà,[65a,65c] A. Giassi,[65a] M. T. Grippo,[65a,z] F. Ligabue,[65a,65c] T. Lomtadze,[65a] L. Martini,[65a,65b] A. Messineo,[65a,65b] C. S. Moon,[65a,aa] F. Palla,[65a,c] A. Rizzi,[65a,65b] A. Savoy-Navarro,[65a,bb] A. T. Serban,[65a] P. Spagnolo,[65a] P. Squillacioti,[65a,z] R. Tenchini,[65a] G. Tonelli,[65a,65b] A. Venturi,[65a] P. G. Verdini,[65a] C. Vernieri,[65a,65c] L. Barone,[66a,66b] F. Cavallari,[66a] G. D'imperio,[66a,66b] D. Del Re,[66a,66b] M. Diemoz,[66a] C. Jorda,[66a] E. Longo,[66a,66b] F. Margaroli,[66a,66b] P. Meridiani,[66a] F. Micheli,[66a,66b,c] G. Organtini,[66a,66b] R. Paramatti,[66a] S. Rahatlou,[66a,66b] C. Rovelli,[66a] F. Santanastasio,[66a,66b] L. Soffi,[66a,66b] P. Traczyk,[66a,66b,c] N. Amapane,[67a,67b] R. Arcidiacono,[67a,67c] S. Argiro,[67a,67b] M. Arneodo,[67a,67c] R. Bellan,[67a,67b] C. Biino,[67a] N. Cartiglia,[67a] S. Casasso,[67a,67b,c] M. Costa,[67a,67b] A. Degano,[67a,67b] N. Demaria,[67a] L. Finco,[67a,67b,c] C. Mariotti,[67a] S. Maselli,[67a] E. Migliore,[67a,67b] V. Monaco,[67a,67b] M. Musich,[67a] M. M. Obertino,[67a,67c] L. Pacher,[67a,67b] N. Pastrone,[67a] M. Pelliccioni,[67a] G. L. Pinna Angioni,[67a,67b] A. Potenza,[67a,67b] A. Romero,[67a,67b] M. Ruspa,[67a,67c] R. Sacchi,[67a,67b] A. Solano,[67a,67b] A. Staiano,[67a] U. Tamponi,[67a] S. Belforte,[68a] V. Candelise,[68a,68b,c] M. Casarsa,[68a] F. Cossutti,[68a] G. Della Ricca,[68a,68b] B. Gobbo,[68a] C. La Licata,[68a,68b] M. Marone,[68a,68b] A. Schizzi,[68a,68b] T. Umer,[68a,68b] A. Zanetti,[68a] S. Chang,[69] A. Kropivnitskaya,[69] S. K. Nam,[69] D. H. Kim,[70] G. N. Kim,[70] M. S. Kim,[70] D. J. Kong,[70] S. Lee,[70] Y. D. Oh,[70] H. Park,[70] A. Sakharov,[70] D. C. Son,[70] T. J. Kim,[71] M. S. Ryu,[71] J. Y. Kim,[72] D. H. Moon,[72] S. Song,[72] S. Choi,[73] D. Gyun,[73] B. Hong,[73] M. Jo,[73] H. Kim,[73] Y. Kim,[73] B. Lee,[73] K. S. Lee,[73] S. K. Park,[73] Y. Roh,[73] H. D. Yoo,[74] M. Choi,[75] J. H. Kim,[75] I. C. Park,[75] G. Ryu,[75] Y. Choi,[76] Y. K. Choi,[76] J. Goh,[76] D. Kim,[76] E. Kwon,[76] J. Lee,[76] I. Yu,[76] A. Juodagalvis,[77] J. R. Komaragiri,[78] M. A. B. Md Ali,[78] E. Casimiro Linares,[79] H. Castilla-Valdez,[79] E. De La Cruz-Burelo,[79] I. Heredia-de La Cruz,[79] A. Hernandez-Almada,[79] R. Lopez-Fernandez,[79] A. Sanchez-Hernandez,[79] S. Carrillo Moreno,[80] F. Vazquez Valencia,[80] I. Pedraza,[81] H. A. Salazar Ibarguen,[81] A. Morelos Pineda,[82] D. Krofcheck,[83] P. H. Butler,[84] S. Reucroft,[84] A. Ahmad,[85] M. Ahmad,[85] Q. Hassan,[85] H. R. Hoorani,[85] W. A. Khan,[85] T. Khurshid,[85] M. Shoaib,[85] H. Bialkowska,[86] M. Bluj,[86] B. Boimska,[86] T. Frueboes,[86] M. Górski,[86] M. Kazana,[86] K. Nawrocki,[86] K. Romanowska-Rybinska,[86] M. Szleper,[86] P. Zalewski,[86] G. Brona,[87] K. Bunkowski,[87] M. Cwiok,[87] W. Dominik,[87] K. Doroba,[87] A. Kalinowski,[87] M. Konecki,[87] J. Krolikowski,[87] M. Misiura,[87] M. Olszewski,[87] P. Bargassa,[88] C. Beirão Da Cruz E Silva,[88] P. Faccioli,[88] P. G. Ferreira Parracho,[88] M. Gallinaro,[88] L. Lloret Iglesias,[88] F. Nguyen,[88] J. Rodrigues Antunes,[88] J. Seixas,[88] J. Varela,[88]

P. Vischia,[88] S. Afanasiev,[89] P. Bunin,[89] M. Gavrilenko,[89] I. Golutvin,[89] I. Gorbunov,[89] A. Kamenev,[89] V. Karjavin,[89] V. Konoplyanikov,[89] A. Lanev,[89] A. Malakhov,[89] V. Matveev,[89,cc] P. Moisenz,[89] V. Palichik,[89] V. Perelygin,[89] S. Shmatov,[89] N. Skatchkov,[89] V. Smirnov,[89] A. Zarubin,[89] V. Golovtsov,[90] Y. Ivanov,[90] V. Kim,[90,dd] P. Levchenko,[90] V. Murzin,[90] V. Oreshkin,[90] I. Smirnov,[90] V. Sulimov,[90] L. Uvarov,[90] S. Vavilov,[90] A. Vorobyev,[90] An. Vorobyev,[90] Yu. Andreev,[91] A. Dermenev,[91] S. Gninenko,[91] N. Golubev,[91] M. Kirsanov,[91] N. Krasnikov,[91] A. Pashenkov,[91] D. Tlisov,[91] A. Toropin,[91] V. Epshteyn,[92] V. Gavrilov,[92] N. Lychkovskaya,[92] V. Popov,[92] I. Pozdnyakov,[92] G. Safronov,[92] S. Semenov,[92] A. Spiridonov,[92] V. Stolin,[92] E. Vlasov,[92] A. Zhokin,[92] V. Andreev,[93] M. Azarkin,[93] I. Dremin,[93] M. Kirakosyan,[93] A. Leonidov,[93] G. Mesyats,[93] S. V. Rusakov,[93] A. Vinogradov,[93] A. Belyaev,[94] E. Boos,[94] V. Bunichev,[94] M. Dubinin,[94,ee] L. Dudko,[94] A. Gribushin,[94] V. Klyukhin,[94] O. Kodolova,[94] I. Lokhtin,[94] S. Obraztsov,[94] M. Perfilov,[94] S. Petrushanko,[94] V. Savrin,[94] I. Azhgirey,[95] I. Bayshev,[95] S. Bitioukov,[95] V. Kachanov,[95] A. Kalinin,[95] D. Konstantinov,[95] V. Krychkine,[95] V. Petrov,[95] R. Ryutin,[95] A. Sobol,[95] L. Tourtchanovitch,[95] S. Troshin,[95] N. Tyurin,[95] A. Uzunian,[95] A. Volkov,[95] P. Adzic,[96,ff] M. Ekmedzic,[96] J. Milosevic,[96] V. Rekovic,[96] J. Alcaraz Maestre,[97] C. Battilana,[97] E. Calvo,[97] M. Cerrada,[97] M. Chamizo Llatas,[97] N. Colino,[97] B. De La Cruz,[97] A. Delgado Peris,[97] D. Domínguez Vázquez,[97] A. Escalante Del Valle,[97] C. Fernandez Bedoya,[97] J. P. Fernández Ramos,[97] J. Flix,[97] M. C. Fouz,[97] P. Garcia-Abia,[97] O. Gonzalez Lopez,[97] S. Goy Lopez,[97] J. M. Hernandez,[97] M. I. Josa,[97] E. Navarro De Martino,[97] A. Pérez-Calero Yzquierdo,[97] J. Puerta Pelayo,[97] A. Quintario Olmeda,[97] I. Redondo,[97] L. Romero,[97] M. S. Soares,[97] C. Albajar,[98] J. F. de Trocóniz,[98] M. Missiroli,[98] D. Moran,[98] H. Brun,[99] J. Cuevas,[99] J. Fernandez Menendez,[99] S. Folgueras,[99] I. Gonzalez Caballero,[99] J. A. Brochero Cifuentes,[100] I. J. Cabrillo,[100] A. Calderon,[100] J. Duarte Campderros,[100] M. Fernandez,[100] G. Gomez,[100] A. Graziano,[100] A. Lopez Virto,[100] J. Marco,[100] R. Marco,[100] C. Martinez Rivero,[100] F. Matorras,[100] F. J. Munoz Sanchez,[100] J. Piedra Gomez,[100] T. Rodrigo,[100] A. Y. Rodríguez-Marrero,[100] A. Ruiz-Jimeno,[100] L. Scodellaro,[100] I. Vila,[100] R. Vilar Cortabitarte,[100] D. Abbaneo,[101] E. Auffray,[101] G. Auzinger,[101] M. Bachtis,[101] P. Baillon,[101] A. H. Ball,[101] D. Barney,[101] A. Benaglia,[101] J. Bendavid,[101] L. Benhabib,[101] J. F. Benitez,[101] P. Bloch,[101] A. Bocci,[101] A. Bonato,[101] O. Bondu,[101] C. Botta,[101] H. Breuker,[101] T. Camporesi,[101] G. Cerminara,[101] S. Colafranceschi,[101,gg] M. D'Alfonso,[101] D. d'Enterria,[101] A. Dabrowski,[101] A. David,[101] F. De Guio,[101] A. De Roeck,[101] S. De Visscher,[101] E. Di Marco,[101] M. Dobson,[101] M. Dordevic,[101] B. Dorney,[101] N. Dupont-Sagorin,[101] A. Elliott-Peisert,[101] G. Franzoni,[101] W. Funk,[101] D. Gigi,[101] K. Gill,[101] D. Giordano,[101] M. Girone,[101] F. Glege,[101] R. Guida,[101] S. Gundacker,[101] M. Guthoff,[101] J. Hammer,[101] M. Hansen,[101] P. Harris,[101] J. Hegeman,[101] V. Innocente,[101] P. Janot,[101] K. Kousouris,[101] K. Krajczar,[101] P. Lecoq,[101] C. Lourenço,[101] N. Magini,[101] L. Malgeri,[101] M. Mannelli,[101] J. Marrouche,[101] L. Masetti,[101] F. Meijers,[101] S. Mersi,[101] E. Meschi,[101] F. Moortgat,[101] S. Morovic,[101] M. Mulders,[101] L. Orsini,[101] L. Pape,[101] E. Perez,[101] A. Petrilli,[101] G. Petrucciani,[101] A. Pfeiffer,[101] M. Pimiä,[101] D. Piparo,[101] M. Plagge,[101] A. Racz,[101] G. Rolandi,[101,hh] M. Rovere,[101] H. Sakulin,[101] C. Schäfer,[101] C. Schwick,[101] A. Sharma,[101] P. Siegrist,[101] P. Silva,[101] M. Simon,[101] P. Sphicas,[101,ii] D. Spiga,[101] J. Steggemann,[101] B. Stieger,[101] M. Stoye,[101] Y. Takahashi,[101] D. Treille,[101] A. Tsirou,[101] G. I. Veres,[101,r] N. Wardle,[101] H. K. Wöhri,[101] H. Wollny,[101] W. D. Zeuner,[101] W. Bertl,[102] K. Deiters,[102] W. Erdmann,[102] R. Horisberger,[102] Q. Ingram,[102] H. C. Kaestli,[102] D. Kotlinski,[102] U. Langenegger,[102] D. Renker,[102] T. Rohe,[102] F. Bachmair,[103] L. Bäni,[103] L. Bianchini,[103] M. A. Buchmann,[103] B. Casal,[103] N. Chanon,[103] G. Dissertori,[103] M. Dittmar,[103] M. Donegà,[103] M. Dünser,[103] P. Eller,[103] C. Grab,[103] D. Hits,[103] J. Hoss,[103] W. Lustermann,[103] B. Mangano,[103] A. C. Marini,[103] M. Marionneau,[103] P. Martinez Ruiz del Arbol,[103] M. Masciovecchio,[103] D. Meister,[103] N. Mohr,[103] P. Musella,[103] C. Nägeli,[103,jj] F. Nessi-Tedaldi,[103] F. Pandolfi,[103] F. Pauss,[103] L. Perrozzi,[103] M. Peruzzi,[103] M. Quittnat,[103] L. Rebane,[103] M. Rossini,[103] A. Starodumov,[103,kk] M. Takahashi,[103] K. Theofilatos,[103] R. Wallny,[103] H. A. Weber,[103] C. Amsler,[104,ll] M. F. Canelli,[104] V. Chiochia,[104] A. De Cosa,[104] A. Hinzmann,[104] T. Hreus,[104] B. Kilminster,[104] C. Lange,[104] B. Millan Mejias,[104] J. Ngadiuba,[104] D. Pinna,[104] P. Robmann,[104] F. J. Ronga,[104] S. Taroni,[104] M. Verzetti,[104] Y. Yang,[104] M. Cardaci,[105] K. H. Chen,[105] C. Ferro,[105] C. M. Kuo,[105] W. Lin,[105] Y. J. Lu,[105] R. Volpe,[105] S. S. Yu,[105] P. Chang,[106] Y. H. Chang,[106] Y. W. Chang,[106] Y. Chao,[106] K. F. Chen,[106] P. H. Chen,[106] C. Dietz,[106] U. Grundler,[106] W.-S. Hou,[106] K. Y. Kao,[106] Y. F. Liu,[106] R.-S. Lu,[106] E. Petrakou,[106] Y. M. Tzeng,[106] R. Wilken,[106] B. Asavapibhop,[107] G. Singh,[107] N. Srimanobhas,[107] N. Suwonjandee,[107] A. Adiguzel,[108] M. N. Bakirci,[108,mm] S. Cerci,[108,nn] C. Dozen,[108] I. Dumanoglu,[108] E. Eskut,[108] S. Girgis,[108] G. Gokbulut,[108] Y. Guler,[108] E. Gurpinar,[108] I. Hos,[108] E. E. Kangal,[108] A. Kayis Topaksu,[108] G. Onengut,[108,oo] K. Ozdemir,[108] S. Ozturk,[108,mm] A. Polatoz,[108] D. Sunar Cerci,[108,nn] B. Tali,[108,nn] H. Topakli,[108,mm] M. Vergili,[108] C. Zorbilmez,[108] I. V. Akin,[109] B. Bilin,[109] S. Bilmis,[109] H. Gamsizkan,[109,pp] B. Isildak,[109,qq] G. Karapinar,[109,rr] K. Ocalan,[109,ss] S. Sekmen,[109] U. E. Surat,[109] M. Yalvac,[109] M. Zeyrek,[109]

E. A. Albayrak,[110,tt] E. Gülmez,[110] M. Kaya,[110,uu] O. Kaya,[110,vv] T. Yetkin,[110,ww] K. Cankocak,[111] F. I. Vardarlı,[111] L. Levchuk,[112] P. Sorokin,[112] J. J. Brooke,[113] E. Clement,[113] D. Cussans,[113] H. Flacher,[113] J. Goldstein,[113] M. Grimes,[113] G. P. Heath,[113] H. F. Heath,[113] J. Jacob,[113] L. Kreczko,[113] C. Lucas,[113] Z. Meng,[113] D. M. Newbold,[113,xx] S. Paramesvaran,[113] A. Poll,[113] T. Sakuma,[113] S. Seif El Nasr-storey,[113] S. Senkin,[113] V. J. Smith,[113] K. W. Bell,[114] A. Belyaev,[114,yy] C. Brew,[114] R. M. Brown,[114] D. J. A. Cockerill,[114] J. A. Coughlan,[114] K. Harder,[114] S. Harper,[114] E. Olaiya,[114] D. Petyt,[114] C. H. Shepherd-Themistocleous,[114] A. Thea,[114] I. R. Tomalin,[114] T. Williams,[114] W. J. Womersley,[114] S. D. Worm,[114] M. Baber,[115] R. Bainbridge,[115] O. Buchmuller,[115] D. Burton,[115] D. Colling,[115] N. Cripps,[115] P. Dauncey,[115] G. Davies,[115] M. Della Negra,[115] P. Dunne,[115] W. Ferguson,[115] J. Fulcher,[115] D. Futyan,[115] G. Hall,[115] G. Iles,[115] M. Jarvis,[115] G. Karapostoli,[115] M. Kenzie,[115] R. Lane,[115] R. Lucas,[115,xx] L. Lyons,[115] A.-M. Magnan,[115] S. Malik,[115] B. Mathias,[115] J. Nash,[115] A. Nikitenko,[115,kk] J. Pela,[115] M. Pesaresi,[115] K. Petridis,[115] D. M. Raymond,[115] S. Rogerson,[115] A. Rose,[115] C. Seez,[115] P. Sharp,[115,a] A. Tapper,[115] M. Vazquez Acosta,[115] T. Virdee,[115] S. C. Zenz,[115] J. E. Cole,[116] P. R. Hobson,[116] A. Khan,[116] P. Kyberd,[116] D. Leggat,[116] D. Leslie,[116] I. D. Reid,[116] P. Symonds,[116] L. Teodorescu,[116] M. Turner,[116] J. Dittmann,[117] K. Hatakeyama,[117] A. Kasmi,[117] H. Liu,[117] T. Scarborough,[117] O. Charaf,[118] S. I. Cooper,[118] C. Henderson,[118] P. Rumerio,[118] A. Avetisyan,[119] T. Bose,[119] C. Fantasia,[119] P. Lawson,[119] C. Richardson,[119] J. Rohlf,[119] J. St. John,[119] L. Sulak,[119] J. Alimena,[120] E. Berry,[120] S. Bhattacharya,[120] G. Christopher,[120] D. Cutts,[120] Z. Demiragli,[120] N. Dhingra,[120] A. Ferapontov,[120] A. Garabedian,[120] U. Heintz,[120] G. Kukartsev,[120] E. Laird,[120] G. Landsberg,[120] M. Luk,[120] M. Narain,[120] M. Segala,[120] T. Sinthuprasith,[120] T. Speer,[120] J. Swanson,[120] R. Breedon,[121] G. Breto,[121] M. Calderon De La Barca Sanchez,[121] S. Chauhan,[121] M. Chertok,[121] J. Conway,[121] R. Conway,[121] P. T. Cox,[121] R. Erbacher,[121] M. Gardner,[121] W. Ko,[121] R. Lander,[121] M. Mulhearn,[121] D. Pellett,[121] J. Pilot,[121] F. Ricci-Tam,[121] S. Shalhout,[121] J. Smith,[121] M. Squires,[121] D. Stolp,[121] M. Tripathi,[121] S. Wilbur,[121] R. Yohay,[121] R. Cousins,[122] P. Everaerts,[122] C. Farrell,[122] J. Hauser,[122] M. Ignatenko,[122] G. Rakness,[122] E. Takasugi,[122] V. Valuev,[122] M. Weber,[122] K. Burt,[123] R. Clare,[123] J. Ellison,[123] J. W. Gary,[123] G. Hanson,[123] J. Heilman,[123] M. Ivova Rikova,[123] P. Jandir,[123] E. Kennedy,[123] F. Lacroix,[123] O. R. Long,[123] A. Luthra,[123] M. Malberti,[123] M. Olmedo Negrete,[123] A. Shrinivas,[123] S. Sumowidagdo,[123] S. Wimpenny,[123] J. G. Branson,[124] G. B. Cerati,[124] S. Cittolin,[124] R. T. D'Agnolo,[124] A. Holzner,[124] R. Kelley,[124] D. Klein,[124] J. Letts,[124] I. Macneill,[124] D. Olivito,[124] S. Padhi,[124] C. Palmer,[124] M. Pieri,[124] M. Sani,[124] V. Sharma,[124] S. Simon,[124] M. Tadel,[124] Y. Tu,[124] A. Vartak,[124] C. Welke,[124] F. Würthwein,[124] A. Yagil,[124] D. Barge,[125] J. Bradmiller-Feld,[125] C. Campagnari,[125] T. Danielson,[125] A. Dishaw,[125] V. Dutta,[125] K. Flowers,[125] M. Franco Sevilla,[125] P. Geffert,[125] C. George,[125] F. Golf,[125] L. Gouskos,[125] J. Incandela,[125] C. Justus,[125] N. Mccoll,[125] J. Richman,[125] D. Stuart,[125] W. To,[125] C. West,[125] J. Yoo,[125] A. Apresyan,[126] A. Bornheim,[126] J. Bunn,[126] Y. Chen,[126] J. Duarte,[126] A. Mott,[126] H. B. Newman,[126] C. Pena,[126] M. Pierini,[126] M. Spiropulu,[126] J. R. Vlimant,[126] R. Wilkinson,[126] S. Xie,[126] R. Y. Zhu,[126] V. Azzolini,[127] A. Calamba,[127] B. Carlson,[127] T. Ferguson,[127] Y. Iiyama,[127] M. Paulini,[127] J. Russ,[127] H. Vogel,[127] I. Vorobiev,[127] J. P. Cumalat,[128] W. T. Ford,[128] A. Gaz,[128] M. Krohn,[128] E. Luiggi Lopez,[128] U. Nauenberg,[128] J. G. Smith,[128] K. Stenson,[128] S. R. Wagner,[128] J. Alexander,[129] A. Chatterjee,[129] J. Chaves,[129] J. Chu,[129] S. Dittmer,[129] N. Eggert,[129] N. Mirman,[129] G. Nicolas Kaufman,[129] J. R. Patterson,[129] A. Ryd,[129] E. Salvati,[129] L. Skinnari,[129] W. Sun,[129] W. D. Teo,[129] J. Thom,[129] J. Thompson,[129] J. Tucker,[129] Y. Weng,[129] L. Winstrom,[129] P. Wittich,[129] D. Winn,[130] S. Abdullin,[131] M. Albrow,[131] J. Anderson,[131] G. Apollinari,[131] L. A. T. Bauerdick,[131] A. Beretvas,[131] J. Berryhill,[131] P. C. Bhat,[131] G. Bolla,[131] K. Burkett,[131] J. N. Butler,[131] H. W. K. Cheung,[131] F. Chlebana,[131] S. Cihangir,[131] V. D. Elvira,[131] I. Fisk,[131] J. Freeman,[131] Y. Gao,[131] E. Gottschalk,[131] L. Gray,[131] D. Green,[131] S. Grünendahl,[131] O. Gutsche,[131] J. Hanlon,[131] D. Hare,[131] R. M. Harris,[131] J. Hirschauer,[131] B. Hooberman,[131] S. Jindariani,[131] M. Johnson,[131] U. Joshi,[131] B. Klima,[131] B. Kreis,[131] S. Kwan,[131,a] J. Linacre,[131] D. Lincoln,[131] R. Lipton,[131] T. Liu,[131] J. Lykken,[131] K. Maeshima,[131] J. M. Marraffino,[131] V. I. Martinez Outschoorn,[131] S. Maruyama,[131] D. Mason,[131] P. McBride,[131] P. Merkel,[131] K. Mishra,[131] S. Mrenna,[131] S. Nahn,[131] C. Newman-Holmes,[131] V. O'Dell,[131] O. Prokofyev,[131] E. Sexton-Kennedy,[131] S. Sharma,[131] A. Soha,[131] W. J. Spalding,[131] L. Spiegel,[131] L. Taylor,[131] S. Tkaczyk,[131] N. V. Tran,[131] L. Uplegger,[131] E. W. Vaandering,[131] R. Vega Morales,[131,zz] R. Vidal,[131] A. Whitbeck,[131] J. Whitmore,[131] F. Yang,[131] D. Acosta,[132] P. Avery,[132] P. Bortignon,[132] D. Bourilkov,[132] M. Carver,[132] D. Curry,[132] S. Das,[132] M. De Gruttola,[132] G. P. Di Giovanni,[132] R. D. Field,[132] M. Fisher,[132] I. K. Furic,[132] J. Gainer,[132] J. Hugon,[132] J. Konigsberg,[132] A. Korytov,[132] T. Kypreos,[132] J. F. Low,[132] K. Matchev,[132] H. Mei,[132] P. Milenovic,[132,aaa] G. Mitselmakher,[132] L. Muniz,[132] A. Rinkevicius,[132] L. Shchutska,[132] M. Snowball,[132] D. Sperka,[132] J. Yelton,[132] M. Zakaria,[132] S. Hewamanage,[133] S. Linn,[133] P. Markowitz,[133] G. Martinez,[133] J. L. Rodriguez,[133] T. Adams,[134] A. Askew,[134] J. Bochenek,[134] B. Diamond,[134] J. Haas,[134] S. Hagopian,[134] V. Hagopian,[134] K. F. Johnson,[134]

H. Prosper,[134] V. Veeraraghavan,[134] M. Weinberg,[134] M. M. Baarmand,[135] M. Hohlmann,[135] H. Kalakhety,[135] F. Yumiceva,[135] M. R. Adams,[136] L. Apanasevich,[136] D. Berry,[136] R. R. Betts,[136] I. Bucinskaite,[136] R. Cavanaugh,[136] O. Evdokimov,[136] L. Gauthier,[136] C. E. Gerber,[136] D. J. Hofman,[136] P. Kurt,[136] C. O'Brien,[136] I. D. Sandoval Gonzalez,[136] C. Silkworth,[136] P. Turner,[136] N. Varelas,[136] B. Bilki,[137,bbb] W. Clarida,[137] K. Dilsiz,[137] M. Haytmyradov,[137] J.-P. Merlo,[137] H. Mermerkaya,[137,ccc] A. Mestvirishvili,[137] A. Moeller,[137] J. Nachtman,[137] H. Ogul,[137] Y. Onel,[137] F. Ozok,[137,tt] A. Penzo,[137] R. Rahmat,[137] S. Sen,[137] P. Tan,[137] E. Tiras,[137] J. Wetzel,[137] K. Yi,[137] I. Anderson,[138] B. A. Barnett,[138] B. Blumenfeld,[138] S. Bolognesi,[138] D. Fehling,[138] A. V. Gritsan,[138] P. Maksimovic,[138] C. Martin,[138] J. Roskes,[138] U. Sarica,[138] M. Swartz,[138] M. Xiao,[138] C. You,[138] P. Baringer,[139] A. Bean,[139] G. Benelli,[139] C. Bruner,[139] J. Gray,[139] R. P. Kenny III,[139] D. Majumder,[139] M. Malek,[139] M. Murray,[139] D. Noonan,[139] S. Sanders,[139] J. Sekaric,[139] R. Stringer,[139] Q. Wang,[139] J. S. Wood,[139] I. Chakaberia,[140] A. Ivanov,[140] K. Kaadze,[140] S. Khalil,[140] M. Makouski,[140] Y. Maravin,[140] L. K. Saini,[140] N. Skhirtladze,[140] I. Svintradze,[140] J. Gronberg,[141] D. Lange,[141] F. Rebassoo,[141] D. Wright,[141] A. Baden,[142] A. Belloni,[142] B. Calvert,[142] S. C. Eno,[142] J. A. Gomez,[142] N. J. Hadley,[142] R. G. Kellogg,[142] T. Kolberg,[142] Y. Lu,[142] A. C. Mignerey,[142] K. Pedro,[142] A. Skuja,[142] M. B. Tonjes,[142] S. C. Tonwar,[142] A. Apyan,[143] R. Barbieri,[143] W. Busza,[143] I. A. Cali,[143] M. Chan,[143] L. Di Matteo,[143] G. Gomez Ceballos,[143] M. Goncharov,[143] D. Gulhan,[143] M. Klute,[143] Y. S. Lai,[143] Y.-J. Lee,[143] A. Levin,[143] P. D. Luckey,[143] C. Paus,[143] D. Ralph,[143] C. Roland,[143] G. Roland,[143] G. S. F. Stephans,[143] K. Sumorok,[143] D. Velicanu,[143] J. Veverka,[143] B. Wyslouch,[143] M. Yang,[143] M. Zanetti,[143] V. Zhukova,[143] B. Dahmes,[144] A. Gude,[144] S. C. Kao,[144] K. Klapoetke,[144] Y. Kubota,[144] J. Mans,[144] S. Nourbakhsh,[144] N. Pastika,[144] R. Rusack,[144] A. Singovsky,[144] N. Tambe,[144] J. Turkewitz,[144] J. G. Acosta,[145] S. Oliveros,[145] E. Avdeeva,[146] K. Bloom,[146] S. Bose,[146] D. R. Claes,[146] A. Dominguez,[146] R. Gonzalez Suarez,[146] J. Keller,[146] D. Knowlton,[146] I. Kravchenko,[146] J. Lazo-Flores,[146] F. Meier,[146] F. Ratnikov,[146] G. R. Snow,[146] M. Zvada,[146] J. Dolen,[147] A. Godshalk,[147] I. Iashvili,[147] A. Kharchilava,[147] A. Kumar,[147] S. Rappoccio,[147] G. Alverson,[148] E. Barberis,[148] D. Baumgartel,[148] M. Chasco,[148] A. Massironi,[148] D. M. Morse,[148] D. Nash,[148] T. Orimoto,[148] D. Trocino,[148] R.-J. Wang,[148] D. Wood,[148] J. Zhang,[148] K. A. Hahn,[149] A. Kubik,[149] N. Mucia,[149] N. Odell,[149] B. Pollack,[149] A. Pozdnyakov,[149] M. Schmitt,[149] S. Stoynev,[149] K. Sung,[149] M. Velasco,[149] S. Won,[149] A. Brinkerhoff,[150] K. M. Chan,[150] A. Drozdetskiy,[150] M. Hildreth,[150] C. Jessop,[150] D. J. Karmgard,[150] N. Kellams,[150] K. Lannon,[150] S. Lynch,[150] N. Marinelli,[150] Y. Musienko,[150,cc] T. Pearson,[150] M. Planer,[150] R. Ruchti,[150] G. Smith,[150] N. Valls,[150] M. Wayne,[150] M. Wolf,[150] A. Woodard,[150] L. Antonelli,[151] J. Brinson,[151] B. Bylsma,[151] L. S. Durkin,[151] S. Flowers,[151] A. Hart,[151] C. Hill,[151] R. Hughes,[151] K. Kotov,[151] T. Y. Ling,[151] W. Luo,[151] D. Puigh,[151] M. Rodenburg,[151] B. L. Winer,[151] H. Wolfe,[151] H. W. Wulsin,[151] O. Driga,[152] P. Elmer,[152] J. Hardenbrook,[152] P. Hebda,[152] S. A. Koay,[152] P. Lujan,[152] D. Marlow,[152] T. Medvedeva,[152] M. Mooney,[152] J. Olsen,[152] P. Piroué,[152] X. Quan,[152] H. Saka,[152] D. Stickland,[152,c] C. Tully,[152] J. S. Werner,[152] A. Zuranski,[152] E. Brownson,[153] S. Malik,[153] H. Mendez,[153] J. E. Ramirez Vargas,[153] V. E. Barnes,[154] D. Benedetti,[154] D. Bortoletto,[154] M. De Mattia,[154] L. Gutay,[154] Z. Hu,[154] M. K. Jha,[154] M. Jones,[154] K. Jung,[154] M. Kress,[154] N. Leonardo,[154] D. H. Miller,[154] N. Neumeister,[154] B. C. Radburn-Smith,[154] X. Shi,[154] I. Shipsey,[154] D. Silvers,[154] A. Svyatkovskiy,[154] F. Wang,[154] W. Xie,[154] L. Xu,[154] J. Zablocki,[154] N. Parashar,[155] J. Stupak,[155] A. Adair,[156] B. Akgun,[156] K. M. Ecklund,[156] F. J. M. Geurts,[156] W. Li,[156] B. Michlin,[156] B. P. Padley,[156] R. Redjimi,[156] J. Roberts,[156] J. Zabel,[156] B. Betchart,[157] A. Bodek,[157] R. Covarelli,[157] P. de Barbaro,[157] R. Demina,[157] Y. Eshaq,[157] T. Ferbel,[157] A. Garcia-Bellido,[157] P. Goldenzweig,[157] J. Han,[157] A. Harel,[157] A. Khukhunaishvili,[157] S. Korjenevski,[157] G. Petrillo,[157] D. Vishnevskiy,[157] R. Ciesielski,[158] L. Demortier,[158] K. Goulianos,[158] C. Mesropian,[158] S. Arora,[159] A. Barker,[159] J. P. Chou,[159] C. Contreras-Campana,[159] E. Contreras-Campana,[159] D. Duggan,[159] D. Ferencek,[159] Y. Gershtein,[159] R. Gray,[159] E. Halkiadakis,[159] D. Hidas,[159] S. Kaplan,[159] A. Lath,[159] S. Panwalkar,[159] M. Park,[159] R. Patel,[159] S. Salur,[159] S. Schnetzer,[159] D. Sheffield,[159] S. Somalwar,[159] R. Stone,[159] S. Thomas,[159] P. Thomassen,[159] M. Walker,[159] K. Rose,[160] S. Spanier,[160] A. York,[160] O. Bouhali,[161,ddd] A. Castaneda Hernandez,[161] R. Eusebi,[161] W. Flanagan,[161] J. Gilmore,[161] T. Kamon,[161,eee] V. Khotilovich,[161] V. Krutelyov,[161] R. Montalvo,[161] I. Osipenkov,[161] Y. Pakhotin,[161] A. Perloff,[161] J. Roe,[161] A. Rose,[161] A. Safonov,[161] I. Suarez,[161] A. Tatarinov,[161] K. A. Ulmer,[161] N. Akchurin,[162] C. Cowden,[162] J. Damgov,[162] C. Dragoiu,[162] P. R. Dudero,[162] J. Faulkner,[162] K. Kovitanggoon,[162] S. Kunori,[162] S. W. Lee,[162] T. Libeiro,[162] I. Volobouev,[162] E. Appelt,[163] A. G. Delannoy,[163] S. Greene,[163] A. Gurrola,[163] W. Johns,[163] C. Maguire,[163] Y. Mao,[163] A. Melo,[163] M. Sharma,[163] P. Sheldon,[163] B. Snook,[163] S. Tuo,[163] J. Velkovska,[163] M. W. Arenton,[164] S. Boutle,[164] B. Cox,[164] B. Francis,[164] J. Goodell,[164] R. Hirosky,[164] A. Ledovskoy,[164] H. Li,[164] C. Lin,[164] C. Neu,[164] J. Wood,[164] C. Clarke,[165] R. Harr,[165] P. E. Karchin,[165] C. Kottachchi Kankanamge Don,[165] P. Lamichhane,[165] J. Sturdy,[165] D. A. Belknap,[166] D. Carlsmith,[166] M. Cepeda,[166] S. Dasu,[166] L. Dodd,[166] S. Duric,[166] E. Friis,[166] R. Hall-Wilton,[166] M. Herndon,[166] A. Hervé,[166] P. Klabbers,[166]

A. Lanaro,[166] C. Lazaridis,[166] A. Levine,[166] R. Loveless,[166] A. Mohapatra,[166] I. Ojalvo,[166] T. Perry,[166] G. A. Pierro,[166] G. Polese,[166] I. Ross,[166] T. Sarangi,[166] A. Savin,[166] W. H. Smith,[166] D. Taylor,[166] C. Vuosalo,[166] and N. Woods[166]

(CMS Collaboration)

[1]*Yerevan Physics Institute, Yerevan, Armenia*
[2]*Institut für Hochenergiephysik der OeAW, Wien, Austria*
[3]*National Centre for Particle and High Energy Physics, Minsk, Belarus*
[4]*Universiteit Antwerpen, Antwerpen, Belgium*
[5]*Vrije Universiteit Brussel, Brussel, Belgium*
[6]*Université Libre de Bruxelles, Bruxelles, Belgium*
[7]*Ghent University, Ghent, Belgium*
[8]*Université Catholique de Louvain, Louvain-la-Neuve, Belgium*
[9]*Université de Mons, Mons, Belgium*
[10]*Centro Brasileiro de Pesquisas Fisicas, Rio de Janeiro, Brazil*
[11]*Universidade do Estado do Rio de Janeiro, Rio de Janeiro, Brazil*
[12a]*Universidade Estadual Paulista, São Paulo, Brazil*
[12b]*Universidade Federal do ABC, São Paulo, Brazil*
[13]*Institute for Nuclear Research and Nuclear Energy, Sofia, Bulgaria*
[14]*University of Sofia, Sofia, Bulgaria*
[15]*Institute of High Energy Physics, Beijing, China*
[16]*State Key Laboratory of Nuclear Physics and Technology, Peking University, Beijing, China*
[17]*Universidad de Los Andes, Bogota, Colombia*
[18]*University of Split, Faculty of Electrical Engineering, Mechanical Engineering and Naval Architecture, Split, Croatia*
[19]*University of Split, Faculty of Science, Split, Croatia*
[20]*Institute Rudjer Boskovic, Zagreb, Croatia*
[21]*University of Cyprus, Nicosia, Cyprus*
[22]*Charles University, Prague, Czech Republic*
[23]*Academy of Scientific Research and Technology of the Arab Republic of Egypt, Egyptian Network of High Energy Physics, Cairo, Egypt*
[24]*National Institute of Chemical Physics and Biophysics, Tallinn, Estonia*
[25]*Department of Physics, University of Helsinki, Helsinki, Finland*
[26]*Helsinki Institute of Physics, Helsinki, Finland*
[27]*Lappeenranta University of Technology, Lappeenranta, Finland*
[28]*DSM/IRFU, CEA/Saclay, Gif-sur-Yvette, France*
[29]*Laboratoire Leprince-Ringuet, Ecole Polytechnique, IN2P3-CNRS, Palaiseau, France*
[30]*Institut Pluridisciplinaire Hubert Curien, Université de Strasbourg, Université de Haute Alsace Mulhouse, CNRS/IN2P3, Strasbourg, France*
[31]*Centre de Calcul de l'Institut National de Physique Nucleaire et de Physique des Particules, CNRS/IN2P3, Villeurbanne, France*
[32]*Université de Lyon, Université Claude Bernard Lyon 1, CNRS-IN2P3, Institut de Physique Nucléaire de Lyon, Villeurbanne, France*
[33]*Institute of High Energy Physics and Informatization, Tbilisi State University, Tbilisi, Georgia*
[34]*RWTH Aachen University, I. Physikalisches Institut, Aachen, Germany*
[35]*RWTH Aachen University, III. Physikalisches Institut A, Aachen, Germany*
[36]*RWTH Aachen University, III. Physikalisches Institut B, Aachen, Germany*
[37]*Deutsches Elektronen-Synchrotron, Hamburg, Germany*
[38]*University of Hamburg, Hamburg, Germany*
[39]*Institut für Experimentelle Kernphysik, Karlsruhe, Germany*
[40]*Institute of Nuclear and Particle Physics (INPP), NCSR Demokritos, Aghia Paraskevi, Greece*
[41]*University of Athens, Athens, Greece*
[42]*University of Ioánnina, Ioánnina, Greece*
[43]*Wigner Research Centre for Physics, Budapest, Hungary*
[44]*Institute of Nuclear Research ATOMKI, Debrecen, Hungary*
[45]*University of Debrecen, Debrecen, Hungary*
[46]*National Institute of Science Education and Research, Bhubaneswar, India*
[47]*Panjab University, Chandigarh, India*
[48]*University of Delhi, Delhi, India*

[49]Saha Institute of Nuclear Physics, Kolkata, India
[50]Bhabha Atomic Research Centre, Mumbai, India
[51]Tata Institute of Fundamental Research, Mumbai, India
[52]Institute for Research in Fundamental Sciences (IPM), Tehran, Iran
[53]University College Dublin, Dublin, Ireland
[54a]INFN Sezione di Bari, Bari, Italy
[54b]Università di Bari, Bari, Italy
[54c]Politecnico di Bari, Bari, Italy
[55a]INFN Sezione di Bologna, Bologna, Italy
[55b]Università di Bologna, Bologna, Italy
[56a]INFN Sezione di Catania, Catania, Italy
[56b]Università di Catania, Catania, Italy
[56c]CSFNSM, Catania, Italy
[57a]INFN Sezione di Firenze, Firenze, Italy
[57b]Università di Firenze, Firenze, Italy
[58]INFN Laboratori Nazionali di Frascati, Frascati, Italy
[59a]INFN Sezione di Genova, Genova, Italy
[59b]Università di Genova, Genova, Italy
[60a]INFN Sezione di Milano-Bicocca, Milano, Italy
[60b]Università di Milano-Bicocca, Milano, Italy
[61a]INFN Sezione di Napoli, Napoli, Italy
[61b]Università di Napoli 'Federico II', Napoli, Italy
[61c]Università della Basilicata (Potenza), Napoli, Italy
[61d]Università G. Marconi (Roma), Napoli, Italy
[62a]INFN Sezione di Padova, Padova, Italy
[62b]Università di Padova, Padova, Italy
[62c]Università di Trento (Trento), Padova, Italy
[63a]INFN Sezione di Pavia, Pavia, Italy
[63b]Università di Pavia, Pavia, Italy
[64a]INFN Sezione di Perugia, Perugia, Italy
[64b]Università di Perugia, Perugia, Italy
[65a]INFN Sezione di Pisa, Pisa, Italy
[65b]Università di Pisa, Pisa, Italy
[65c]Scuola Normale Superiore di Pisa, Pisa, Italy
[66a]INFN Sezione di Roma, Roma, Italy
[66b]Università di Roma, Roma, Italy
[67a]INFN Sezione di Torino, Torino, Italy
[67b]Università di Torino, Torino, Italy
[67c]Università del Piemonte Orientale (Novara), Torino, Italy
[68a]INFN Sezione di Trieste, Trieste, Italy
[68b]Università di Trieste, Trieste, Italy
[69]Kangwon National University, Chunchon, Korea
[70]Kyungpook National University, Daegu, Korea
[71]Chonbuk National University, Jeonju, Korea
[72]Chonnam National University, Institute for Universe and Elementary Particles, Kwangju, Korea
[73]Korea University, Seoul, Korea
[74]Seoul National University, Seoul, Korea
[75]University of Seoul, Seoul, Korea
[76]Sungkyunkwan University, Suwon, Korea
[77]Vilnius University, Vilnius, Lithuania
[78]National Centre for Particle Physics, Universiti Malaya, Kuala Lumpur, Malaysia
[79]Centro de Investigacion y de Estudios Avanzados del IPN, Mexico City, Mexico
[80]Universidad Iberoamericana, Mexico City, Mexico
[81]Benemerita Universidad Autonoma de Puebla, Puebla, Mexico
[82]Universidad Autónoma de San Luis Potosí, San Luis Potosí, Mexico
[83]University of Auckland, Auckland, New Zealand
[84]University of Canterbury, Christchurch, New Zealand
[85]National Centre for Physics, Quaid-I-Azam University, Islamabad, Pakistan
[86]National Centre for Nuclear Research, Swierk, Poland
[87]Institute of Experimental Physics, Faculty of Physics, University of Warsaw, Warsaw, Poland

[88]*Laboratório de Instrumentação e Física Experimental de Partículas, Lisboa, Portugal*
[89]*Joint Institute for Nuclear Research, Dubna, Russia*
[90]*Petersburg Nuclear Physics Institute, Gatchina (St. Petersburg), Russia*
[91]*Institute for Nuclear Research, Moscow, Russia*
[92]*Institute for Theoretical and Experimental Physics, Moscow, Russia*
[93]*P.N. Lebedev Physical Institute, Moscow, Russia*
[94]*Skobeltsyn Institute of Nuclear Physics, Lomonosov Moscow State University, Moscow, Russia*
[95]*State Research Center of Russian Federation, Institute for High Energy Physics, Protvino, Russia*
[96]*University of Belgrade, Faculty of Physics and Vinca Institute of Nuclear Sciences, Belgrade, Serbia*
[97]*Centro de Investigaciones Energéticas Medioambientales y Tecnológicas (CIEMAT), Madrid, Spain*
[98]*Universidad Autónoma de Madrid, Madrid, Spain*
[99]*Universidad de Oviedo, Oviedo, Spain*
[100]*Instituto de Física de Cantabria (IFCA), CSIC-Universidad de Cantabria, Santander, Spain*
[101]*CERN, European Organization for Nuclear Research, Geneva, Switzerland*
[102]*Paul Scherrer Institut, Villigen, Switzerland*
[103]*Institute for Particle Physics, ETH Zurich, Zurich, Switzerland*
[104]*Universität Zürich, Zurich, Switzerland*
[105]*National Central University, Chung-Li, Taiwan*
[106]*National Taiwan University (NTU), Taipei, Taiwan*
[107]*Chulalongkorn University, Faculty of Science, Department of Physics, Bangkok, Thailand*
[108]*Cukurova University, Adana, Turkey*
[109]*Middle East Technical University, Physics Department, Ankara, Turkey*
[110]*Bogazici University, Istanbul, Turkey*
[111]*Istanbul Technical University, Istanbul, Turkey*
[112]*National Scientific Center, Kharkov Institute of Physics and Technology, Kharkov, Ukraine*
[113]*University of Bristol, Bristol, United Kingdom*
[114]*Rutherford Appleton Laboratory, Didcot, United Kingdom*
[115]*Imperial College, London, United Kingdom*
[116]*Brunel University, Uxbridge, United Kingdom*
[117]*Baylor University, Waco, USA*
[118]*The University of Alabama, Tuscaloosa, USA*
[119]*Boston University, Boston, USA*
[120]*Brown University, Providence, USA*
[121]*University of California, Davis, Davis, USA*
[122]*University of California, Los Angeles, USA*
[123]*University of California, Riverside, Riverside, USA*
[124]*University of California, San Diego, La Jolla, USA*
[125]*University of California, Santa Barbara, Santa Barbara, USA*
[126]*California Institute of Technology, Pasadena, USA*
[127]*Carnegie Mellon University, Pittsburgh, USA*
[128]*University of Colorado at Boulder, Boulder, USA*
[129]*Cornell University, Ithaca, USA*
[130]*Fairfield University, Fairfield, USA*
[131]*Fermi National Accelerator Laboratory, Batavia, USA*
[132]*University of Florida, Gainesville, USA*
[133]*Florida International University, Miami, USA*
[134]*Florida State University, Tallahassee, USA*
[135]*Florida Institute of Technology, Melbourne, USA*
[136]*University of Illinois at Chicago (UIC), Chicago, USA*
[137]*The University of Iowa, Iowa City, USA*
[138]*Johns Hopkins University, Baltimore, USA*
[139]*The University of Kansas, Lawrence, USA*
[140]*Kansas State University, Manhattan, USA*
[141]*Lawrence Livermore National Laboratory, Livermore, USA*
[142]*University of Maryland, College Park, USA*
[143]*Massachusetts Institute of Technology, Cambridge, USA*
[144]*University of Minnesota, Minneapolis, USA*
[145]*University of Mississippi, Oxford, USA*
[146]*University of Nebraska-Lincoln, Lincoln, USA*
[147]*State University of New York at Buffalo, Buffalo, USA*

[148]Northeastern University, Boston, USA
[149]Northwestern University, Evanston, USA
[150]University of Notre Dame, Notre Dame, USA
[151]The Ohio State University, Columbus, USA
[152]Princeton University, Princeton, USA
[153]University of Puerto Rico, Mayaguez, USA
[154]Purdue University, West Lafayette, USA
[155]Purdue University Calumet, Hammond, USA
[156]Rice University, Houston, USA
[157]University of Rochester, Rochester, USA
[158]The Rockefeller University, New York, USA
[159]Rutgers, The State University of New Jersey, Piscataway, USA
[160]University of Tennessee, Knoxville, USA
[161]Texas A&M University, College Station, USA
[162]Texas Tech University, Lubbock, USA
[163]Vanderbilt University, Nashville, USA
[164]University of Virginia, Charlottesville, USA
[165]Wayne State University, Detroit, USA
[166]University of Wisconsin, Madison, USA

[a]Deceased.
[b]Also at Vienna University of Technology, Vienna, Austria.
[c]Also at CERN, European Organization for Nuclear Research, Geneva, Switzerland.
[d]Also at Institut Pluridisciplinaire Hubert Curien, Université de Strasbourg, Université de Haute Alsace Mulhouse, CNRS/IN2P3, Strasbourg, France.
[e]Also at National Institute of Chemical Physics and Biophysics, Tallinn, Estonia.
[f]Also at Skobeltsyn Institute of Nuclear Physics, Lomonosov Moscow State University, Moscow, Russia.
[g]Also at Universidade Estadual de Campinas, Campinas, Brazil.
[h]Also at Laboratoire Leprince-Ringuet, Ecole Polytechnique, IN2P3-CNRS, Palaiseau, France.
[i]Also at Joint Institute for Nuclear Research, Dubna, Russia.
[j]Also at Suez University, Suez, Egypt.
[k]Also at Cairo University, Cairo, Egypt.
[l]Also at Fayoum University, El-Fayoum, Egypt.
[m]Also at British University in Egypt, Cairo, Egypt.
[n]Also at Sultan Qaboos University, Muscat, Oman.
[o]Also at Université de Haute Alsace, Mulhouse, France.
[p]Also at Brandenburg University of Technology, Cottbus, Germany.
[q]Also at Institute of Nuclear Research ATOMKI, Debrecen, Hungary.
[r]Also at Eötvös Loránd University, Budapest, Hungary.
[s]Also at University of Debrecen, Debrecen, Hungary.
[t]Also at University of Visva-Bharati, Santiniketan, India.
[u]Also at King Abdulaziz University, Jeddah, Saudi Arabia.
[v]Also at University of Ruhuna, Matara, Sri Lanka.
[w]Also at Isfahan University of Technology, Isfahan, Iran.
[x]Also at University of Tehran, Department of Engineering Science, Tehran, Iran.
[y]Also at Plasma Physics Research Center, Science and Research Branch, Islamic Azad University, Tehran, Iran.
[z]Also at Università degli Studi di Siena, Siena, Italy.
[aa]Also at Centre National de la Recherche Scientifique (CNRS)-IN2P3, Paris, France.
[bb]Also at Purdue University, West Lafayette, USA.
[cc]Also at Institute for Nuclear Research, Moscow, Russia.
[dd]Also at St. Petersburg State Polytechnical University, St. Petersburg, Russia.
[ee]Also at California Institute of Technology, Pasadena, USA.
[ff]Also at Faculty of Physics, University of Belgrade, Belgrade, Serbia.
[gg]Also at Facoltà Ingegneria, Università di Roma, Roma, Italy.
[hh]Also at Scuola Normale e Sezione dell'INFN, Pisa, Italy.
[ii]Also at University of Athens, Athens, Greece.
[jj]Also at Paul Scherrer Institut, Villigen, Switzerland.
[kk]Also at Institute for Theoretical and Experimental Physics, Moscow, Russia.
[ll]Also at Albert Einstein Center for Fundamental Physics, Bern, Switzerland.
[mm]Also at Gaziosmanpasa University, Tokat, Turkey.

[nn]Also at Adiyaman University, Adiyaman, Turkey.
[oo]Also at Cag University, Mersin, Turkey.
[pp]Also at Anadolu University, Eskisehir, Turkey.
[qq]Also at Ozyegin University, Istanbul, Turkey.
[rr]Also at Izmir Institute of Technology, Izmir, Turkey.
[ss]Also at Necmettin Erbakan University, Konya, Turkey.
[tt]Also at Mimar Sinan University, Istanbul, Istanbul, Turkey.
[uu]Also at Marmara University, Istanbul, Turkey.
[vv]Also at Kafkas University, Kars, Turkey.
[ww]Also at Yildiz Technical University, Istanbul, Turkey.
[xx]Also at Rutherford Appleton Laboratory, Didcot, United Kingdom.
[yy]Also at School of Physics and Astronomy, University of Southampton, Southampton, United Kingdom.
[zz]Also at Université Paris-Sud, Orsay, France.
[aaa]Also at University of Belgrade, Faculty of Physics and Vinca Institute of Nuclear Sciences, Belgrade, Serbia.
[bbb]Also at Argonne National Laboratory, Argonne, USA.
[ccc]Also at Erzincan University, Erzincan, Turkey.
[ddd]Also at Texas A&M University at Qatar, Doha, Qatar.
[eee]Also at Kyungpook National University, Daegu, Korea.